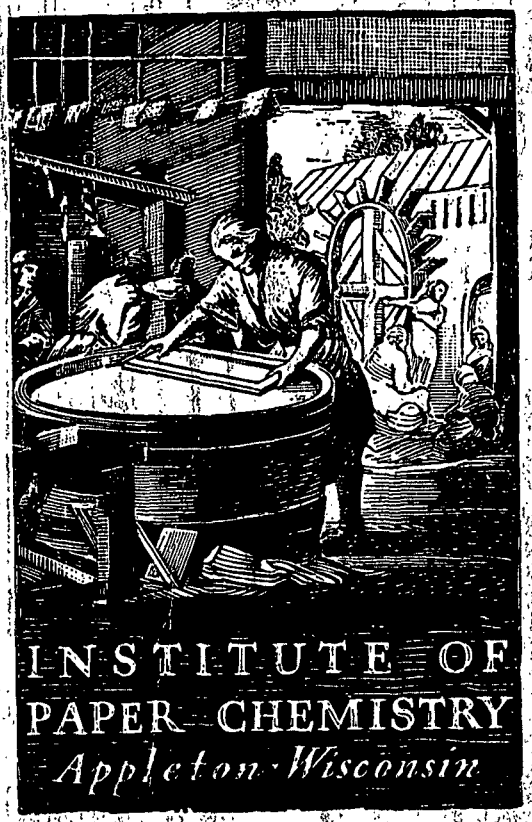

A FUNDAMENTAL RHEOLOGICAL STUDY OF THE BLADE COATING PROCESS

Project 3069

Report One

A Progress Report

to

MEMBERS OF GROUP PROJECT 3069

July 27, 1973

THE INSTITUTE OF PAPER CHEMISTRY

Appleton, Wisconsin

A FUNDAMENTAL RHEOLOGICAL STUDY OF THE BLADE COATING PROCESS

Project 3069

Report One

A Progress Report

to

MEMBERS OF GROUP PROJECT 3069

July 27, 1973

MEMBERS OF GROUP PROJECT 3069

Air Products and Chemicals, Inc.

American Can Company

Appleton Papers, Inc.

Blandin Paper Company

Champion International

Continental Can Company, Inc.

The Dow Chemical Corporation

Georgia Kaolin Company

P. H. Glatfelter Co.

Great Northern Paper Company

Potlatch Corporation

Thiele Kaolin Company

Union Camp Corporation

TABLE OF CONTENTS

THE INSTITUTE OF PAPER CHEMISTRY

Appleton, Wisconsin

A FUNDAMENTAL RHEOLOGICAL STUDY OF THE BLADE COATING PROCESS

SUMMARY

This project was begun as part of the research effort of one of the sponsoring companies and has been continued at The Institute of Paper Chemistry as Group Project 3069 with the support of manufacturers of coated papers and suppliers of coating materials.

The original purposes of the work were to permit comparison of theoretical and experimental flow behavior, to enable pertinent fluid properties to be measured under realistic conditions, and to apply the results to actual coating problems. The experimental approach to these goals was to generate high shear flow in a model nip. The original purposes remain unchanged. Work to date has been concerned with the first two goals, with a considerable degree of success. The projected continuation of the project involves refinement of the experimental equipment and techniques, extension of the experiments to a wider variety of machine parameters and coating compositions, and application of the results to pilot and commercial coating operations.

The analytical device built for this research work is called the "Blade Nip Rheometer." It physically resembles a blade coater, with the blade and roll both being inflexible. The nip is formed by the blade and roll, with no base stock involved. A unique double blade device was designed to permit operating over a wide range of variables with no change in blade angle. The blade angle was fixed at ten degrees for the work done to date.

In order to adequately describe flow in the nip and to evaluate fluid properties, the following operating variables were measured:

$\underline{V_o}$: the roll surface velocity,

$\underline{DR}$: the film thickness under the blade nip,

$\underline{DX}$: the fluid drag on the roll, and

$\underline{F}$: the normal force applied to the blades.

The shear rate varies throughout the nip, of course, but one can adequately describe a maximum shear rate characteristic of given operating parameters as being equal to $\underline{V_o}/\underline{DR}$.

In order to utilize the experimental results, it was necessary to mathematically describe theoretical flow in the nip. The flow was assumed to be viscometric (simple shear), a practice followed in all mathematical models of flow in nips. Fluids were considered to be generally viscoelastic, with the viscosity function conforming to the power law model. The application of the theory to the experimental results yields two measurements of fluid properties:

$\eta(\underline{D})$: a function of $\underline{V_o}$, $\underline{DR}$, and $\underline{DX}$, and

$\eta(\underline{F})$: a function of $\underline{V_o}$, $\underline{DR}$, and $\underline{F}$.

The parameter $\eta(\underline{D})$ is the usual viscosity function. The parameter $\eta(\underline{F})$ is characteristic of both viscous and elastic fluid properties. For inelastic fluids, $\eta(\underline{F})$ is also the usual viscosity function; for viscoelastic fluids, $\eta(\underline{F})$ is the sum of the viscosity and a contribution of the viscoelastic normal stress combination $\underline{p_{11}}-\underline{p_{22}}$. According to viscometric flow theory, these fluid parameters completely characterize a fluid flowing in any nip.

In anticipation of necessary corrections to experimental results, theoretical analyses were made for corrections due to viscous heating and for cross-flow resulting from the pressure drop from the center of the nip to the edges.

An extensive series of measurements was made on Newtonian fluids, glycerin-water mixtures. A statistical analysis was made on the results to determine the sources of random error. It was determined that the techniques used to measure the physical variables are adequate, and that random error is largely due to uncertainties concerning the exact physical description of the nip and the condition of fluid in the nip. The random error was reflected mainly in the film thickness, $\underline{DR}$, not the measurement of the value but true random variation in the parameter. The error level in the results was generally not so great as to be unacceptable but large enough to suggest improvement.

The results on Newtonian fluids were independent of roll velocity, $\underline{V}_o$, at levels of 1000 and 2000 ft./min. At low shear rate and low viscosity, the viscosity results were generally larger than theoretical, probably due to turbulence in the nip. For high viscosity fluids at high shear rates, the viscosity results were generally lower than theoretical, for reasons unknown. At moderate viscosity values (0.6-1.0 poise) the results generally conformed to the theory except that $\eta(\underline{D})$ showed a sharp decrease at high shear rate. Since a similar decrease for coatings was not observed, it is possible that this is a real fluid effect and not an aberration of the instrument. Shear rates attained in the measurements were generally in the range 10^4-10^6 sec.$^{-1}$ Shear rates of two million were easily attained.

A wide variety of coating compositions was tested. As a standard, a starch-clay coating was tested in most of the experiments. Viscoelastic behavior was presumed to be absent in the standard; the difference between $\eta(\underline{F})$ and $\eta(\underline{D})$ was fairly small, and both functions decreased monotonously with increasing shear rates. Both viscosity functions were independent of velocity at 1000 and 2000 ft./min.

The effect of various additives, such as carboxymethyl cellulose, urea, and calcium stearate, on the standard altered the levels of the viscosity functions but made no change in the basic form of the results. Comparable results were obtained by substituting various mineral pigments for clay.

Latex- and protein-clay coatings showed significant departures from the rheological behavior of the standard.

Coatings containing polyvinyl alcohol as part or all of the binder exhibited strong viscoelastic behavior. Contrary to theory, $\eta(\underline{D})$ was affected by viscoelasticity, and $\eta(\underline{F})$ was affected in a manner that only conformed to the theory in part. It is apparent from the results that the presence of viscoelasticity alters the presumed viscometric flow in the nip. Viscoelastic behavior was also seen in the results for starch binder, without pigment.

Starch-plastic pigment coatings were prepared with starch-pigment ratios the same as the standard, on a volume basis. Contrary to expectations, these coatings exhibited basically different flow behavior than the standard. A comparison with the PVA containing coatings indicated moderate levels of viscoelasticity.

A point of particular importance can be seen in comparing Rheometer results with those obtained with the Hercules viscometer. The Rheometer makes a clear distinction between the flow behaviors of various coatings that appear to be very similar in the Hercules rheograms. In fact, of all the coatings tested, only the latex-clay coating showed a basically different type of flow behavior in the Hercules instrument. An additional advantage of the Rheometer in characterizing coatings is that, even though the theoretical explanation of the results is not completely understood, results are being transferred from a measuring device with

the same type of flow geometry, and operating under the same high shear conditions, as the coating process.

A survey of the results to date has led to the conclusion that certain problems in the Rheometer should be corrected. Chief among these is the necessity to avoid pumping fluid to the nips since, in many cases, the results were somewhat affected by insufficient fluid in the nips. Other problems are a lack of temperature control, the requirement for large amounts of test materials, the lack of assurance that the relative positions of blade and roll are always where they are presumed to be, the problem of entrained air due to the fluid circulation system, and the impracticality of testing nonaqueous systems. Some preliminary work has already been done on the redesign of the Rheometer to correct these problems, without altering the essential features that operate satisfactorily. Some consideration has also been given to methods by which the Rheometer concept and equipment can be used to measure viscosity and normal stresses independent of the nonideal conditions existing in nips. This would provide an invaluable tool for the description of nip flow in terms of basic fluid parameters.

INTRODUCTION

Research in blade coating rheology has made significant advances in recent years. Mathematical descriptions of flow in the blade nip have provided a means of predicting the response of changes in such variables as blade angle, blade thickness, blade load, coater velocity, and coating viscosity. This research has emphasized that the maximum shear rate reached in the nip is of the order of one million reciprocal seconds, compared with values of about 20,000 in commercial viscometers. This has led to investigations conducted with such high shear instruments as the band and the jet viscometers, neither of which is commercially available. There has been a little interest shown in the possible importanc of coating viscoelasticity.

The motivations for this project were to determine how well existing theory describes flow in the blade nip, to determine what fluid properties are important, and to provide a means of measuring these properties. In order to make significant progress in reaching these goals, it was considered necessary to use the essential part of the blade coater, the blade nip, as an analytical tool. The result was the design and construction of the Blade Nip Rheometer. Results obtained with this instrument have a validity uncommon to previous measurements; they are obtained at shear rates comparable to those existing in the blade coater, and, due to similarities in geometry, the results are directly applicable to coater operation.

It became apparent during the use of the instrument that the flow behavior of certain types of coatings is dependent on other rheological properties in addition to viscosity, suggesting that the Rheometer may have a unique applicability in the characterization of coating rheology.

FUTURE WORK

1. It was shown in the work done to date that coatings with similar viscosity functions can behave very differently in the blade nip. It is important to investigate how these differences affect coater operation by comparing Rheometer results with coating behavior on pilot and commercial coaters. This is an area in which feedback from the sponsors should be particularly useful since the materials studied so far have been used in commercial coatings.

The use of the Rheometer offers a unique opportunity to study the effects of fluid properties and nip variables on coat weight. It is projected that Rheometer and coater results be used in conjunction to separate the relative amounts of coating which are sheared in the nip and which are carried through as part of the base stock. This approach may be useful in contributing to information on the extent of coating-base stock interaction.

2. The results to date were obtained with a single blade configuration, with only the film thickness being varied. Future work will include the application of variable blade angles and nip shapes.

3. It was seen from the results that where coatings exhibit viscoelastic behavior, the commonly applied viscometric flow theory is inadequate. Work will be undertaken to revise the theory to better describe the behavior of these materials.

4. Some preliminary work has been done in the redesign of the Rheometer in order to eliminate certain problems that have become apparent:

(a) Coating is collected as overflow from the nips and recirculated by pumping. Undesirable effects resulting from the need to

recirculate coating are that the pumping rate is insufficient in some cases to fill the nips, the recirculation of coatings leads to considerable amounts of entrained air in the coatings, and pumping provides an unwanted thixotropic breakdown of coatings.

(b) The amount of coating required for a test is of the order of four to five liters, an amount difficult to produce on a laboratory scale.

(c) There is no temperature control on the instrument.

(d) Because of the original design of the instrument, there is a degree of uncertainty concerning the maintenance of the blades on a parallel with the center line of the roll.

(e) The instrument is limited to the testing of water-based materials.

BACKGROUND

THE PRINCIPLE OF BLADE DOCTORING

Consider the schematic model of the blade nip illustrated in Fig. 1. A force balance is given by Equation (1):

$$F(b) = F(p) + F(ve) \tag{1}$$

in which $\underline{F}(\underline{b})$ is the mechanical load applied to the blade, $\underline{F}(\underline{p})$ is the pressure force exerted by the fluid on the blade, and $\underline{F}(\underline{\underline{ve}})$ is the viscoelastic normal stress force exerted by the fluid on the blade. The fluid forces are given by:

$$F(p) = \int p \, dx \tag{2}$$

$$F(ve) = \int (p_{11}-p_{22})_{|\Gamma|_{min}} \, dx \tag{3}$$

in which $(\underline{p}_{11}-\underline{p}_{22})$ is the first normal stress difference, and $|\Gamma|_{min}$ is the minimum absolute value of shear rate. See Appendix II for arguments supporting the particular normal stress function used.

The flow shown in Fig. 1(a) is stable for two reasons: (1) because of blade bending, even large changes in $\underline{h}_o$ do not appreciably change the mechanical blade load, $\underline{F}(\underline{b})$; and (2) any change in $\underline{h}_o$ alters the fluid forces in a manner tending to restore the original value. For example, a sudden decrease in $\underline{h}_o$ increases both $\underline{F}(\underline{p})$ and $\underline{F}(\underline{\underline{ve}})$, which increases the lifting force on the blade.

The fluid forces depend on fluid properties and process variables. For a Newtonian fluid, the pressure force is of the form:

$$[F(p)/(\eta * V_o)] = f(h_o) \tag{4}$$

in which η is the fluid viscosity.

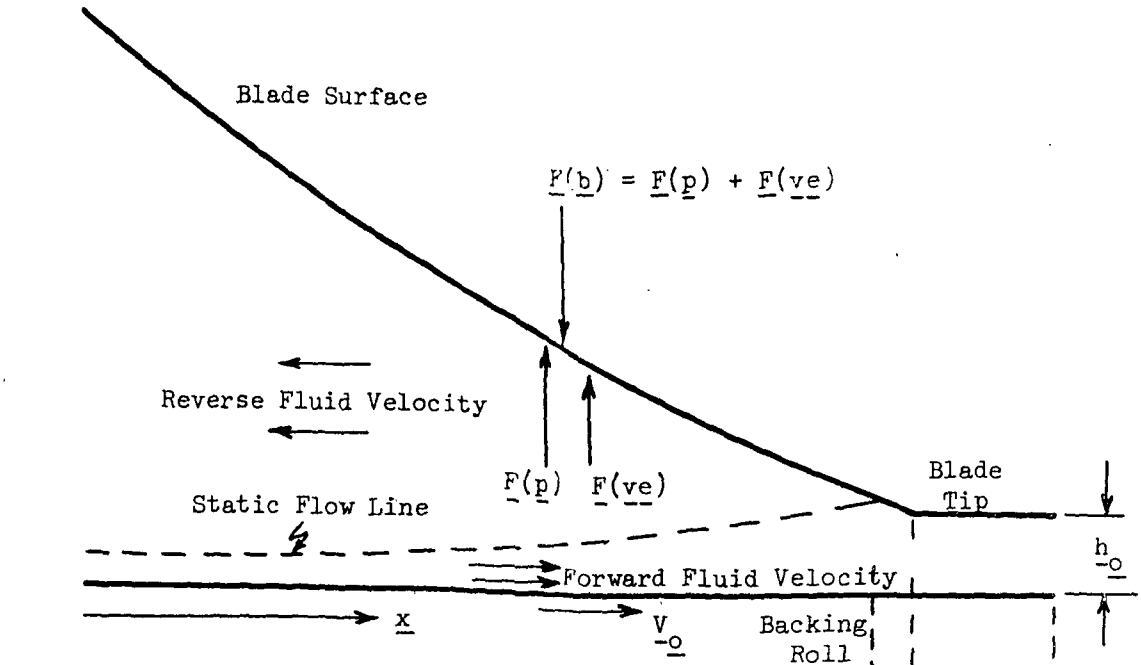

(a) Velocity, and Force Balance

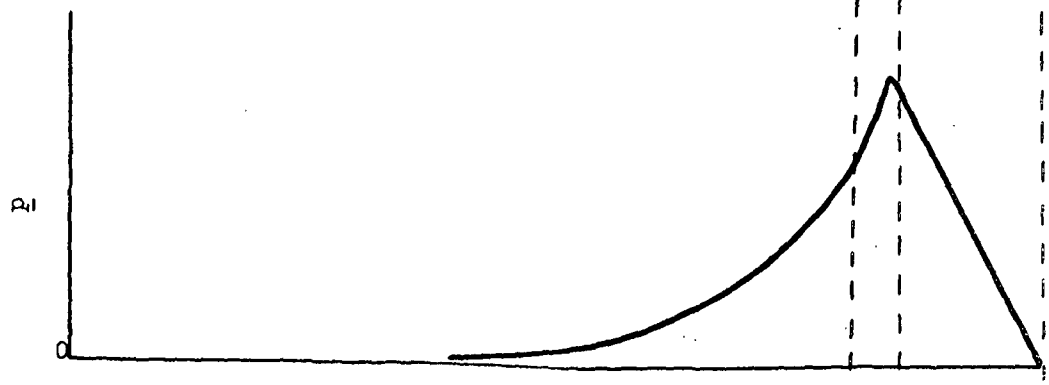

(b) Pressure Profile

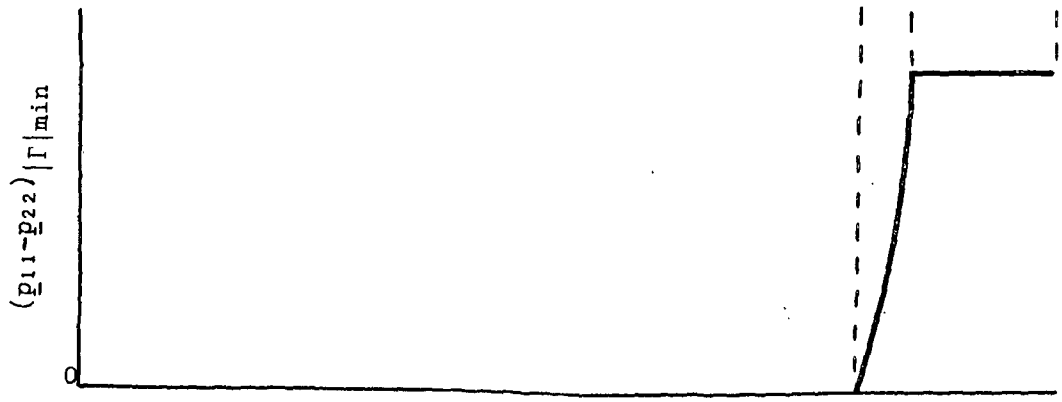

(c) Effective Normal Stress Difference

Figure 1. Schematic Model of the Blade Nip

The nature of the functionality of Equation (4) depends on the nip geometry, but it is always inverse. One can then expect an increase in coat weight with an increase in velocity, an increase in fluid viscosity, or a decrease in blade load.

PUBLISHED ANALYSES

The expected effect of process and coating variables on coat weight has generally been confirmed in practice. Coat weight is reduced by increasing the blade load (1-4). It was shown that at sufficiently large blade loads the coat weight is nearly constant, presumably because the doctored film thickness is insignificant when compared with the coating within the sheet and that trapped by the surface roughness (2). Coat weight increases with coating viscosity, whether this is achieved by increasing solids (1,2), by reducing the temperature (2), or by increasing penetration (which increases the solids and thus the viscosity) (1,2,5). In Reference (2) it was reported that originally lower viscosity can result in higher coat weight due to increased penetration. All else equal, coat weight increases with a decrease in blade angle (1). Windle and Beazley have estimated that the viscoelastic normal stress and pressure lifting forces are comparable in magnitude (6).

Published mathematical analyses of lubrication flow in the blade nip have been restricted to the viscometric flow of Newtonian fluids, except for a very recent presentation which considers the power law model (3). Follette and Fowells made a semiempirical analysis and correctly, but only qualitatively, predicted the effect of process variables on coat weight (1). Bohmer (7), Bliesner (8), and Hayward (4) made quantitative calculations with the assumption that the blade tip forms a small converging angle with the sheet.

Turai considered the effect of lubrication flow in a parallel channel under the blade tip (9-11). His model assumes a restricted channel at the nip outlet due to paper compression, which results in the prediction of reverse pressure driven flow under the blade tip.

Windle and Beazley approximated the nip as a plane wedge or by a plano-cylindrical wedge and erroneously concluded in both cases that a stable free film is impossible (5). For the plane wedge they neglected the fact that a change in film thickness produces a change in blade lift that tends to restore the film thickness. For the plano-cylindrical wedge they conclude that the pressure liftir force is independent of the minimum film thickness. They give no derivation for their equation and this author has been unable to duplicate it.

CONVERGING VS. PARALLEL FLOW CHANNEL UNDER THE BLADE TIP

In contrast to the parallel flow channel under the blade tip assumed as the model in this report, at least three previous studies have considered the channel to be converging (4,7,8). The arguments in favor of a parallel channel are as follows:

(1) During coater operation, the blade is quickly ground to a steady-state geometry relative to the base stock.

(2) The rate of blade wear is presumed to be roughly proportional to the shear stress at the blade surface. The shear stress is presumed to be approximately proportional to the inverse of the film thickness.

(3) As a result, the blade tip will wear such that a parallel flow channel is attained. Because of paper and backing roll deformation, the channel may have some curvature but still not vary in thickness.

EQUIPMENT

DESCRIPTION OF THE RHEOMETER

A schematic drawing of the Rheometer is given in Fig. 2. A list of the commercial parts of the equipment follows:

Pump

Jabsco pump; Marathon Electric; Wausau, Wis.; Model 7QJ 48C 17D157H-ECC1 1/3 hp.; 1725 r.p.m.

Dial Indicator

Starrett dial indicator; L.S. Starrett Co.; Athol, Mass.; No. 656-611; 0.2-in. range; 0.0001-in. units.

SCR Drive

T. B. Wood's Sons Co.; Chambersburg, Pa.; Ultracon SCR Drive Control; Model U-300; 230 volts.

Motor

T. B. Wood's Sons Co.; Chambersburg, Pa.; Model MU-300; 3 hp.; d.c. motor.

Tackometer

Zero Max Co.; Tackometer generator set; Model B2420; dual range: 0-5000 ft./min., 0-1000 ft./min.

Force Gage

Dillon Co.; 14620 Keswick St.; Van Nuys, Calif.; Model XC; Code WORO-X; Serial 17614; 0-50 lb.

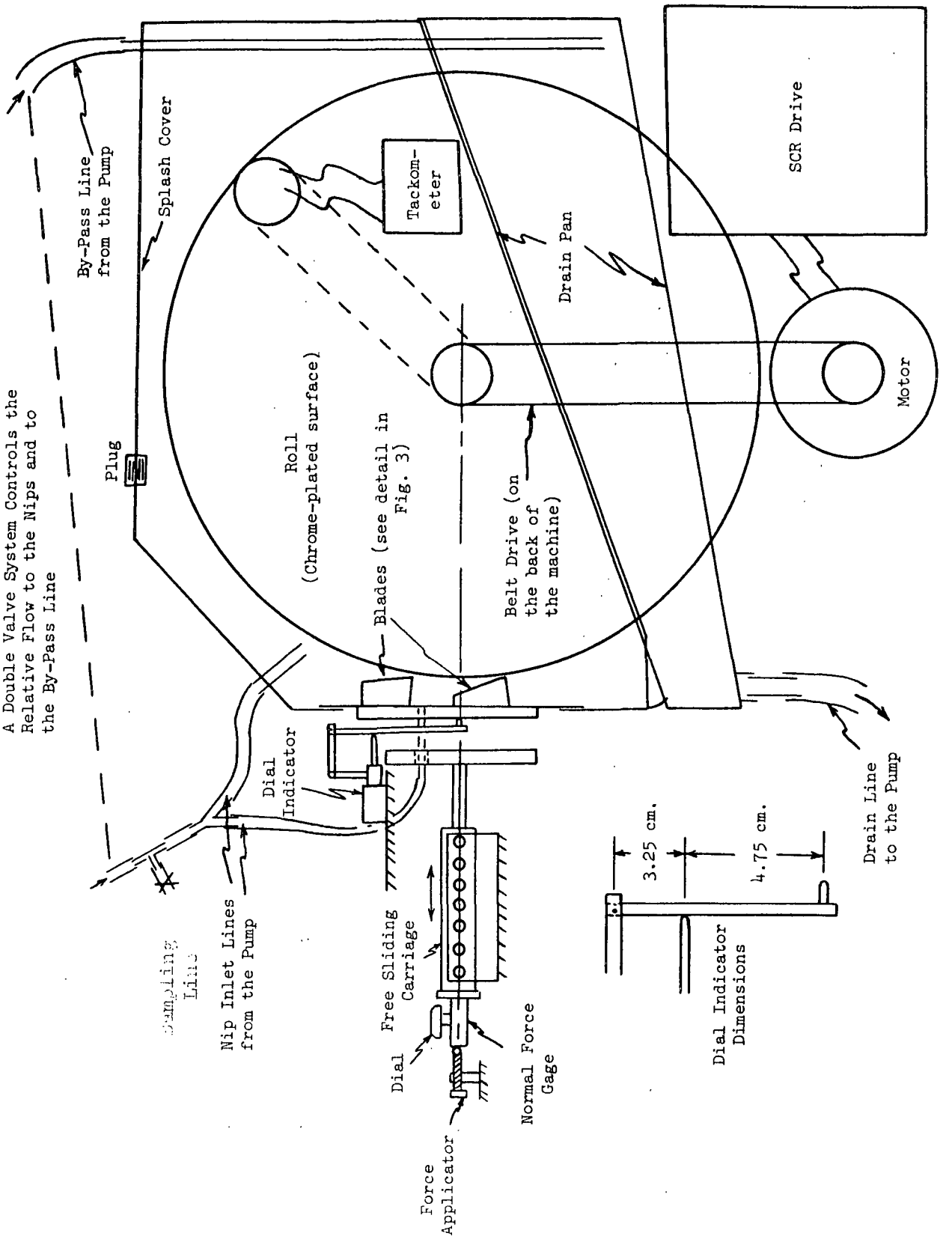

Figure 2. Schematic Drawing of the Rheometer

DETAILED DESCRIPTION OF THE DOUBLE BLADES

Principle of the Double Blade Operation

A detailed, full-scale drawing of the double blade assembly is given i Fig. 3.

The blade on a coater immediately adjusts to roll-base stock changes t maintain a constant blade load. The mechanism for this adjustment is blade bending; small changes in the position of the blade tip do not change the blade bending to any significant extent. The function of blade bending in the double blade operation is replaced by the springs loading the blade holder. The double blade must conform to an additional condition not required of the blade coater: blade angle must remain constant over extreme changes in blade load. The maintenance of constant blade angle is assured by the mutual action of the blade the virtual contact of each blade tip and roll keeps the angle constant on the other blade.

Torque Balance

The fluid and mechanical forces exerted on the blade assembly are show in Fig. 4. Some comments concerning the various forces and dimensions:

F_1, F_2: normal forces exerted by the fluid on the blades. It assumes that these forces are exerted at the blade tips.

D_1, D_2: tangential forces exerted by the fluid on the blades. These values are not determined experimentally. See below for additional comment.

S: mechanical force exerted on the blade holder by springs.

W(850 g.): weight of the blade assembly.

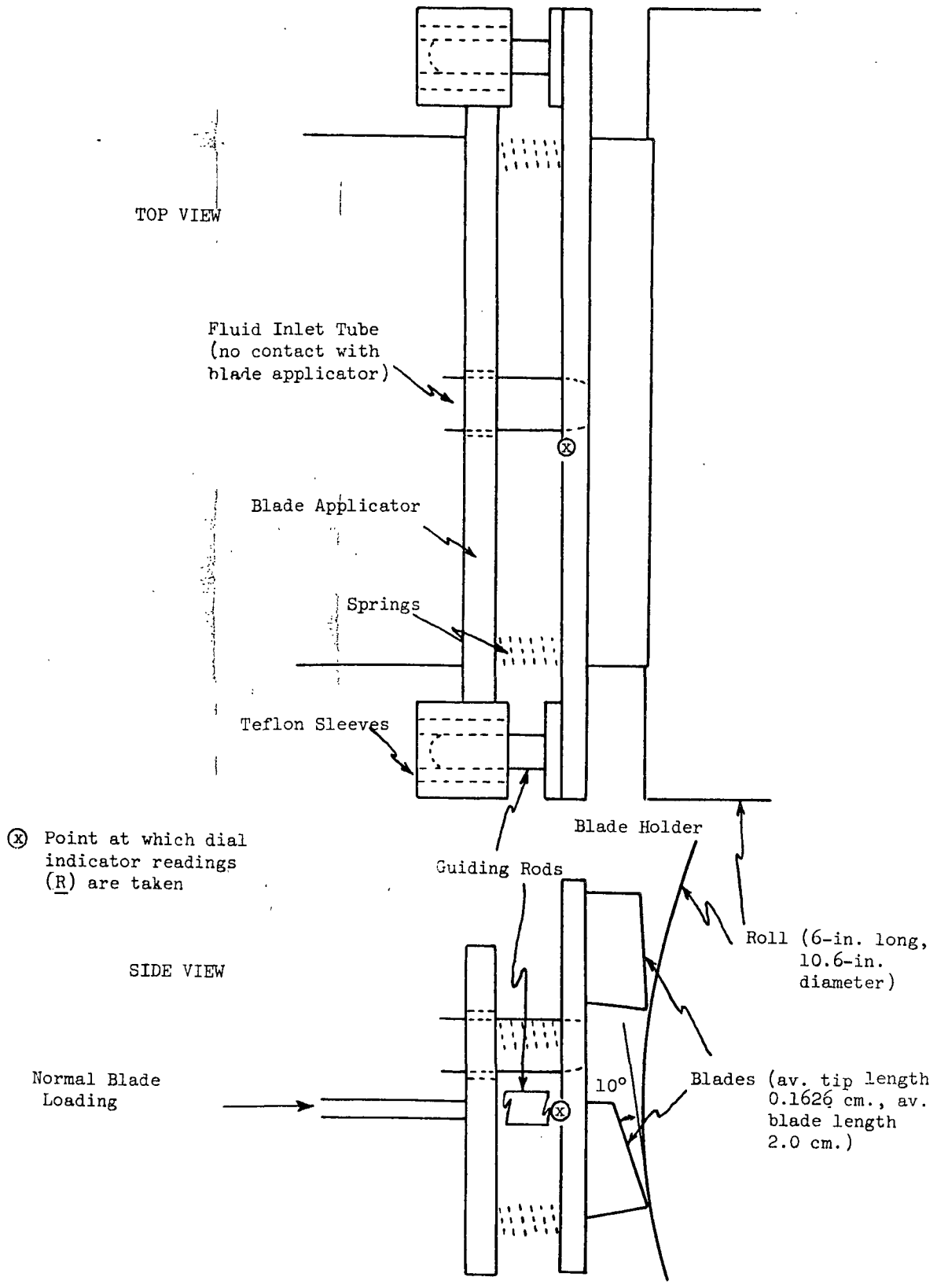

Figure 3. Details of the Double Blade Device

$\underline{F}_r$: force exerted by the blade applicator on the guiding rods. It is presumed that the teflon sleeves holding the guiding rods can exert a vertical force only and not exert a couple on the guiding rods.

Δ_1(3.8 cm.): distances from the reference point, $\underline{O}$, to the blade tips.

Δ_2(1.45 cm.), Δ_3(2.25 cm.): distances from the reference point to the centers of the springs.

Δ_4(3.5 cm.): distance from the reference point to the point of force application on the guiding rods. This distance is an estimate only since the part of the teflon sleeve which supports the rods is unknown.

Δ_5(1.1 cm.): distance from the reference point to the mass center of the assembly.

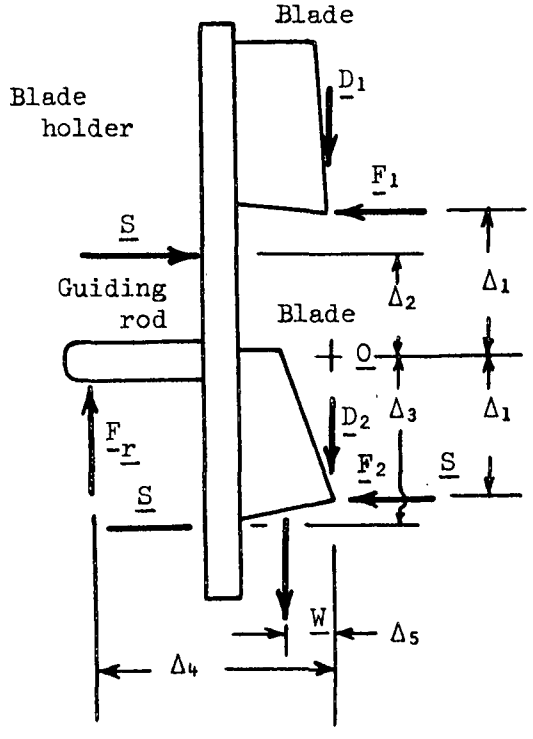

Figure 4. Forces Applied to the Blade Assembly

A point of particular interest concerns the fluid tangential forces $\underline{D}_1$ and $\underline{D}_2$. Calculations for this nip geometry covering a wide range of film thicknesses and power law exponents gave tangential forces on the blade and roll that were identical, within a few percent, but opposite in sign. This is a physically reasonable result. However, the drag on the roll is due only to fluid shear and the tangential force on the blades consists of both shear and the tangential component of pressure force on the blade surfaces. The shearing forces on the blade tip and blade surface are opposite and in some cases virtually cancel out, and yet the pressure force on the blade surface gives a result which is numerically equal to shear drag on the roll. This fortunate result leads to the conclusion that the tangential force on a blade can be set equal to the negative roll drag.

The vertical force balance gives:

$$F_r = D_1 + D_2 + W. \tag{5}$$

The horizontal force balance gives:

$$2\,S = F_1 + F_2. \tag{6}$$

A torque balance about point $\underline{O}$ gives:

$$S(\Delta_3-\Delta_2) + (F_1-F_2)\Delta_1 - F_r\,\Delta_4 + W\,\Delta_5 = 0. \tag{7}$$

Equations (5)-(7) are combined and after some manipulation give Equation (8):

$$F_1-F_2 = (F_1+F_2)\left(\frac{\Delta_2-\Delta_3}{2\,\Delta_1} + \frac{\Delta_4}{\Delta_1}\,\frac{D_1+D_2}{F_1+F_2}\right) + W(\Delta_4-\Delta_5)/\Delta_1. \tag{8}$$

In terms of experimental quantities, $\underline{F}$ and $\underline{DX}$:

$$\left.\begin{aligned} D_1 + D_2 \text{ (g.)} &= 14.2 \text{ DX} \\ F_1 + F_2 \text{ (g.)} &= 480 \text{ F.} \end{aligned}\right\} \qquad (9)$$

Substituting the numerical values given into Equation (8):

$$\Delta F = F(0.0275*DX/F - 0.106) + 1.12 \qquad (10)$$

in which ΔF is F_1-F_2 expressed in experimental units.

Equation (10) gives a means of using experimental results to check the presumed equal normal forces on the two blades.

EXPERIMENTAL PROCEDURES

GRINDING THE BLADES

The blades were ground while installed in place on the Rheometer. With the roll wrapped with coarse emery paper, the blades were ground to about the depth desired. The normal blade load was about 10 lb. and the roll surface velocity about 40 ft./min.

After removing the emery paper, the blades were fine ground using a water paste of 400 grit carborundum. The load and roll velocity were the same as for the coarse grinding. The blades were tested for fit on the roll by marking lines across the roll with a felt tip pen and turning the roll by hand with various loads on the blades. After about 20 minutes of grinding the even scraping of the lines by the blades indicated a near perfect fit of blade tips and roll surface.

The relative horizontal positions of the two edges of the blades were measured with a depth micrometer on top of the blade holder. The relative values were later duplicated, as closely as possible, for experimental runs.

The blade tip lengths (TL) were measured at various positions across the blades, with the results given in Table I.

PREPARING FOR AN EXPERIMENT

The splash cover, pan, and blades were installed. The relative position of the blades were checked with a depth micrometer on the blade holder. If the difference between the two depths was within 0.002 in. of the difference measured when the blades were ground, no correction was made; if not within 0.002 in., various adjustments in the machine were made to obtain a satisfactory difference.

The adjustments were required only in a few cases in early experiments. In the first few experiments, the ink line test described above was used to confirm goo blade tip-roll surface fit.

TABLE I

BLADE TIP DIMENSIONS

		Top Blade TL, cm.	Bottom Blade TL, cm.
Front of the Rheometer	1	0.162	0.160
	2	0.162	0.158
	3	0.162	0.160
	4	0.162	0.158
	5	0.164	0.158
	6	0.164	0.158
	7	0.162	0.158
	8	0.164	0.162
	9	0.162	0.164
	10	0.164	0.174
Back of the Rheometer	11	0.164	0.174
	Average	0.1629	0.1622
	Total average	0.1626	

The various circulation lines were connected. The cooling water was turned on. The voltmeter used to measure roll drag was connected to the drive control. The dial indicator was installed and adjusted to insure readings could not go off scale. The normal force gage was set at zero on the dial with no load on the blades.

Fluid was introduced through the top of the splash cover. In the case of glycerin-water, 2500 ml. was introduced and the dilution by water in the lines was part of the fluid tested. In testing coatings, the system was first flushed

out with about 2-3 liters of coating before introduction of the 2500 ml. of coating to be tested. This procedure led to very little dilution of the coating tested. It was estimated that the volume of fluid in the system during a test was about 3000 ml. The pump was turned on and fluid was circulated through both the nip lines and the by-pass line to insure thorough mixing.

In glycerin experiments, a change of fluid was made by adding dilution water. In one case, pure glycerin was added to reverse the order of progressive lower glycerin-water ratios. In testing coatings, each new coating was used to flush out the system before introduction of the 2500-ml. sample to be tested.

PROCEDURE FOLLOWED DURING AN EXPERIMENT

In the usual case, a fluid was tested by making two runs, the first at 1000 ft./min. and the second at 2000 ft./min. A sample was taken from a drain on the nip line between runs.

During a given run, the following information was recorded:

(1) The starting temperature, t_i, of overflow from the blades.

(2) With the blades held off the roll as far as possible and the roll velocity at V_o, X_o was recorded on the voltmeter. In experiments after the first two, this measurement was deleted.

(3) Normal force, F, was applied to the blades in successively increasing steps, with roll velocity held constant at V_o. At each step, F, X, and R were recorded, in which:

F = normal force applied (see Appendix V for calibration),

X = drive control voltage (see Appendix V for calibration), and

R = dial indicator reading (distance in cm. = $R/16070$).

(4) At the maximum force, the velocity was cut to $V_o/4$ and a reading of R was taken, R_o'.

(5) With the velocity at V_o and the blades backed off, the X reading was recorded as X_o.

(6) The final temperature, t_f, was taken.

CONCLUSION OF AN EXPERIMENT

In early experiments, the depth readings on the blade holder were checked. In no case was there a significant change and the practice was abandon in later experiments.

DETERMINATION OF VISCOSITY RESULTS FROM THE EXPERIMENTAL DATA

INPUT DATA FOR A RUN

V_o = roll surface velocity

t_i, t_f = temperatures at the start and end of a run

k = fluid thermal conductivity

ρ = fluid density

c_p = fluid heat capacity

β = viscosity-temperature coefficient; i.e., $\eta = \eta_o \exp[-\beta(t-t_o)]$

$F(J), J = 1, JJ$ = blade load, with $F(1)$ being the first and lowest value and $F(JJ)$ being the last and largest value (see Appendix V for the calibration)

$X(J), J = 1, JJ$ = drive control voltage corresponding to $F(J)$ values (see Appendix V for calibration)

$R(J), J = 1, JJ$ = dial indicator readings corresponding to $F(J)$ values. $[R(J)-R_o]/16070$ = film thickness under the blade tip in cm., with R_o being the blade-roll "contact" value of R

X_o = value of X with the blades backed off to the limit. Under this condition there is no fluid contact apparent between blades and roll. Where X_o values were taken at the start and end of a run, the second value is used

R_o' = R value with $F = F(JJ)$ and velocity = $V_o/4$

N = power law exponent; i.e., shear stress = viscosity*shear rate^N

$\eta_o(30)$ (glycerin-water mixtures only) = fluid viscosity at 30°C.

COMPUTATION OF VISCOSITY RESULTS

Subroutine Operations

(1) Assuming the geometry under the blade surface is a plane wedge and the fluid is Newtonian, there are exact analytical solutions for DD = DX/[η(D)*V_o] and FF = F/[η(F)*V_o] as functions of DR. Based on results obtained for the general fluid, described in Appendix II, empirical corrections were mad for DD and FF as functions of DR and N. Therefore, with N and DR as input, FF and DD are obtained as output.

(2) The viscous heat program of Appendix IV is much too time consumi to be used for each set of data. Results from the program were empirically cor lated with fluid properties, ρ, c_p, k, and viscosity; and nip variables, DR and The output results are:

$$\left.\begin{aligned} VHF &= \frac{\eta(F)(\text{uncorrected})}{\eta(F)(\text{corrected for viscous heat})} \\ VHD &= \frac{\eta(D)(\text{uncorrected})}{\eta(D)(\text{corrected for viscous heat}).} \end{aligned}\right\} \quad (1$$

(3) The results from the cross flow corrections of Appendix III were empirically correlated with DR as:

$$\left.\begin{aligned} CFF &= \frac{\eta(F)(\text{uncorrected})}{\eta(F)(\text{corrected for cross flow})} \\ CFD &= \frac{\eta(D)(\text{uncorrected})}{\eta(D)(\text{corrected for cross flow}).} \end{aligned}\right\} \quad (1$$

Computational Steps

(1) It is assumed that the temperature rises faster at higher blade loads and the temperature at each step, t(J), is assumed to be given by:

$$t(J) = t_i + (t_f - t_i)\ (\frac{J-1}{JJ-1})^2. \qquad (\quad)$$

(2) The first three values of $\underline{X}$ are corrected for a reversible decrease in $\underline{X}_o$ according to the formula:

$$\left.\begin{aligned} X(1)_{corrected} &= X(1) - V_o/250 \\ X(2)_{corrected} &= X(2) - V_o/500 \\ X(3)_{corrected} &= X(3) - V_o/1000. \end{aligned}\right\} \qquad (\quad)$$

The measure of roll drag, $\underline{DX}$, is:

$$DX(J) = X(J) - X_o. \qquad (\quad)$$

(3) All dial indicator readings, $\underline{R}_o'$ and $\underline{R}(\underline{J})$, $\underline{J} = 1, \underline{JJ}$, are corrected for blade load to a common load, $\underline{F} = 50$, according to the procedure given in Appendix V.

(4) The value of $\underline{R}$ for zero film thickness, $\underline{R}_o$, is obtained from $\underline{R}(\underline{JJ})$ and $\underline{R}_o'$. It is assumed that $\eta(\underline{F})$ has a common value at film thicknesses $\underline{DR}(\underline{JJ}) = \underline{R}(\underline{JJ}) - \underline{R}_o$ and $\underline{DR}' = \underline{R}_o' - \underline{R}_o$. For an assumed value of $\underline{R}_o$, $\underline{FF}$, $\underline{VHF}$, and $\underline{CFF}$ are obtained for $\underline{DR}(\underline{JJ})$ and $\underline{DR}'$ from the subroutines. The resulting viscosities are

$$\eta(F)_{DR(JJ)} = \frac{F(JJ)}{FF_{DR(JJ)} * V_o} * VHF_{DR(JJ)} * CFF_{DR(JJ)} \qquad (\quad)$$

$$\eta(F)_{DR'} = \frac{F(JJ)}{FF_{DR'} * V_o/4} * VHF_{DR'} * CFF_{DR'}. \qquad (\quad)$$

The value of $\underline{R}_o$ is altered until the two calculated viscosities are acceptably close.

(5) Film thickness values, $\underline{DR}(\underline{J})$, are:

$$DR(J) = R(J) - R_o. \qquad (\quad)$$

(6) The estimates of maximum shear rate, Γ, are:

$$\Gamma(J) = V_o/DR(J). \tag{19}$$

(7) The derived viscosity values $\eta(\underline{F})$ and $\eta(\underline{D})$ are determined. From the subroutines, FF, DD, VHF, VHD, CFF, and CFD are obtained for each point. The viscosities are given by:

$$\eta(F)(J) = \frac{F(J)}{FF(J)*V_o} * VHF(J) * CFF(J), J = 1,JJ \tag{20}$$

$$\eta(D)(J) = \frac{DX(J)}{DD(J)*V_o} * VHD(J) * CFD(J), J = 1,JJ. \tag{21}$$

There is an element of trial and error involved in these calculations since viscous heating depends on the viscosity. Rapid convergence is obtained by setti VHF and VHD equal to one for a first trial, using the resulting viscosities for an estimate of VHF and VHD, and repeating the procedure a few times using succeed values of $\eta(\underline{F})$ and $\eta(\underline{D})$.

(8) For coatings, the exponent $\underline{N}$ is not known until the results are obtained. To facilitate trial and error determination of $\underline{N}$, it is desirable to calculate apparent $\underline{N}$ values from both $\eta(\underline{F})$ and $\eta(\underline{D})$. To do this, the viscosity results are corrected to a common temperature by:

$$\eta(30°) = \eta(t) * \exp[-\beta*(30°-t)]. \tag{22}$$

The exponent $\underline{N}$ is then determined by the log-log slope of η vs. Γ, using a least squares technique. To avoid points that are obviously erroneous, the first two points, $\underline{J} = 1,2$, are not used in evaluating $\underline{N}$.

RANDOM ERROR IN THE NEWTONIAN FLUID RESULTS

INTRODUCTION

Knowledge of random error of measurement is always important in describing physical phenomena. It is of particular importance in this work because the evolution of a technique for describing fluid properties is at least as important as the experimental results. The analysis of random error is one way of indicating how the techniques of measurement can be improved.

MEASUREMENTS MADE: QUALITATIVE COMMENTS

(1) The glycerin concentration in the glycerin-water mixtures. These values were determined from carefully determined viscosity values and are not considered subject to significant error. During long experiments, changes in concentration were determined by repeat samplings.

(2) Temperatures of the fluid were taken at the start (t_i) and the end (t_f) of each run. These temperatures were measured at the overflow from the blades and are not considered important sources of error. In the case of large temperature changes during a run (up to the order of 3°C.) the presumed time-temperature relationship could lead to some uncertainty, but in general fluid temperature measurement is not considered a problem.

(3) The roll surface velocity, V_o (ft./min.), is measured with a tackometer and is not considered a significant source of error.

(4) The normal force applied to the blades is given as F, with the force in lb. equal to $F/1.056$. These values are considered unlikely to significantly contribute to error, and later evidence qualitatively supports this contention.

(5) Roll drag is measured as $\underline{DX} = \underline{X}-\underline{X}_o$, with the drag in lb. being $\underline{DX}/32.0$. $\underline{X}$ is a measure of power input to the drive motor and $\underline{X}_o$ is the value of $\underline{X}$ at infinite film thickness (i.e., no roll drag by the fluid). Both $\underline{X}$ and $\underline{X}_o$ are considered possible sources of random error, either measurement error or true physical variance, or both.

(6) Film thickness under the blade tip is given by $\underline{DR} = \underline{R}-\underline{R}_o$, with the units being film thickness in cm. equal to $\underline{DR}/16070$. Both $\underline{R}$ and $\underline{R}_o$ are considered possible sources of random error, either due to measurement error or true physical variance, or both.

(7) Two derived values are employed in the following discussions. The true fluid viscosity, η_o, is determined from the glycerin concentration and the temperature. The shear rate, $\Gamma(\text{sec.}^{-1})$, is the ratio of roll velocity to film thickness under the blade tip. Obviously, the shear rate varies through the nip and Γ is considered to be a fairly precise measure of the maximum shear rate.

RANDOM ERROR IN $\underline{DR}$

Calculated Random Error in $\underline{DR}$

Consider plots of $\underline{DR}$ vs. η_o, with $\underline{F}$ and $\underline{V}_o$ as parameters, in Fig. 5. Two things are obvious: there is a dependence of $\underline{DR}$ on η_o, and there is random scatter in the data. It is desired to estimate error (scatter) in the data after removal of the $\underline{DR}$-η_o dependence. Each set of data is fit by a straight line or a quadratic curve using the least squares technique. If the second-order coefficie in the quadratic equation is statistically significant, that equation is consider as the best fit of the data; if not, then the straight line is considered the bes fit. The best lines, and their equations, are shown in Fig. 5.

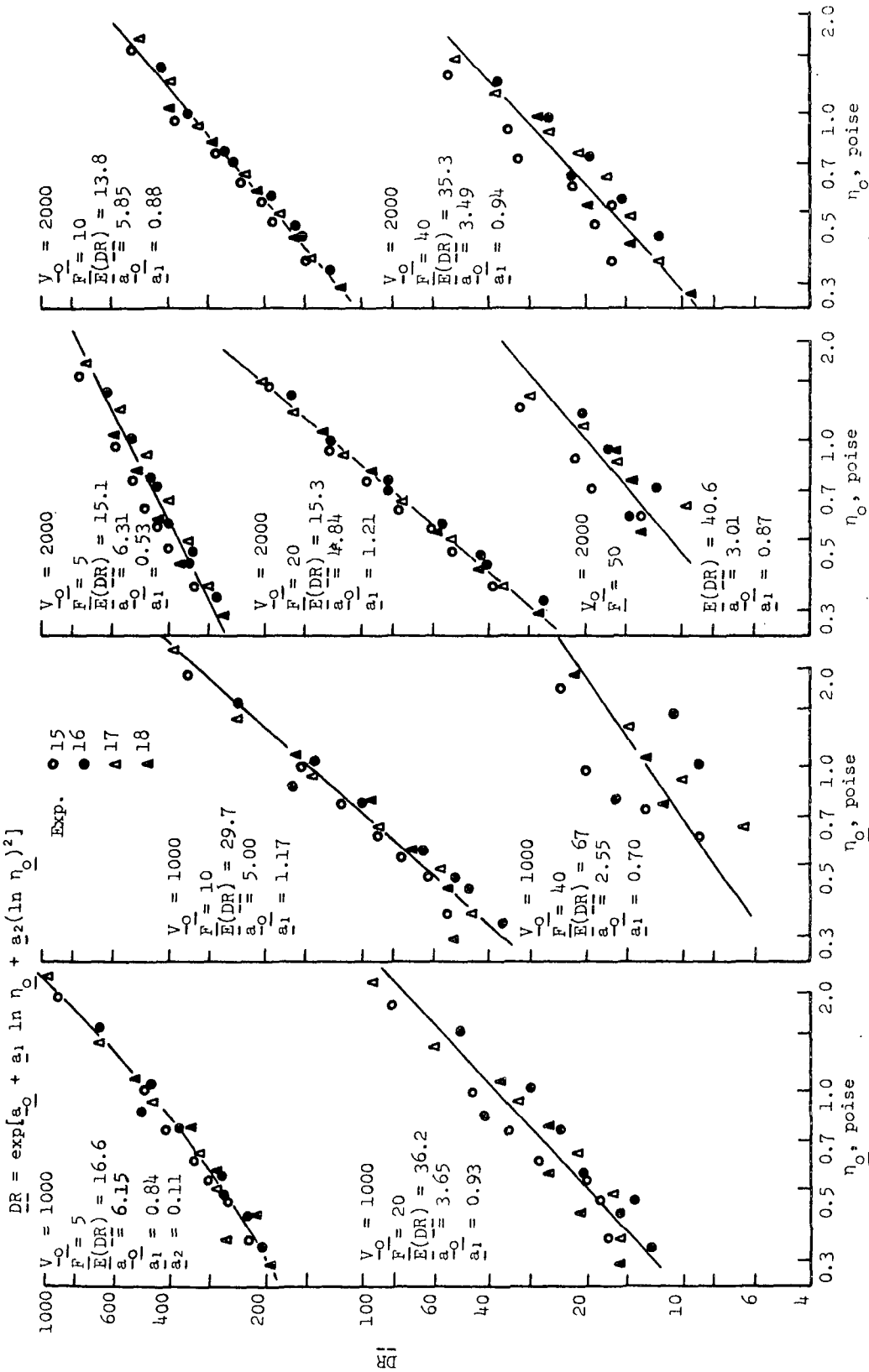

Figure 5. DR as a Function of Newtonian Viscosity, with F and V_0 Parameters

Scatter in the data may be due to error in $\underline{DR}$, η_o, $\underline{V_o}$, $\underline{F}$, or to interactions. It was indicated in previous discussion that, of these four, $\underline{DR}$ is the predominant source of error and the analysis proceeds on the assumption that all scatter is due to $\underline{DR}$. The residual sums of squares ($\underline{RSS}$) about a line is considered to be a measure of variance of the data unexplained by the $\underline{DR}$-η_o correlation. A measure of confidence in the data is assumed to be given by the standard formula:

$$\text{C.I.} = \text{confidence interval} = \pm t_{n,0.975}\sqrt{RSS/n} \tag{23}$$

in which $t_{n,0.975}$ is the usual student $\underline{t}$ at 95% confidence and $\underline{n}$ is the number of data points minus the number of coefficients in the line through the data.

Since the data in Fig. 5 (and all other data in this discussion) are on a log-log plot, the confidence interval in $\underline{DR}$ is:

$$DR(\text{predicted})*\exp(\pm\ \text{C.I.}). \tag{24}$$

The error is expressed in percent variation from the predicted value. Up to quit large values of $\underline{C.I.}$, the average percent error is given by $100*\underline{C.I.}$ For example if $\underline{C.I.}$ is 0.5:

$$\text{change (increase)} = 65\%$$
$$\text{change (decrease)} = 39\%$$
$$\text{change (average)} = 52\% .$$

Thus, by definition, error in $\underline{DR}$ is considered for each set of data to be:

$$E(DR) = 100*\text{C.I.} \tag{25}$$

The error E(DR) is not assigned to any particular part of a set of data but is considered an average for all the data. Thus, E(DR) for a given set of data is presumed to be the percent deviation from a predicted value DR which, on the average, will enclose 95% of the data.

Error Between Experiments

The plots of Fig. 5 are composed of results from four experiments. Using standard statistical techniques, tests were made to determine if there is a significant difference between the experiments (12). The results are presented in Table II. It is apparent from the results that there is a noticeable difference for V_o = 1000 and a major difference for V_o = 2000.

TABLE II

COMPARISON OF DR VS. η_o PLOTS BETWEEN EXPERIMENTS

Key: V: Difference in variance between experiments
S: Difference in slopes between experiments
E: Difference in elevation between experiments
All determined at 95% confidence

Experiments	15/16	15/17	15/18	16/17	16/18	17/18
F			V_o = 1000			
5		V	E			
10	E		V		S	S
20	E		S			S
F			V_o = 2000			
5	E	E	V/E		E	E
10	E	E			E	S
20	E	E	E		E	
40	E	E	E			

Also, tests were made to determine if random error could be reduced by ruling out changes between experiments, again using standard statistical techniques and a 95% confidence limit (12). The results, presented in Table III, show that there would be little if any reduction in random error for V_o = 1000, but a significant improvement for V_o = 2000.

Random Error in Reading the Dial Indicator

Vibration or short-time wander in readings is considered reading error. It is important to know how significant this is compared with the overall error in the results. If significant, reading error can be improved; e.g., by electronic damping. In Experiment 27, the effect of feed rate of fluid to the blades was investigated. Duplicate readings at maximum feed rate were taken, with perhaps 30-60 sec. between readings. The results of changes in DR are given in Table IV. These changes are presumed to be due to reading error plus true changes in DR over the time period. Comparison of the results of Table IV with the E(DR) results given in Fig. 5 leads to the conclusion that dial reading error is not a major source contributing to random DR error, E(DR).

Random Error in Determining R_o

The dial indicator value for zero gap between blade tip and roll, R_o, is calculated from values recorded at maximum blade load and velocity equal to V_o and $V_o/4$. One value of R_o is used for all points in a given run. A correction for the effect of blade load on R_o is given in Appendix V.

The best test of random variation in R_o is plots of R_o vs. run number, given in Fig. 6 for three experiments. The change in R_o between runs is a potential source of small systematic error in the results. The deviation of R_o values from smooth progression of the changes is considered evidence of random

TABLE III

TEST OF DIFFERENCE BETWEEN COMBINED DR ERROR AND EXPERIMENT AND POOLED VALUES

Experiment	E(DR)	Different from Combined
V_o = 1000, F = 5		
15	11.2	No
16	20.2	No
17	30.1	No
18	22.3	No
Pooled	16.5	No
Combined	16.6	--
V_o = 1000, F = 10		
15	17.2	Yes
16	35.5	No
17	19.2	No
18	21.9	No
Pooled	21.3	No
Combined	29.7	--
V_o = 1000, F = 20		
15	26.7	No
16	44.2	No
17	40.4	No
18	28.1	No
Pooled	29.6	No
Combined	36.2	--

Experiment	E(DR)	Different from Combined
V_o = 2000, F = 5		
15	5.2	Yes
16	6.8	Yes
17	3.8	Yes
18	15.2	No
Pooled	6.0	Yes
Combined	15.1	--
V_o = 2000, F = 10		
15	13.6	No
16	8.6	No
17	10.2	No
18	13.4	No
Pooled	8.9	Yes
Combined	13.8	--
V_o = 2000, F = 20		
15	12.5	No
16	15.2	No
17	13.5	No
18	7.5	Yes
Pooled	10.6	Yes
Combined	15.3	--
V_o = 2000, F = 40		
15	36.0	No
16	30.1	No
17	14.0	Yes
18	36.7	No
Pooled	24.0	No
Combined	35.3	--

TABLE IV

"SHORT TIME" CHANGES IN DR VALUES

V_o	F	DR (av.)	Δ(DR)	% Change
	Fluid 271, $\eta_o \sim 1.4$			
1000	20	46	0	0
2000	5	555	12	2
1000	3	770	15	2
2000	50	22	3	14
1000	10	118	2	2
2000	30	48	1	2
1000	50	5	0	0
2000	10	321	2	1
1000	5	400	5	1
2000	20	108	9	8
1000	30	16	0	0
2000	3	560	4	1
	Fluid 272, $\eta_o \sim 0.7$			
1000	20	22	1	5
2000	5	390	0	0
1000	3	445	2	0
2000	40	20	1	5

V_o	F	DR (av.)	Δ(DR)	% Change
	Fluid 272, $\eta_o \sim 0.7$			
1000	10	62	0	0
2000	10	180	10	6
1000	30	14	0	0
2000	20	55	0	0
1000	5	209	0	0
2000	3	413	2	0
	Fluid 273, $\eta_o \sim 0.17$			
1000	5	54	2	4
2000	30	8	1	13
1000	20	8	0	0
2000	5	146	5	3
1000	3	134	7	5
2000	10	57	2	4
1000	10	20	0	0
2000	3	225	2	1

error. Such evidence is generally lacking in the results shown. A careful examination of the data in Fig. 5 indicates that those points in Fig. 6 which show jumps in continuity do not correspond to especially large errors in DR.

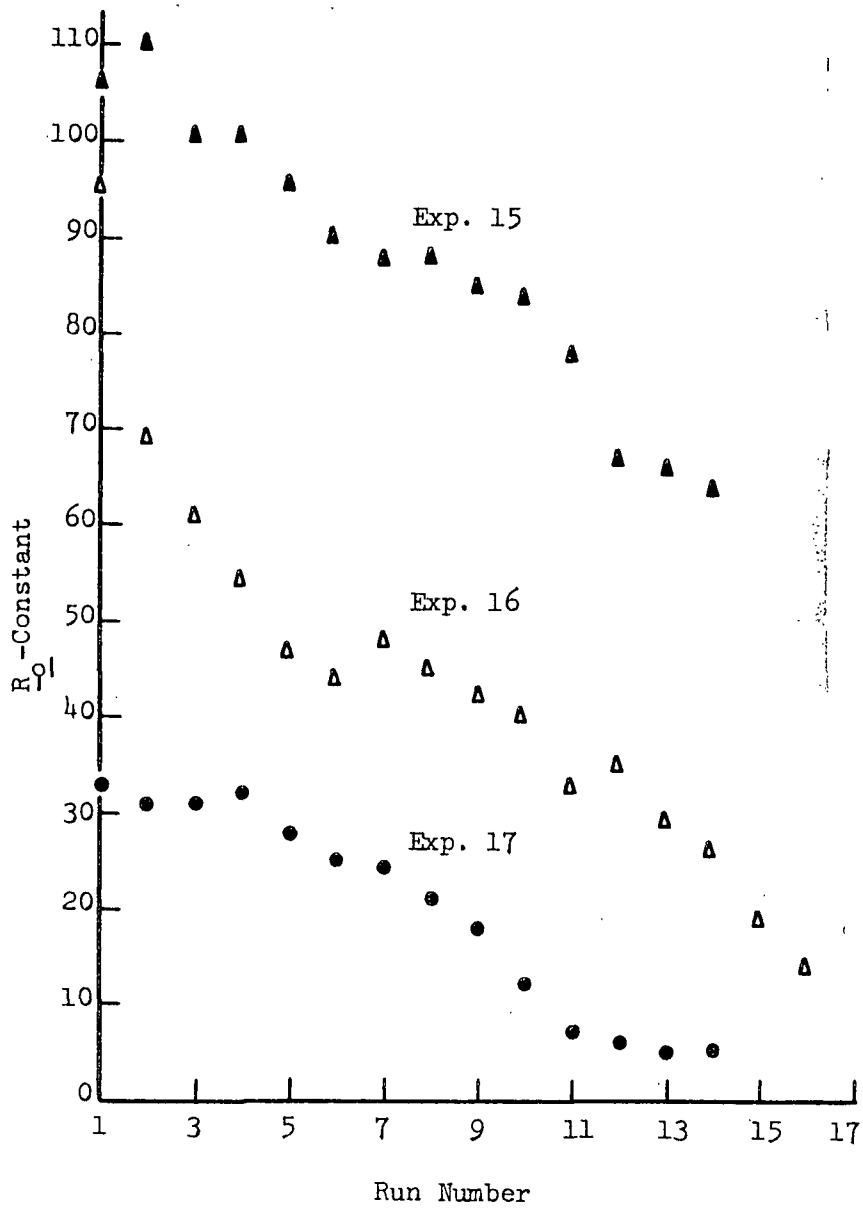

Figure 6. Change of Dial Indicator Zero Reading with Run Number

Of course, where $\underline{DR}$ is small, e.g., values of 20 or less, even small random changes in $\underline{R}_o$ can be significant. Another test was made in Experiments 15 and 16. At the end of each run, repeat measurements were made of $\underline{R}(\underline{F}_{max},\underline{V}_o)$ and $\underline{R}(\underline{F}_{max},\underline{V}_o/4)$. The difference between the two values changed by zero units 14 times, by one unit 8 times, and by two units twice. The change is quite small compared with the error values given in Fig. 5 for large values of $\underline{F}$.

Conclusion

Error in $\underline{DR}$ is in large part due to real physical variance caused by reasons unknown. The contribution of reading error is considered small.

RANDOM ERROR IN $\underline{DX}$

Calculated Error in $\underline{DX}$

In Fig. 7, $\underline{DX}$ is plotted vs. η_o, with $\underline{F}$ and $\underline{V}_o$ as parameters. In the manner discussed above, random percent error in $\underline{DX}$, $\underline{E}(\underline{DX})$, was determined and the results are given in Fig. 7.

Random Error in Reading $\underline{X}$

There was no noticeable rapid vibration of the voltmeter needle in measuring $\underline{X}$ values. A small amount of reading variation over the short term was generally observed, generally of the order of ±1 unit. This is not considered sufficient to be the major source of error in $\underline{DX}$.

The Problem of Determining $\underline{X}_o$

There is generally a reduction in $\underline{X}_o$ during an experiment, presumably due to heating of the bearings. This reduction is particularly marked during the first few runs of an experiment. Consider the values given in Table V. Due to the time change in $\underline{X}_o$ and the additional random variation in values, it is concluded that part, but not all, of $\underline{E}(\underline{DX})$, is due to random variation in $\underline{X}_o$.

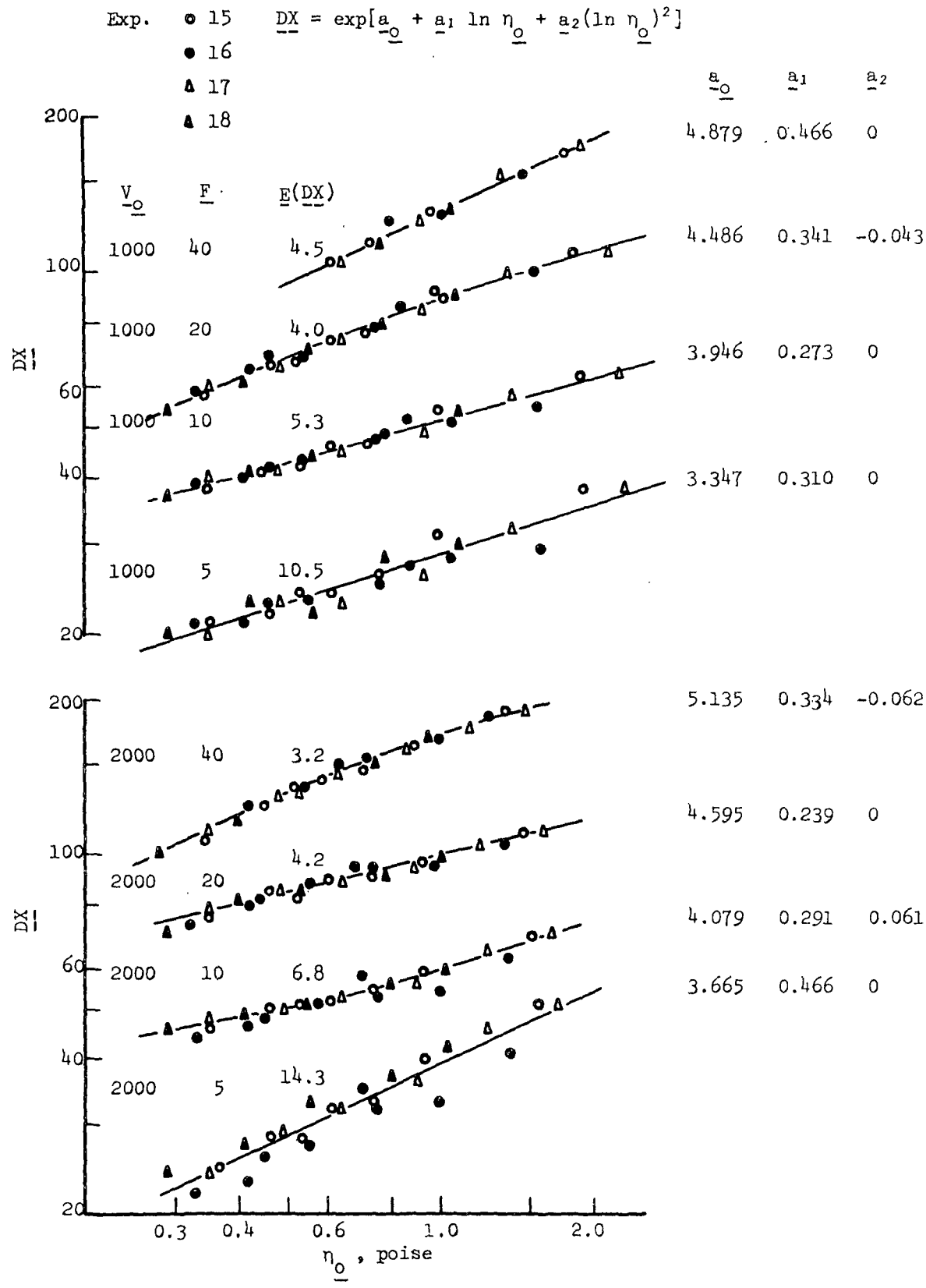

Figure 7. DX as a Function of Newtonian Viscosity, with F and V_o Parameters

TABLE V

CHANGE OF $\underline{X}_o$ WITH RUN NUMBER

Experiment 15				Experiment 16				Experiment 17			
$\underline{V}_o$ = 1000		$\underline{V}_o$ = 2000		$\underline{V}_o$ = 1000		$\underline{V}_o$ = 2000		$\underline{V}_o$ = 1000		$\underline{V}_o$ = 2000	
No.	$\underline{X}_o$	No.	$\underline{X}_o$	No.	$\underline{X}_o$	No.	$\underline{X}_o$	No.	$\underline{X}_o$	No.	$\underline{X}_o$
1	157	2	173	1	147	2	172	1	143	2	167
3	144	4	168	3	145	4	172	3	138	4	163
5	142	6	163	5	143	6	171	5	137	6	163
7	139	8	163	7	141	8	167	7	137	8	163
9	139	10	163	9	137	10	167	9	137	10	164
11	139	12	162	11	138	12	163	11	137	12	164
13	137	14	163	13	138	14	163				
				15	137	16	165				

In the usual experimental procedure, $\underline{X}_o$ is measured at the end of a run and, due to a reversible change in $\underline{X}_o$ during a run, the first three values of $\underline{X}$ are corrected. In Experiments 15 and 16, $\underline{X}_o$ was measured at the start of each run as well as at the end, with the first value of $\underline{F}$ being five in each case. To determine how much reduction in $\underline{E}(\underline{DR})$ might be possible for the first point, the error analysis was carried out using both $\underline{X}_o$ determinations. The results are given in Table VI. It is apparent that in future work it would be an advantage to measure $\underline{X}_o$ at the start and end of each run.

TABLE VI

EFFECT OF X_o MEASUREMENT ON DX ERROR

Experiments 15 and 16 Only

$\Gamma = 5$

V_o	1000	2000
	E(DX)	
X_o measured at end of run	11.8	15.9
X_o measured at start of run	9.7	12.5

RANDOM ERROR IN CALCULATED VISCOSITY VALUES

Viscosities determined from blade lift, $\eta(F)$, and from roll drag, $\eta(D)$, are presented in Fig. 8 as $\eta(F)/\eta_o$ and $\eta(D)/\eta_o$ vs. η_o, with V_o and Γ as parameters. An error analysis similar to that discussed above was used to determine percent error in the viscosity values, with the results being given on the figure.

The dotted curves enveloping the least squares line through each set of points are the locus of confidence intervals for predicted values of $\eta(F)/\eta_o$ and $\eta(D)/\eta_o$. That is, they give the limits of confidence that a point on the line is a true value. These values are at 95% confidence and were determined by standard statistical techniques (12).

APPLICATION OF DR AND DX ERROR TO THE VISCOSITY RESULTS

In order to assign E(DR) and E(DX) values to the viscosity curves of Fig. 8, each set of results must be characterized by a representative value of η_o. This is done by assuming that the midpoint value of η_o, $\bar{\eta}_o$, characterizes

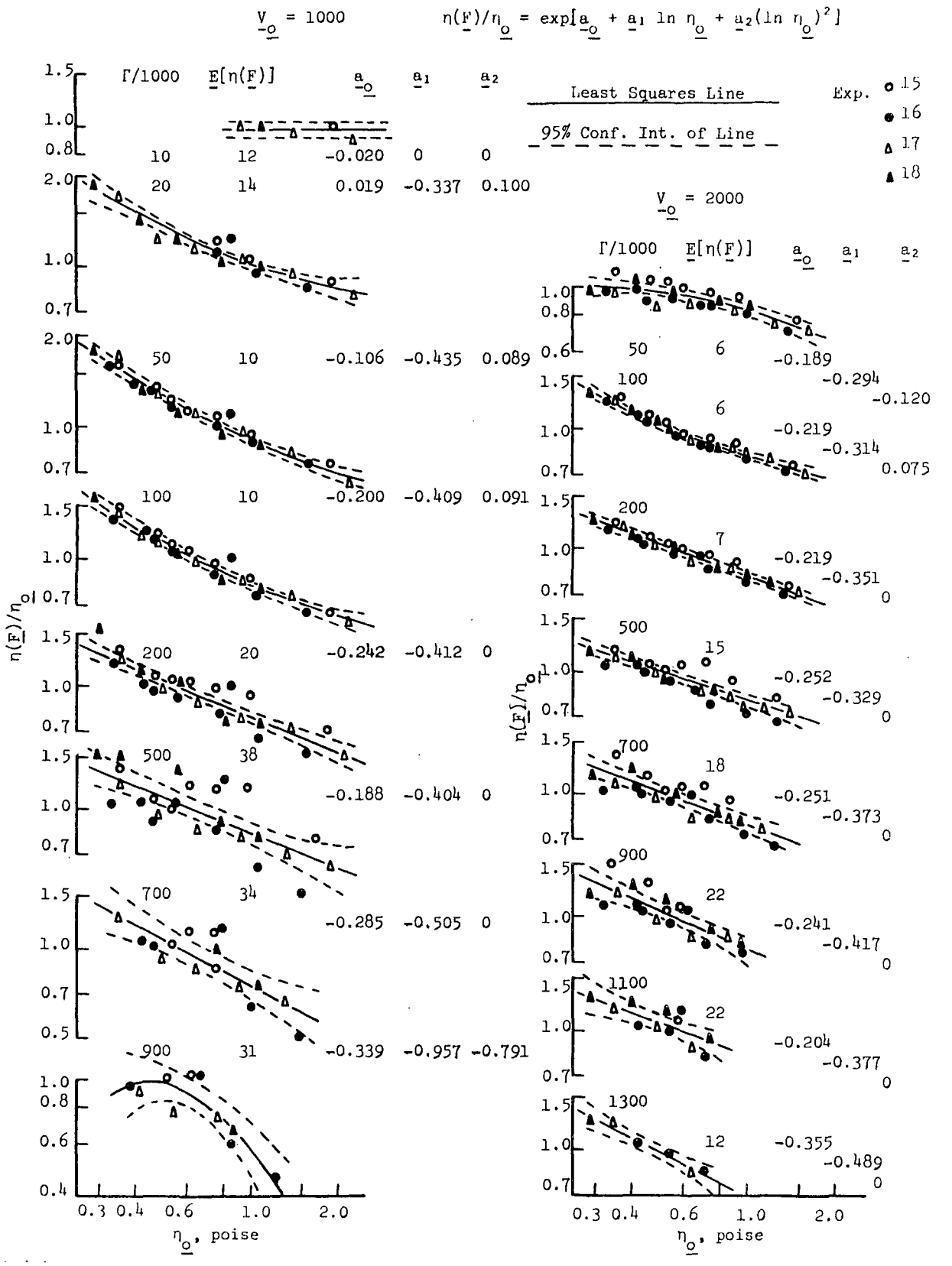

Figure 8. Experimental vs. True Viscosity for Glycerin

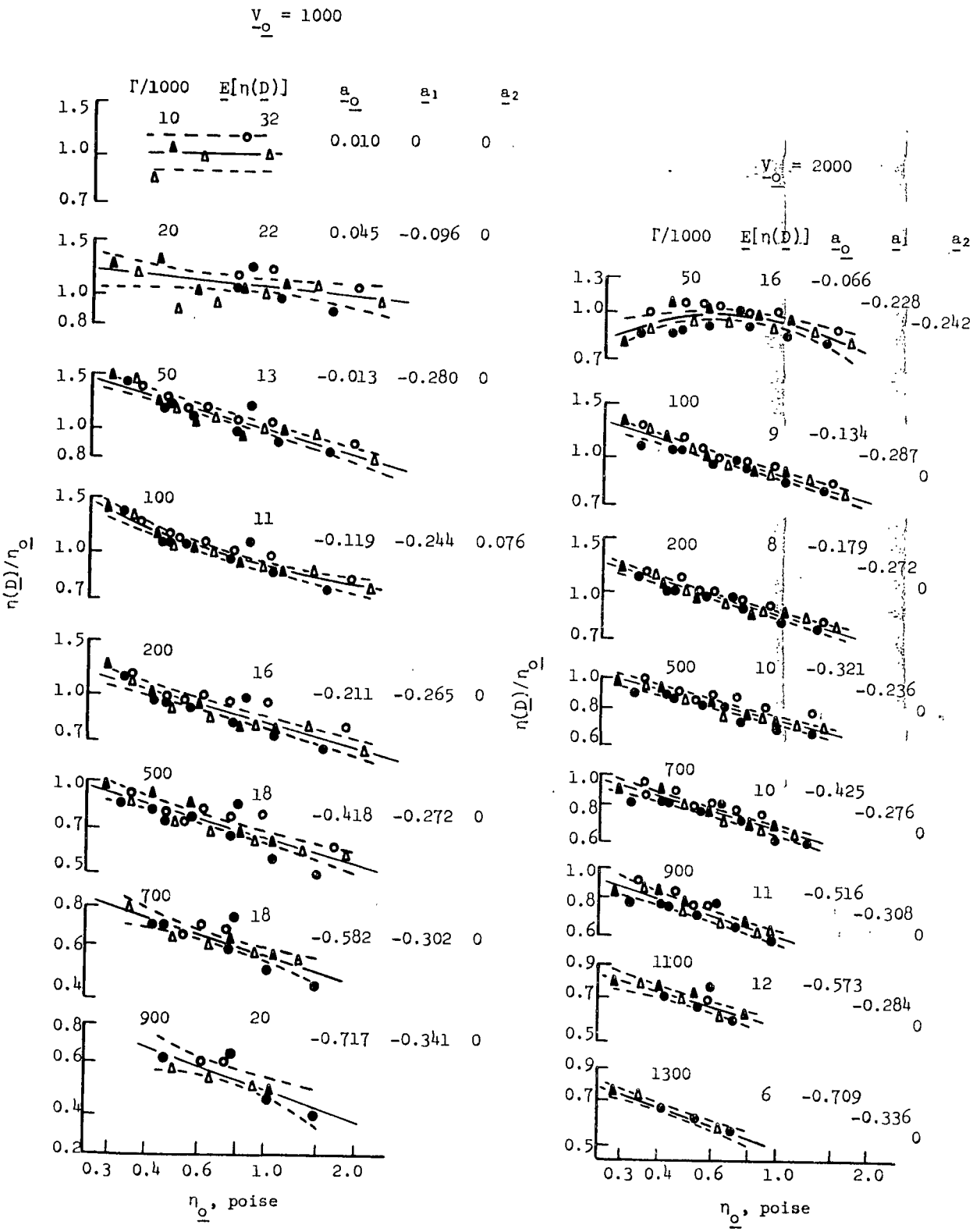

Figure 8 (cont'd). Experimental vs. True Viscosity for Glycerin

each set of points. The corresponding values of E(DR) and E(DX) are taken from Fig. 9. These results are given in Table VII.

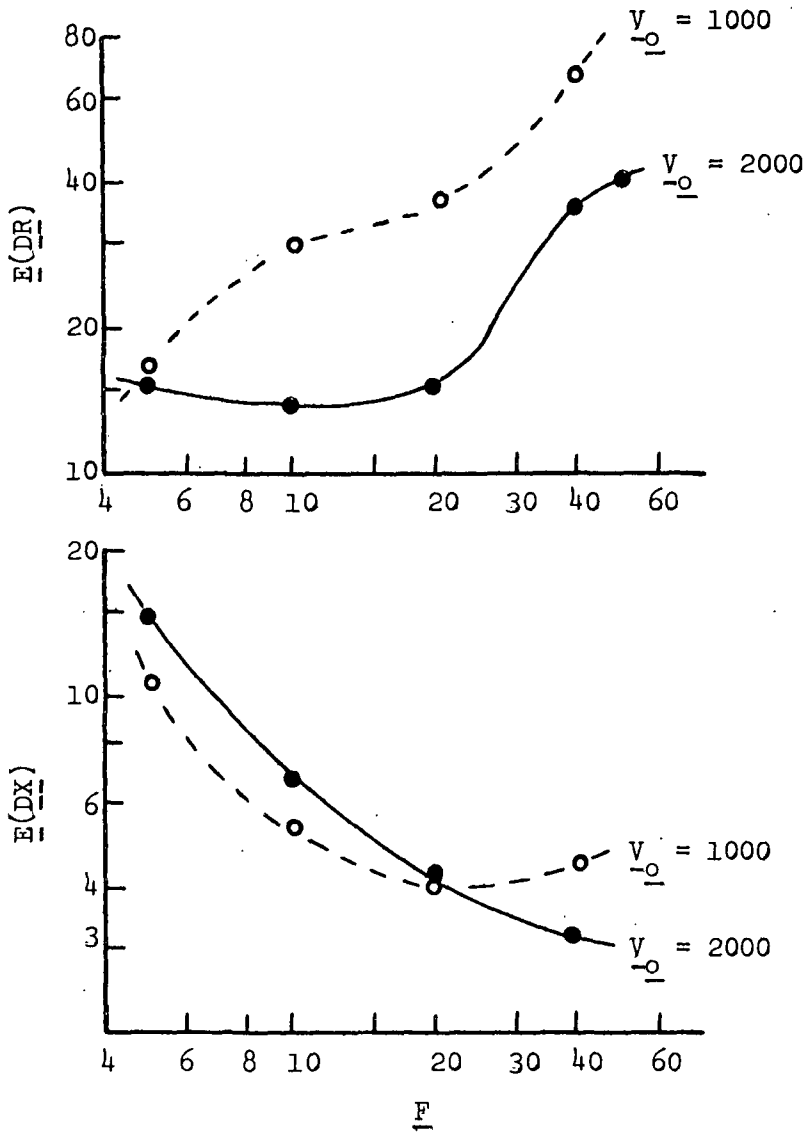

Figure 9. Random Errors (Percent) in DR and DX as Functions of F

Since DX/[η(D)*V_o] is virtually a unique function of DR, there is a direct 1:1 application of E(DX) to E[η(D)].

TABLE VII

PREDICTED AND ACTUAL RANDOM ERRORS IN VISCOSITIES

Γ/1000	$\underline{DR}$	$\bar{\eta}_o$	$\bar{F}$	$E(\underline{DR})$[a]	$E[\eta(\underline{F})/\underline{DR}]$	$E[\eta(\underline{D})/\underline{DR}]$	$E(\underline{DX})$[a]	$E[\eta(\underline{F})]$		$E[\eta(\underline{D})]$	
								Predicted	Actual	Predicted	Actual
					V_o = 1000 ft./min.						
10	820.0	1.40	3.8	11(90)	1.10	0.85	14(4)	12	12	17	32
20	410.0	0.82	4.8	16(66)	0.77	0.76	11(3)	12	14	16	22
50	164.0	0.62	7.3	25(41)	0.49	0.43	7(2)	12	10	13	13
100	82.0	0.62	10.3	30(25)	0.48	0.39	5(2)	14	10	13	11
200	41.0	0.62	14.3	31(13)	0.56	0.39	5(3)	17	20	13	16
500	16.4	0.26	26.0	44(7)	0.80	0.40	4(3)	35	38	18	18
700	11.7	0.76	34.4	58(7)	0.70	0.30	4(4)	41	34	18	18
900	9.1	0.76	43.5	73(7)	0.50	0.22	5(6)	36	31	17	20
					V_o = 2000 ft./min.						
50	328.0	0.60	7.2	14(46)	1.03	0.86	10(4)	14	6	16	16
100	164.0	0.60	12.0	14(23)	0.63	0.53	6(4)	9	6	9	9
200	82.0	0.60	18.7	15(12)	0.52	0.40	4(3)	8	7	7	8
500	32.8	0.60	29.1	22(7)	0.56	0.37	4(5)	12	15	9	10
700	23.4	0.60	34.7	30(7)	0.66	0.38	3(4)	19	18	11	10
900	18.2	0.52	38.3	34(6)	0.69	0.35	3(4)	23	22	12	11
1100	14.9	0.52	42.1	37(6)	0.70	0.28	3(4)	26	22	10	12
1300	12.6	0.52	45.4	39(5)	0.73	0.27	3(4)	29	12	11	6

[a] Error is normally reported as percent. The values in parentheses are in $\underline{DR}$ and $\underline{DX}$ units.

The application of $\underline{E}(\underline{DR})$ to the viscosity results is more complicated, and it was decided that the best means of determining the effect was to simulate $\underline{E}(\underline{DR})$. A variation of ±10% in $\underline{DR}$ was applied to all the experimental results. The resulting changes in viscosities at each set of parameters was determined and the following conversion factors are defined:

$$\left.\begin{aligned} E[\eta(F)/DR] &= \text{Average}\left(\frac{\%\text{ change in }\eta(F)}{\%\text{ change in DR}}\right) \\ E[\eta(D)/DR] &= \text{Average}\left(\frac{\%\text{ change in }\eta(D)}{\%\text{ change in DR}}\right). \end{aligned}\right\} \tag{26}$$

Therefore,

$$\left.\begin{aligned} &\text{DR error applied to } \eta(F) = E(DR)*E[\eta(F)/DR] \\ &\text{DR error applied to } \eta(D) = E(DR)*E[\eta(D)/DR]. \end{aligned}\right\} \tag{27}$$

For $\eta(\underline{F})$ the only error contribution is from $\underline{E}(\underline{DR})$; for $\eta(\underline{D})$, both $\underline{E}(\underline{DR})$ and $\underline{E}(\underline{DX})$ contribute. Making the usual assumption that variances are additive:

$$E[\eta(D)]_{\text{predicted}} = \sqrt{E(DX)^2 + E(DR)^2*E[\eta(D)/DR]^2}. \tag{28}$$

The resulting predicted and actual viscosity errors are given in Table VII.

The effect of attributing error to $\underline{F}$ would be to reduce the error contributions of $\underline{DR}$ and $\underline{DX}$ at low shear rates in Table VII. The effect would be small at high shear rates. For both values of $\underline{V}_{\underline{o}}$, this would increase the differences between predicted and actual errors in the viscosities. It is concluded, therefore that error in measuring $\underline{F}$ is not significant.

Certain interesting results are evident from Table VII:

(1) With a few obvious exceptions, the predicted and actual errors in $\eta(\underline{F})$ and $\eta(\underline{D})$ are fairly close.

(2) At low shear rates the error in $\eta(\underline{D})$ is greater than that in $\eta(\underline{F})$, due mainly to the contribution of error in $\underline{DX}$.

(3) At high shear rates, error in $\eta(\underline{F})$ is greater than that in $\eta(\underline{D})$ due to the greater sensitivity of $\eta(\underline{F})$ to $\underline{DR}$.

(4) In general, the greatest source of error is that due to $\underline{DR}$.

(5) The random errors in $\underline{DR}$ and in the calculated viscosities are considerably less at $\underline{V_o}$ = 2000 than $\underline{V_o}$ = 1000.

GENERAL SUMMARY OF RANDOM ERROR ANALYSIS

The techniques used to measure blade lift, roll drag, and film thickness are generally acceptable. In order to significantly reduce random error in viscosity determinations, it will be necessary to better reproduce physical conditions in the system at the time of measurement. Four areas of improvement are recognized as possibilities in future work:

(1) A great deal of entrained air was generally observed at the top nip entrance. If a large portion of this air is carried through the nips it could lead to both random and systematic error. It would be preferable to have a closed system completely flooded with fluid.

(2) Flexibility was built into the Rheometer to enable changes to be made in blade position and angle of approach. As much as possible, the flexibility was "frozen" in and a given set of

conditions was used in the experiments; but even so there exists conditions which can lead to random changes in the blade-roll relative positions. In future work, a simpler means of applying the blades to the roll (or other moving surface) should be considered

(3) The blades are not in fact symmetric. Changes in stresses applied to the blade combination affect the effective stress applied to each blade differently. For example, a downward force on the blades has the tendency to push the top blade toward the roll more than the lower. Consideration should be given to applying the operating principle of the double blades, which has proven very successful, in a manner such that the blades are truly equivalent.

(4) There is considerable uncertainty concerning the variation of film thickness across the blades due to blade and/or roll tilt.

It is estimated that there is an uncertainty of the order of 0.002-0.003 cm. in relative horizontal positions between the edges of the blades from the value set when grinding the blades, due to physical changes in the machine during an experiment and between experiments.

It was seen in Fig. 6 that, over the course of an experiment, the roll can shift horizontally an amount of the order of 0.003 cm. If this movement in the roll bearings is comparable in the vertical direction and is different for the two sides (e.g., due to the belt drive on the back side of the machine), a roll tilt from one edge of the blades to the other of the order of 0.001 cm. could occur.

The change in film thickness under the blade tip from one edge to the other, δ, due to relative tilt, Δ, is given by:

$$\delta = 0.5\ \Delta\ 1/r = 0.137\ \Delta \qquad (29)$$

in which $\underline{l}$ is the vertical distance between blades and $\underline{r}$ is the roll radius. If then Δ is considered to be of the order of 0.002 cm. (= $32\underline{R}$ units), δ is of the order of $4\underline{R}$ units.

This degree of uncertainty in $\underline{DR}$ from one side of the blades to the other could certainly be a source of random error within or between experiments, especially at low values of $\underline{DR}$.

DISCUSSION OF THE NEWTONIAN RESULTS

EXPERIMENTAL RESULTS

Viscosity results taken from the curves of Fig. 8 are presented in Fig. 10. The parameter is the true fluid viscosity, η_o. The double points on the figure indicate the confidence limits of each value.

In beginning the discussion of these results, two experimental factors affecting the amount of fluid in the nip are considered: the effect of fluid feed rate to the nips, and the effect of a force imbalance on the blades.

THE EFFECT OF FLUID FEED RATE TO THE NIPS

Experiment 27 was designed to deal particularly with the effect of feed rate. With velocity, V_o, and blade load, F, held constant, the rate of fluid feed was altered by using the by-pass valve. The results of this experiment are presented in Fig. 11. The maximum flow rate in each case corresponds to the normal experimental operating condition.

In order to reduce the problem to more manageable proportions, the results of Fig. 11 are combined to give Fig. 12. Fifteen sets of results were obtained at each velocity. These were combined into two groups of three by ranking the film thickness values $\overline{DR}$. Each set of results was shifted up or down on the viscosity axis to a common point at a feed rate of 100 ml./sec., in order to produce comparable results for each set. It is only the change in viscosity that is important, not absolute values.

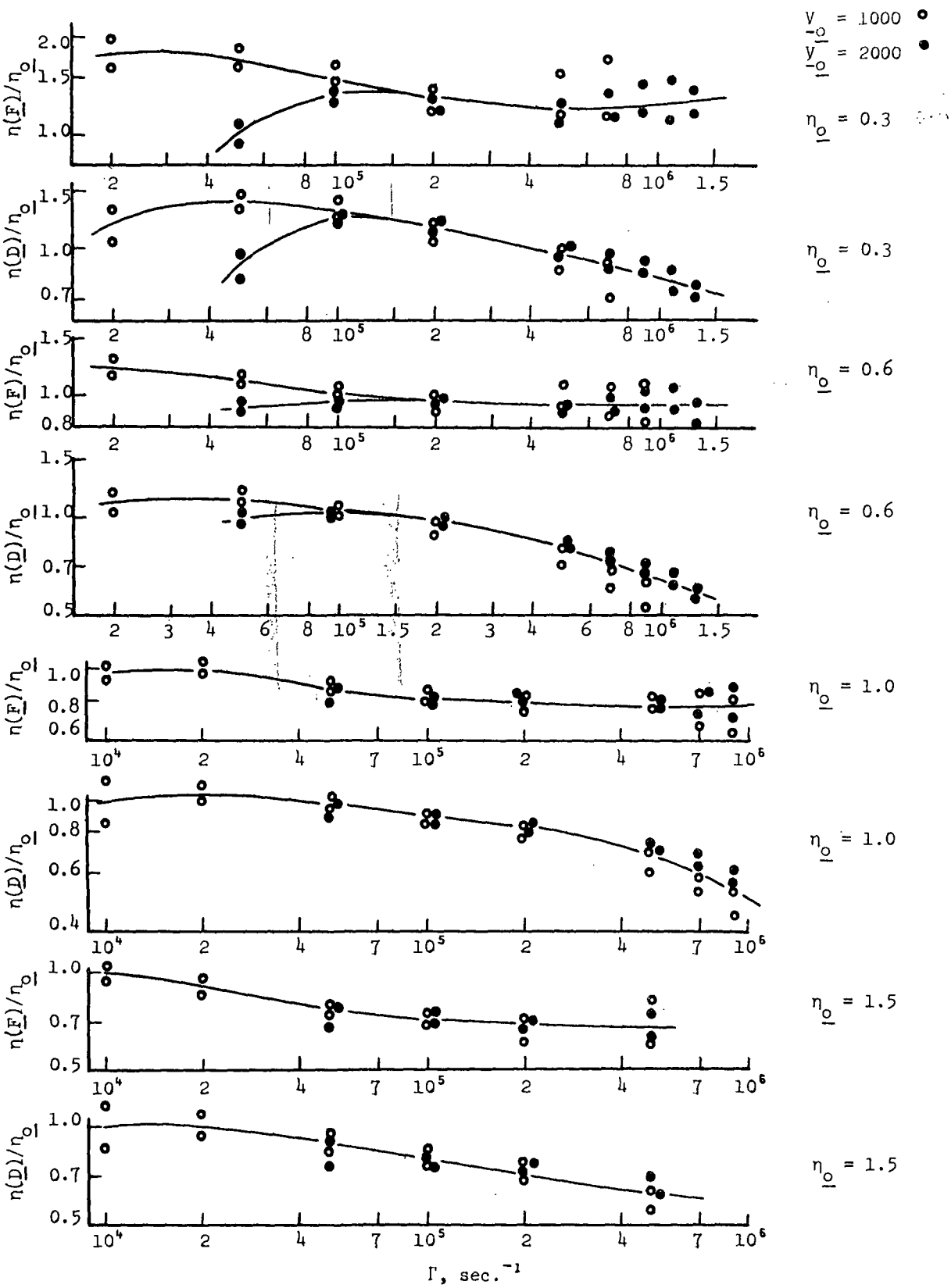

Figure 10. Viscosity vs. Shear Rate (Newtonian Fluids)

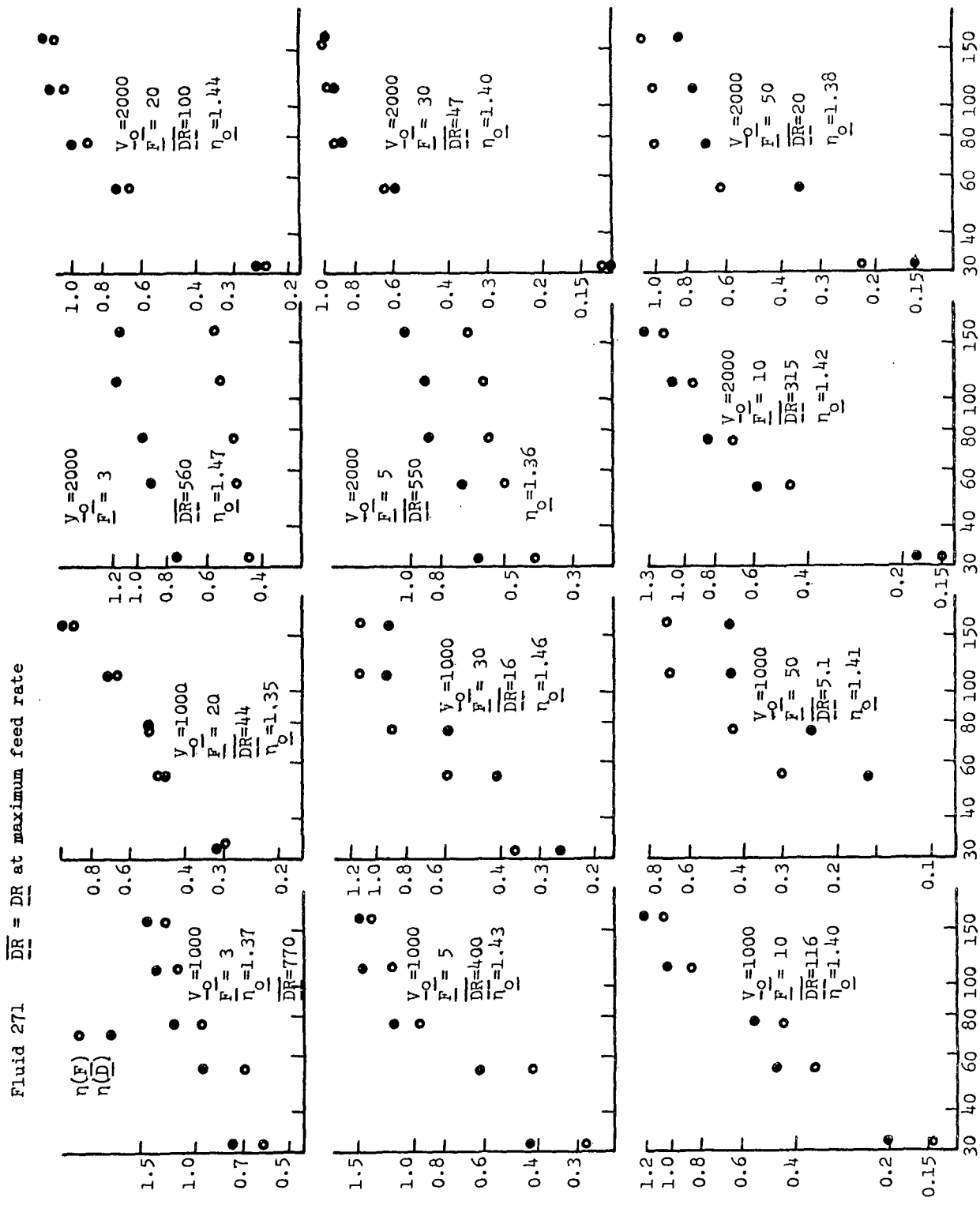

Figure 11. Effect of Feed Rate on Viscosity Results

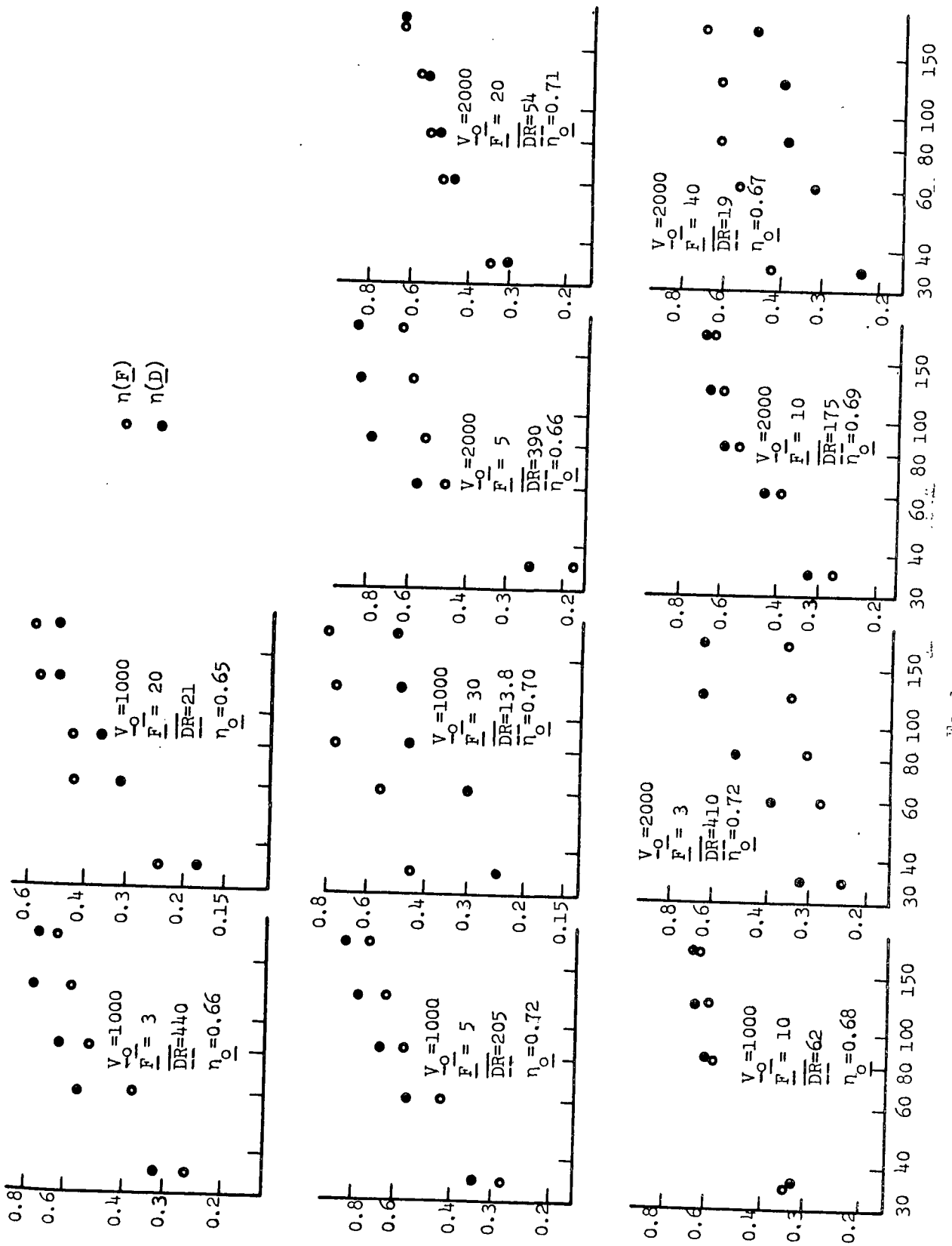

Figure 11 (cont'd). Effect of Feed Rate on Viscosity Results

Fluid 273 $\overline{DR}$ = DR at maximum feed rate

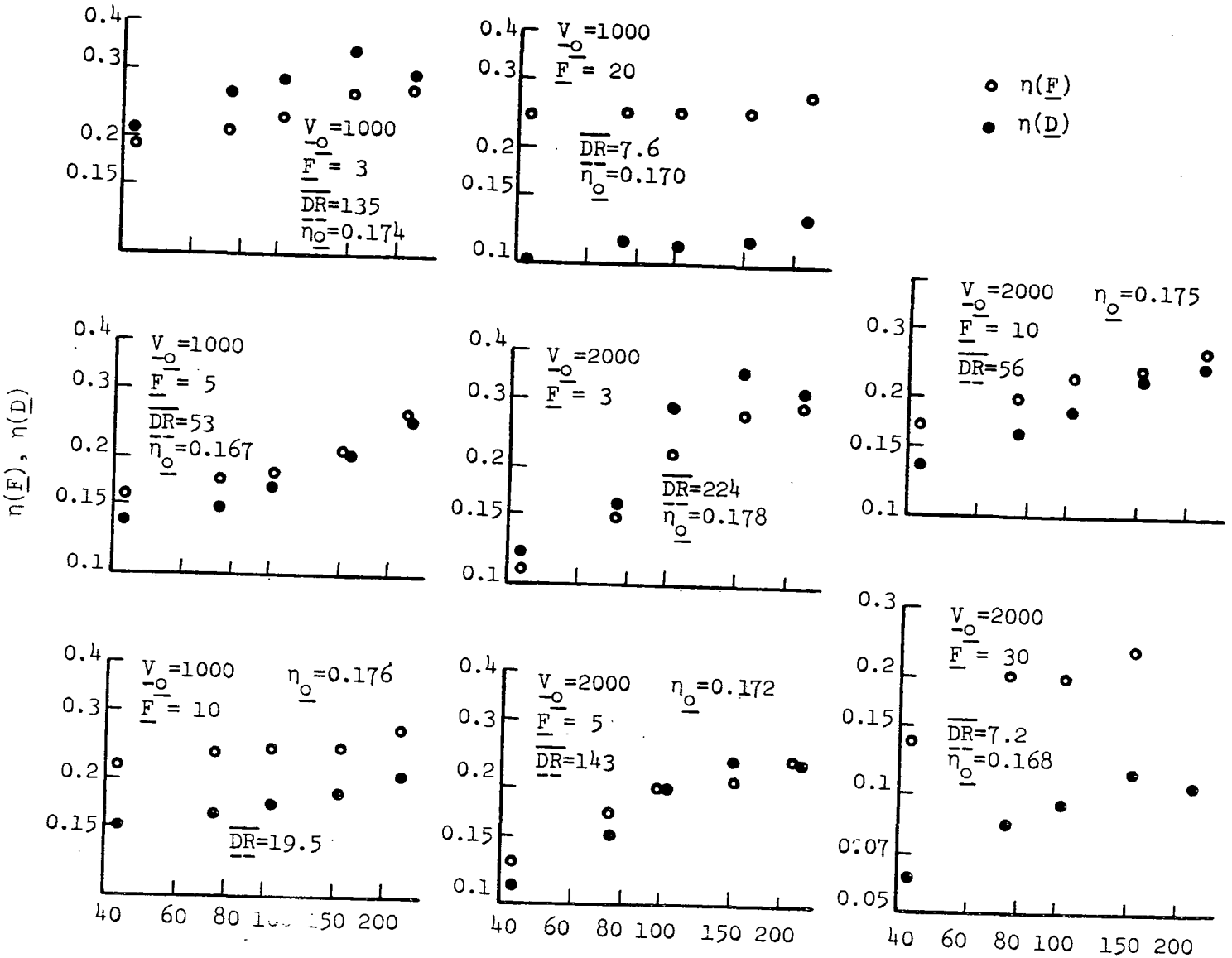

Figure 11 (cont'd). Effect of Feed Rate on Viscosity Results

$\underline{V}_o$ = 1000 O.F.R.: Optimum Feed Rate

——— Theoretical results based on median $\overline{DR}$ values

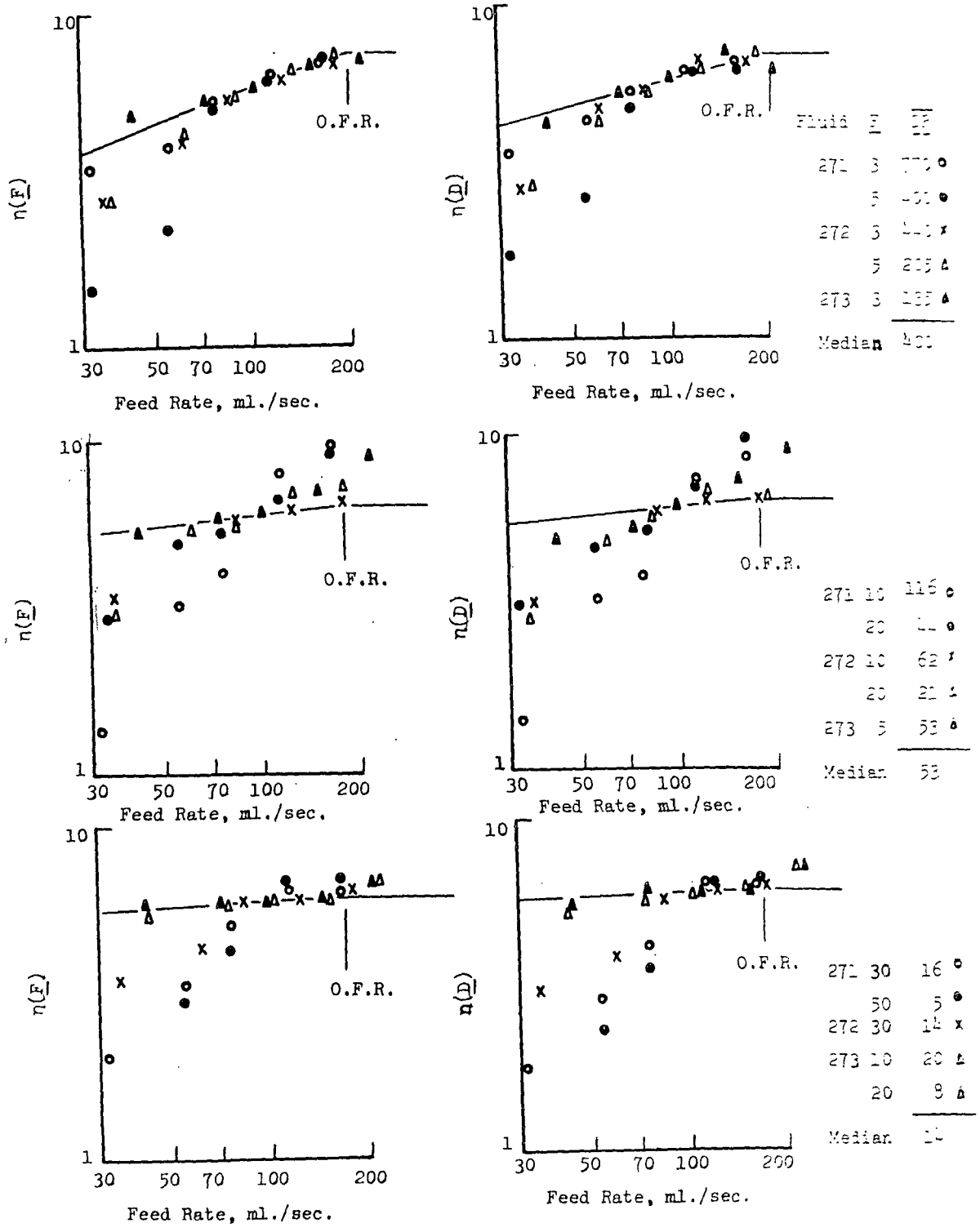

Figure 12. Composite Viscosity-Feed Rate Data

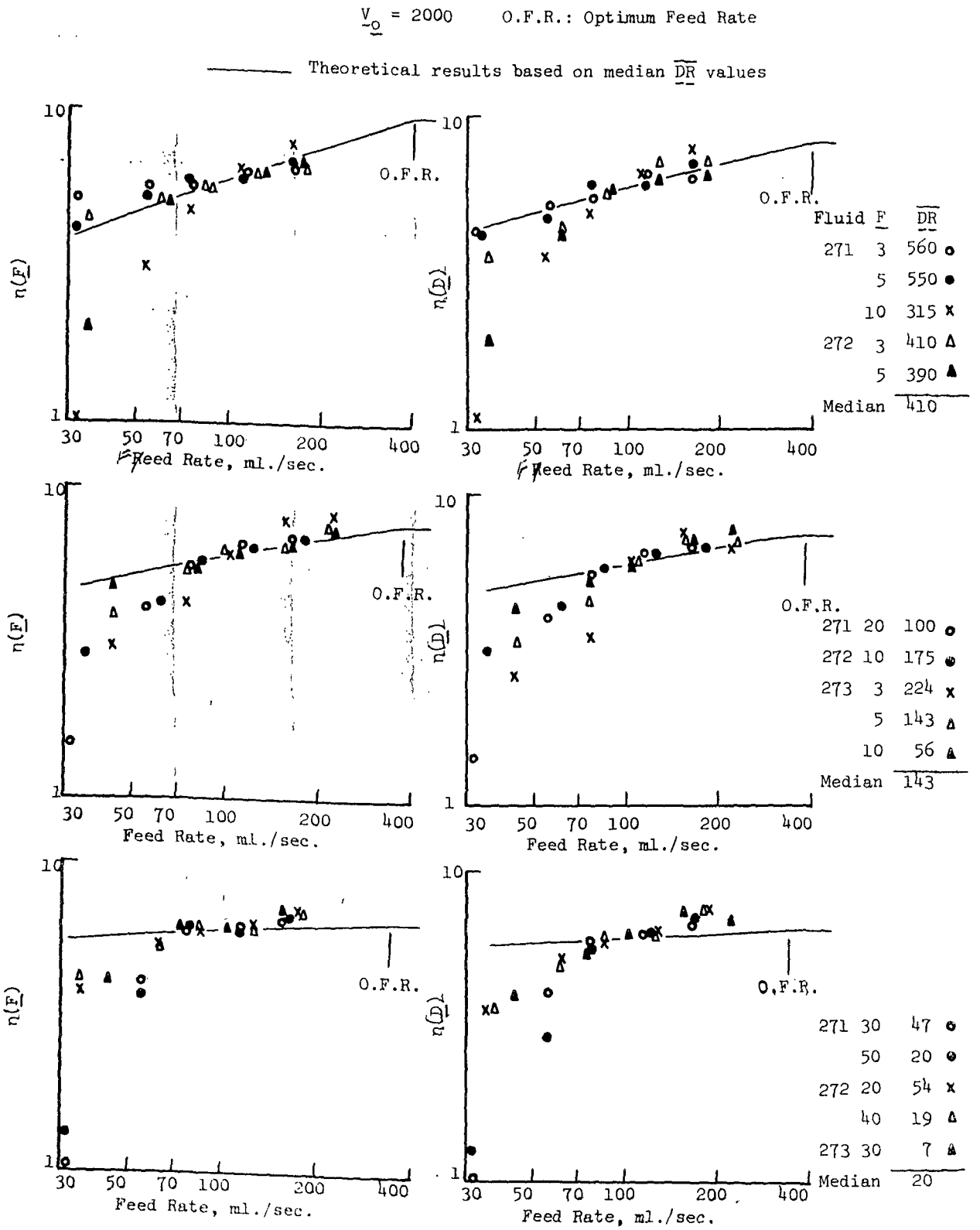

Figure 12 (cont'd). Composite Viscosity-Feed Rate Data

It is presumed that fluid leaving each blade is carried to the next without loss. Then the feed rate required to maintain full nips is determined from the flow rates out the sides obtained from Appendix III. These values are labeled O.F.R. (optimum feed rate) on the figure. Any greater feed rate and excess pressure could conceivably occur in the nips; lower feed rates have to cause some manner of void in the nips.

The theoretical effect of deficient feed rates on the results can be determined if one assumes that the fluid level drops uniformly across the nip. This gives a smaller effective blade surface exposed to flow. Calculations were made of the predicted combination as a function of feed rate and the results are shown as the lines in Fig. 12. The calculated lines were shifted on the viscosity axis to coincide with the common value at 100 ml./sec. used for the experimental results. Physically, the predictions are quite reasonable; the less the film thickness under the blade tip the less important the effect of blade length.

The results of Fig. 12 obviously do not conform to the expressed theory, except at large values of $\overline{\underline{DR}}$ and at flow rate approaching the optimum. The probable reason for this is to be found in the observation made during the experiments: where flow to the top nip is deficient, the effect is not to uniformly lower level across the nip but to remain full in the center and fall off as the edge is approached. (Note: the bottom nip was not visible due to overflow from the top.) This suggests a combination of lower blade length and blade width, especially as the feed rate falls much lower than optimum.

For roll velocity 1000 ft./min., the maximum feed rate approaches the optimum reasonably closely. The general leveling off of the calculated viscosities as the optimum feed rate is approached gives confidence that experimental results at this velocity and maximum experimental feed rates are independent of feed rate.

At roll velocity V_o = 2000 ft./min., the maximum feed rates are about one-half optimum. Extrapolating the results to optimum feed rate suggests a small to moderate error in results at low DR values and larger error at large DR. This effect suggests one reason for the considerable drop in viscosities at V_o = 2000 and low shear rate (at large DR) observed in Fig. 10. The phenomena to be discussed next also deal with probable fluid deficiency in a nip.

THE EFFECT OF UNEQUAL FORCES ON THE BLADES

In an earlier discussion of the equipment, Equation (10) was developed to permit calculation of the difference in normal load applied to the two blades. The application of Equation (10) to the experimental data gives the results of Table VIII. It is assumed in calculating viscosities that the results for the two blades can be averaged. Trial calculations for two cases in which F(top) and F(bottom) differ greatly have shown little error to be introduced in averaging.

Considering the results of Table VIII, it is apparent that, since the load on the top blade is greater than that on the bottom, the film thickness is greater on the bottom blade. Calculations of the apparent film thicknesses (under the blade tips) for the top blade, h_t, and the bottom blade, h_b, resulted in the figures given in Table IX. The excess flow, Q_e, is the amount of fluid which must be added to the bottom blade to make up the lower supply from the top blade. This value is in excess of the loss out of the sides of the blades which was considered in previous discussion.

The values in Table IX suggest that the viscosity results for low shear rate and low true viscosity, η_o, are artificially low due to unequal blade load.

TABLE VIII

SEPARATE NORMAL FORCE EXERTED BY THE BLADES

		V_o = 1000					V_o = 2000		
Γ/1000	η_o	DX/F	F(top)	F(bottom)	Γ/1000	η_o	DX/F	F(top)	F(bottom)
10	1.0	6.8	2.08	0.74	50	0.3	4.5	2.6	1.3
	2.0	6.7	3.6	2.0		0.8	5.7	5.3	3.7
20	0.3	3.6	1.98	0.88		1.5	5.9	7.9	6.0
	0.8	5.3	3.0	1.8	100	0.3	4.5	4.7	3.4
	2.0	6.4	5.4	3.7		0.8	5.2	8.0	6.4
50	0.3	3.8	3.2	2.1		1.5	5.1	12.3	10.3
	0.8	5.0	4.8	3.4	200	0.3	4.2	6.6	5.4
	2.0	5.7	8.0	6.2		0.8	4.5	12.1	10.6
100	0.3	3.9	4.2	3.1		1.5	5.7	17.9	16.2
	0.8	4.6	6.5	5.1	500	0.3	3.6	10.2	9.3
	2.0	5.3	11.4	9.4		0.8	4.1	18.0	16.7
200	0.3	3.8	5.2	4.1		1.5	4.5	26.0	24.0
	0.8	4.4	9.0	7.6	700	0.3	3.4	12.4	11.8
	2.0	5.0	14.7	12.7		0.8	3.9	20.9	19.8
500	0.3	2.9	9.5	8.9	900	0.3	3.1	15.2	14.8
	0.8	3.4	15.8	15.1		0.8	3.6	24.2	23.4
	2.0	4.3	24.0	22.0	1100	0.3	3.0	16.4	16.0
700	0.4	3.7	13.5	13.3		0.8	3.5	26.5	25.9
	0.8	3.1	18.3	18.0	1300	0.3	2.8	17.8	17.8
	1.5	3.5	25.0	24.0		0.8	3.7	25.0	24.0
900	0.5	2.7	16.2	16.1					
	0.8	2.7	21.6	21.9					
	1.5	4.5	20.7	18.9					

TABLE IX

"EXCESS" FLOW REQUIRED FOR THE BOTTOM BLADE

$\Gamma(sec.^{-1})/1000$	η_o, poise	h_t, cm.	h_b, cm.	Q_e, ml./sec.
	$V_o = 1000$			
10	1.0	0.034	0.085	130
	2.0	0.039	0.069	76
	0.3	0.0159	0.0440	71
20	0.8	0.0189	0.0349	41
	2.0	0.0204	0.0324	30
	0.3	0.0077	0.0146	18
50	0.8	0.0082	0.0138	14
	2.0	0.0088	0.0128	10
	$V_o = 2000$			
50	0.3	0.0134	0.0352	111
	0.8	0.0162	0.0268	54
	1.5	0.0172	0.0248	39
100	0.3	0.0083	0.0132	25
	0.8	0.0088	0.0121	17
	1.5	0.0089	0.0116	14
200	0.3	0.0043	0.0061	9
	0.8	0.0046	0.0057	6
	1.5	0.0047	0.0057	5

The combined effects of unequal blade loading and flow out the sides of the blades leads to the conclusion that the low shear rate, low true viscosity, results are in error; in particular those values at $\underline{V}_o$ = 2000 since both phenomena are in effect. It is thereby concluded that the decreasing lower ends of the results of Fig. 10 are to be discarded. It is further concluded that the calculated viscosity results are independent of velocity. With these conclusions, the results are repeated in Fig. 13, permitting a comparison of the two calculated viscosity functions, $\eta(\underline{F})$ and $\eta(\underline{D})$.

POSSIBLE REASONS FOR DEVIATION OF THE VISCOSITY RESULTS FROM THEORY

It is quite impossible to give convincing explanations for deviations from theory observed in Fig. 13. Sufficient data are not available. Four possibilities considered to be most likely sources of deviations are as follows.

Turbulence

Because of the rapidly spreading flow at the nip entrance, accompanied by rapid reverse flow out of the nip, it is likely that a condition of turbulence exists at that point. In some cases, wild turbulence could be observed in the top blade. It is equally likely that flow near, and under, the blade tip is laminar due to extremely low Reynolds numbers. The rate of change from turbulent to laminar flow, and the effect of the turbulent flow, is not known. If turbulence is an important factor, it is expected to be most significant at low shear rates and at low viscosities. This could possibly account for the large excess experimental viscosity values, $\eta(\underline{F})$ and $\eta(\underline{D})$, observed under these conditions.

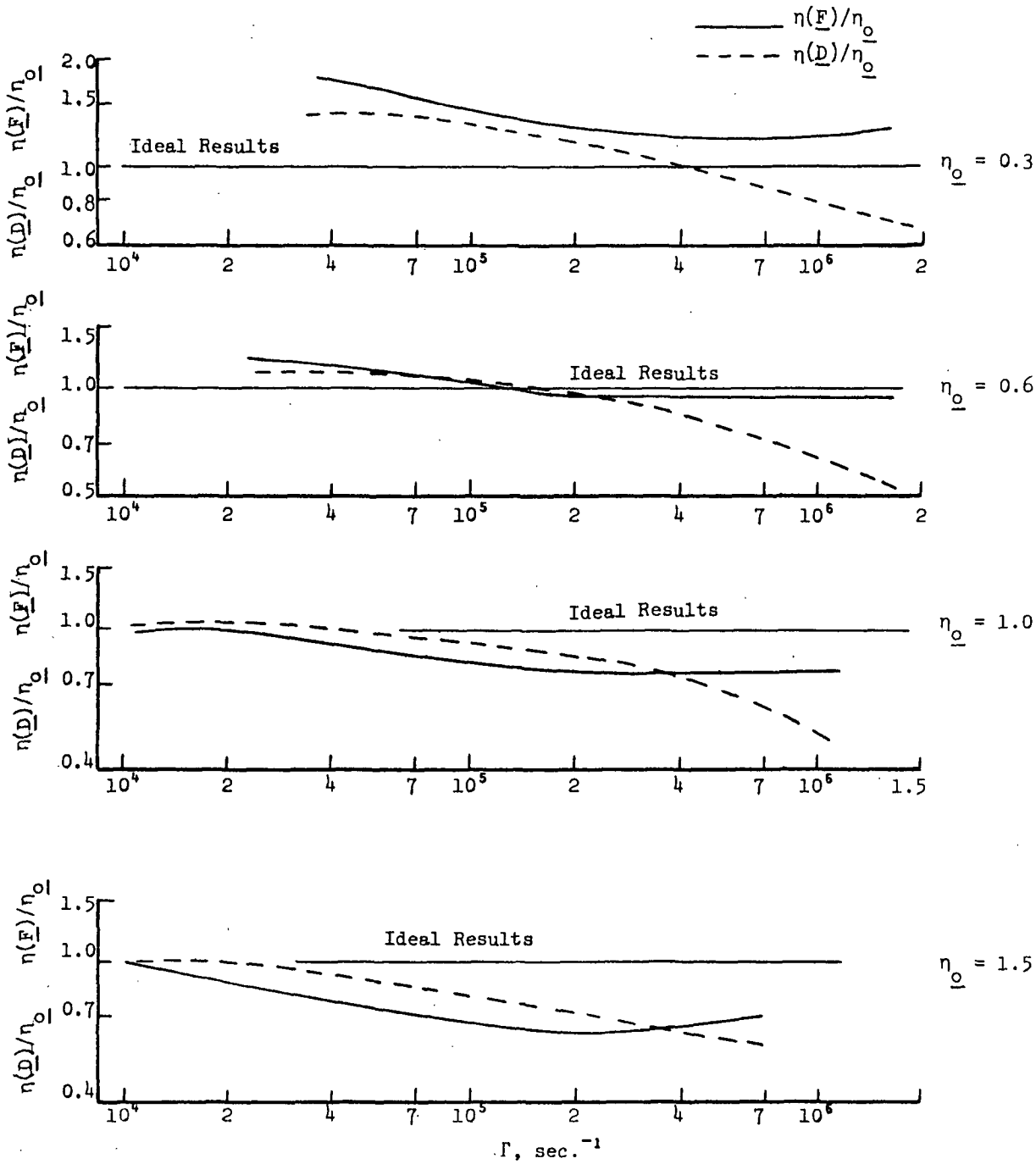

Figure 13. Comparison of η(F) and η(D)

Entrained Air

The circulation system of the Rheometer unfortunately leads to the apparent incorporation of large amounts of entrained air in fluids. The importance of entrained air, the extent to which it is carried into the interior of the nip, and the effect of experimental variables are all unknown. It is considered of greatest importance to revise experimental techniques in the future to avoid this problem.

Blade-Roll Tilt

In previous discussion of random error, it was shown that possible tilt of the blade and/or the roll could lead to significant difference in film thickness from one side of the blade to the other. It is expected that if this is an important factor it would affect the high shear rate results most. Possibly this could be one factor causing the considerable drop in $\eta(\underline{D})$ values at high shear rates.

Nonviscometric Flow

Flow in a converging nip can be calculated as viscometric flow but it cannot be true viscometric flow. There is, of necessity, elongational and compressional flow. It is considered best to hold nonviscometric flow in abeyance as a factor causing deviation from ideal results, at least until the possibilities discussed above are brought under better control.

THE TESTING OF COATINGS IN THE RHEOMETER

INTRODUCTION

When work was begun on the testing of coatings, it was not known what to expect. The basic plan was to test a variety of compositions and follow up the more interesting ones in more detail. There was no intent to evaluate materials for usefulness as coatings but only to investigate flow behavior in the blade nip geometry.

Composition variations tested were binder type, pigment type, and the effect of additives. The most interesting result was the apparent viscoelastic behavior of coatings containing polyvinyl alcohol, and a variety of compositions were tested. In retrospect, it can be seen that other differences are subtle but real and worthy of continued interest. Included in these are the difference between starch and protein binder and the difference in rheological behavior of coatings containing mineral pigment and plastic pigment. Combination binders containing latex were not tested and should be considered in future work.

A point of continuing interest has been the evaluating of the experimental technique. The experiments on coatings have pointed out certain areas which require improvement.

MATERIAL DESCRIPTIONS

Clay: Special Hydratex and KCS Hydrosperse No. 2 grade coating clay, 0.8 μm. particle size, density = 2.6

Delaminated clay: NuClay, 0.2-0.4 μm. particle thickness, density = 2.6

Calcium carbonate: Pure Cal, precipitated, av. particle size 0.2 μm., density = 2.7

Titanium dioxide: Glidden R-77, rutile form, av. particle size 0.2 μm., density = 4.1

Latex: Dow 636, SBR, density = 1.05

Starch: Staco M, oxidized, density = 1.5

Polyvinyl alcohol: DuPont Elvanol 71-30, density = 1.3

Protein: Central Soya Delta Protein DP-5449B, density = 1.3

Carboxyl methyl cellulose (CMC): Hercules 70 low viscosity

Urea

Calcium stearate: Nopco C104

Plastic pigment: Dow XD-7226.00, density = 1.05

There was a general lack of information on the thermal properties of the coating materials. It was assumed that the heat capacity is the sum of the constituent values on a weight basis, and the thermal conductivity is the sum of the constituent values on a volume basis. Heat capacity was assumed to be 0.22 and 0.35 cal./g./°C. for mineral pigment and plastic (all binders and plastic pigment), respectively. Thermal conductivity was assumed to be 0.0003 and 0.0006 cal./°C./cm./sec. for mineral pigment and plastic, respectively. Fortunately, the viscosity-temperature coefficient for most of the coatings was sufficiently small that errors in thermal properties would not change the viscous heat corrections appreciably.

COATING COMPOSITIONS AND PROPERTIES

The coating compositions and properties are given in Table X. The binder and pigment contents are given as percentage of the solid content of the coating on an ovendry basis. In all but Experiment 19, percentage solids was measured on samples taken during the Rheometer test. Units of the physical properties are as follows:

TABLE X

COATING DESCRIPTIONS

Experiment	Coating	Binder	Pigment	Solids, % Calc.	Solids, % Exp.	β	$\underline{k}$	ρ	$\underline{c}_p$
19	1	Latex 15.3	Clay 84.7	65.0	--	0.04	0.00093	1.52	0.51
	2	PVA 4.76	Clay 95.2	50.0	--	0.018	0.00109	1.43	0.61
	3	Starch 15.3	Clay 84.7	53.0	--	0.010	0.00106	1.43	0.60
	4	Protein 13.8	Clay 86.2	49.3	--	0.010	0.00109	1.38	0.62
20	5	Starch/PVA 0/4.76	Clay 95.2	52.5	52.5	0.018	0.00109	1.43	0.61
	6	Starch/PVA 4.16/3.45	Clay 92.4	52.5	53.0	0.016	0.00107	1.46	0.59
	7	Starch/PVA 8.08/2.24	Clay 89.8	52.7	53.0	0.014	0.00106	1.45	0.59
	8	Starch/PVA 11.8/1.10	Clay 87.0	52.9	52.8	0.012	0.00107	1.44	0.60
	9	Starch/PVA 15.3/0	Clay 84.7	53.0	53.1	0.010	0.00106	1.43	0.60
21	10	Starch 100	Clay 0	25.0	29.6	0.040	0.00122	1.11	0.81
	11	Starch 35.3	Clay 64.7	42.5	43.4	0.030	0.00114	1.29	0.68
	12	Starch 21.3	Clay 78.7	49.7	47.8	0.020	0.00111	1.36	0.64
	13	Starch 15.3	Clay 84.7	53.0	52.4	0.010	0.00106	1.43	0.60
22	14	Starch/Calcium stearate 15.1/1.00	Clay 83.9	53.0	52.9	0.010	0.00106	1.43	0.60
	15	Starch/CMC 15.1/0.75	Clay 84.1	50.6	51.0	0.010	0.00106	1.43	0.60
	16	Starch/Urea 14.6/0.66	Clay 84.7	53.0	53.2	0.010	0.00106	1.43	0.60
	17	Starch 15.3	Clay 84.7	53.0	53.3	0.010	0.00106	1.43	0.60

TABLE X (Continued)

COATING DESCRIPTIONS

Experiment	Coating	Binder	Pigment	Solids, % Calc.	Solids, % Exp.	β	k	ρ	c_p
23	18	PVA 100	Clay 0	10.0	13.2	0.032	0.00132	1.03	0.91
	19	PVA 13.0	Clay 87.0	38.2	39.1	0.027	0.00118	1.28	0.70
	20	PVA 7.0	Clay 93.0	46.5	46.4	0.022	0.00112	1.38	0.64
	21	PVA 4.76	Clay 95.2	50.0	50.2	0.018	0.00109	1.43	0.61
24	22	Starch 15.3	Clay 84.7	53.0	53.0	0.010	0.00106	1.43	0.60
	23	Starch 15.3	Delaminated clay 84.7	55.2	56.5	0.010	0.00103	1.48	0.57
	24	Starch 16.4	Calcium carbonate 83.6	59.0	59.2	0.010	0.00101	1.52	0.55
	25	Starch 11.2	Titanium dioxide 88.8	59.7	61.2	0.010	0.00108	1.77	0.53
25	26	Starch 15.3	Clay 84.7	53.2	53.3	0.010	0.00106	1.43	0.60
	27	Starch 15.3	Clay 84.7	53.2	53.3	0.010	0.00106	1.43	0.60
26	28	Starch 30.8	Plastic pigment 69.2	40.9	40.8	0.010	0.00110	1.06	0.73
	29	Starch 30.8	Plastic pigment 69.2	39.1	39.3	0.010	0.00111	1.06	0.74
	30	Starch 30.8	Plastic pigment 69.2	37.6	38.1	0.010	0.00112	1.05	0.75

$\underline{k}$: thermal conductivity in cal./°C./cm./sec.

$\underline{c_p}$: heat capacity in cal./g./°C.

ρ: density in g./cm.^{3}

β: dimensionless viscosity-temperature coefficient determined from Hercules viscosity results, defined by $\eta_2/\eta_1 = \exp[-\beta(\underline{t}_2-\underline{t}_1)]$, in which η_2 and η_1 are viscosities in poises at temperatures $\underline{t}_2$ and $\underline{t}_1$, °C., respectively.

THE EFFECT OF FEED RATE TO THE NIPS ON STARCH-CLAY COATING VISCOSITY

In Experiment 28, viscosities of starch-clay coating were determined as functions of feed rate to the nips. The results are presented in Fig. 14. In Appendix III, the results of calculations of flow rate out the sides of the nips are reported. The two determinations for a non-Newtonian fluid ($\underline{N}$ = 0.9) were fairly close to the Newtonian fluid results, and it is assumed that the Newtonian fluid results are valid for the starch-clay coating with $\underline{N}$ = 0.7. Theoretical results for the effect of blade length on viscosity were determined using the computer program of Appendix II, also for $\underline{N}$ = 0.7. These results were combined to calculate the theoretical lines shown in Fig. 14. The lines are moved on the viscosity axis to coincide with the data at feed rates of 100 ml./sec. The assumption here is that less than full nips cause an even drop in fluid level across the nips. It is apparent that, contrary to earlier results for glycerin, there is a fairly good fit of the data to the theory.

The theoretical lines were extrapolated to the optimum feed rate (full nips) to estimate a theoretical error due to low feed rate. The results are given in Table XI. It will be seen later that the differences between viscosity results for $\underline{V}_o$ = 2000 and $\underline{V}_o$ = 1000 are much less than the difference in extrapolated results. In fact, the results obtained at maximum possible experimental feed

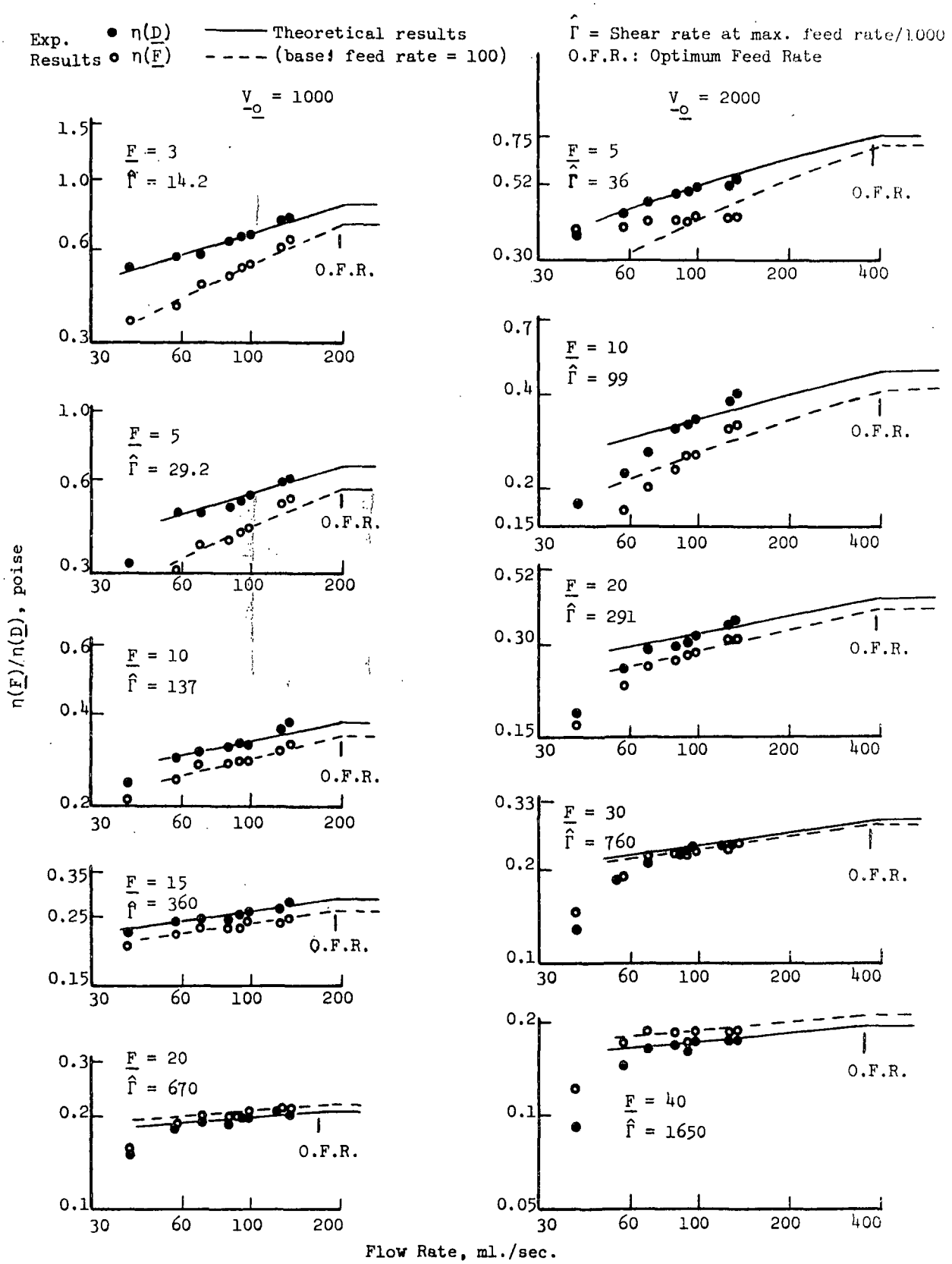

Figure 14. Effect of Feed Rate on Starch-Clay Coating Viscosity

rates are the same for the two velocities, within experimental variations. Whether the extrapolations are faulty, or there are true differences in results at the two velocities, is not known.

TABLE XI

INCREASE IN $\eta(\underline{F})$ AND $\eta(\underline{D})$ WITH THEORETICAL EXTRAPOLATION TO OPTIMUM FEED RATE

	$\underline{V}_o$ = 1000		$\underline{V}_o$ = 2000		Difference in % Increase ($\underline{V}_o$ = 2000 - $\underline{V}_o$ = 1000)	
	% Increase in		% Increase in			
$\Gamma(\text{sec.}^{-1})/1000$	$\eta(\underline{F})$	$\eta(\underline{D})$	$\eta(\underline{F})$	$\eta(\underline{D})$	$\eta(\underline{F})$	$\eta(\underline{D})$
15	18	11				
30	17	11	50	32	33	21
60	14	11	47	30	33	19
100	11	10	42	28	31	18
200	8	7	32	25	24	18
500	4	3	20	18	16	15
1000	0	0	12	12	12	12
1500	0	0	9	9	9	9

The general effect of the presumed error in results due to feed rate is one of reducing viscosity results at all points, with the maximum reduction being at low shear rate. This would have the effect of giving an experimental power law coefficient, $\underline{N}$, lower than the presumed true value.

In comparing different coatings, the feed rate effect could conceivably mask subtle differences between coatings. That is, higher viscosity would result in lower feed rate which would lead to lower experimental viscosities. Considering the slopes of the curves in Fig. 14, and the fairly slow change in pumping rate with viscosity change observed with glycerine solutions, it would not seem

probable that this effect would be major. Unfortunately, no feed rate measurements were made for other coatings. In later discussions of coating results, it will be seen that there is, in fact, some evidence of a dampening of differences between coatings due to the feed rate problem.

THIXOTROPY

History

In the usual coating high shear rheograms, e.g., Hercules or Shirley Feranti, one obtains a measure of thixotropic breakdown, i.e., a reduction of viscosity due to energy input to the fluid. This information is an advantage when describing phenomena presumed to be affected by thixotropy, e.g., see the paper by Smith, et al., on the roll coating process (13). It is, on the other hand, misleading to artificially reduce viscosity in a manner that is contradictory to actual coater operation. Flow in the blade nip is an extremely rapid process and one would expect an effective viscosity larger than that obtained in the usual instruments. It is considered an advantage to measure viscosity in the Rheometer since the technique of measurement corresponds somewhat to the actual coating process.

Energy Input to Coatings in the Rheometer, and Recovery Time

Coating is pumped directly from the pump to the nips, with very little recovery time. The recovery time after nip flow to the pump is about 23 sec. It is concluded that the net pumping effect is to impart a more or less constant thixotropic breakdown to coatings being tested.

Most of the coating entering the nips leaves by flow out the sides. The coating passing completely through a nip will absorb considerable energy and

presumably undergo some breakdown. If the same coating remains on the roll and goes through the nips repeatedly, the situation would be comparable to the usual viscometer. Considering the constant input of new fluid to the nips and the large amount of flow out the sides it is very unlikely that there is not a constant renewal of coating passing all the way through the nips. So, assuming that the entire mass of coating can be treated as an average, consider the calculated times of recovery of an element of coating given in Table XII. These results are based on a total volume of 3000 ml. The recovery time is seen to be fairly large in all cases and especially for the conditions of highest shear rates. One might possibly expect to have some evidence of accumulated nip breakdown at low shear.

TABLE XII

RECOVERY TIME FROM NIP FLOW

Shear Rate (Γ), sec.$^{-1}$	DR[Film Thickness (cm.)/16070]	Recovery Time, sec.
	V_o = 1000, ft./min.	
10^4	820.0	11.6
10^5	82.0	116.0
10^6	8.2	1160.0
	V_o = 2000, ft./min.	
10^5	164.0	29.0
10^6	16.4	290.0

Low Shear Results at V_o = 2000 Ft./Min.

The usual experimental procedure was to make a run at V_o = 1000 from low to high shear and then repeat the process at V_o = 2000. The first few points at the higher velocity invariably show very low viscosity. Any possibility that this effect might be due to thixotropic breakdown at high shear during the

first run is completely masked by the effect of unequal forces on the blades at low shear and high speed.

Effects of Changes in Experimental Procedure

Changes in experimental procedure were used to test the possible effect of accumulated thixotropic breakdown due to flow in the nips.

In the usual procedure, the first data points are at low shear and at $\underline{V}_{\underline{o}}$ = 1000 ft./min. If there is an effect of breakdown in the nips which accumulates, it is possible that the results would show this in lower viscosity when the order of gathering data is changed.

In Experiment 22, the two runs were repeated, with the results shown in Fig. 15. The first several points (at low shear rate) are for $\underline{V}_{\underline{o}}$ = 1000. There is some evidence of accumulated breakdown at very low shear rate. In contrast, consider the results of Experiment 28, Fig. 16. In this experiment, the effect of feed rate to the nips was tested and the points were obtained in random order. It is apparent that there is no dominant effect of reduced viscosity at low shear rate due to accumulated effects. Comparable results were obtained in another experiment in which the velocity and load order were both reversed. The two coatings, No. 26 and 27, had identical solids and approximately the same Hercules rheograms. For Coating 27, the reverse order would give the maximum possible chance for accumulation of breakdown to affect the results at $\underline{V}_{\underline{o}}$ = 1000 and $\underline{V}_{\underline{o}}$ = 500. It is seen in Fig. 17 that there is a small drop in some of the viscosity results for the reverse order fluid (27) but the effect is certainly not major. In an experiment with starch-plastic pigment to be considered later, the procedure was altered to show the same possible effect, and very little effect of accumulated breakdown was evident.

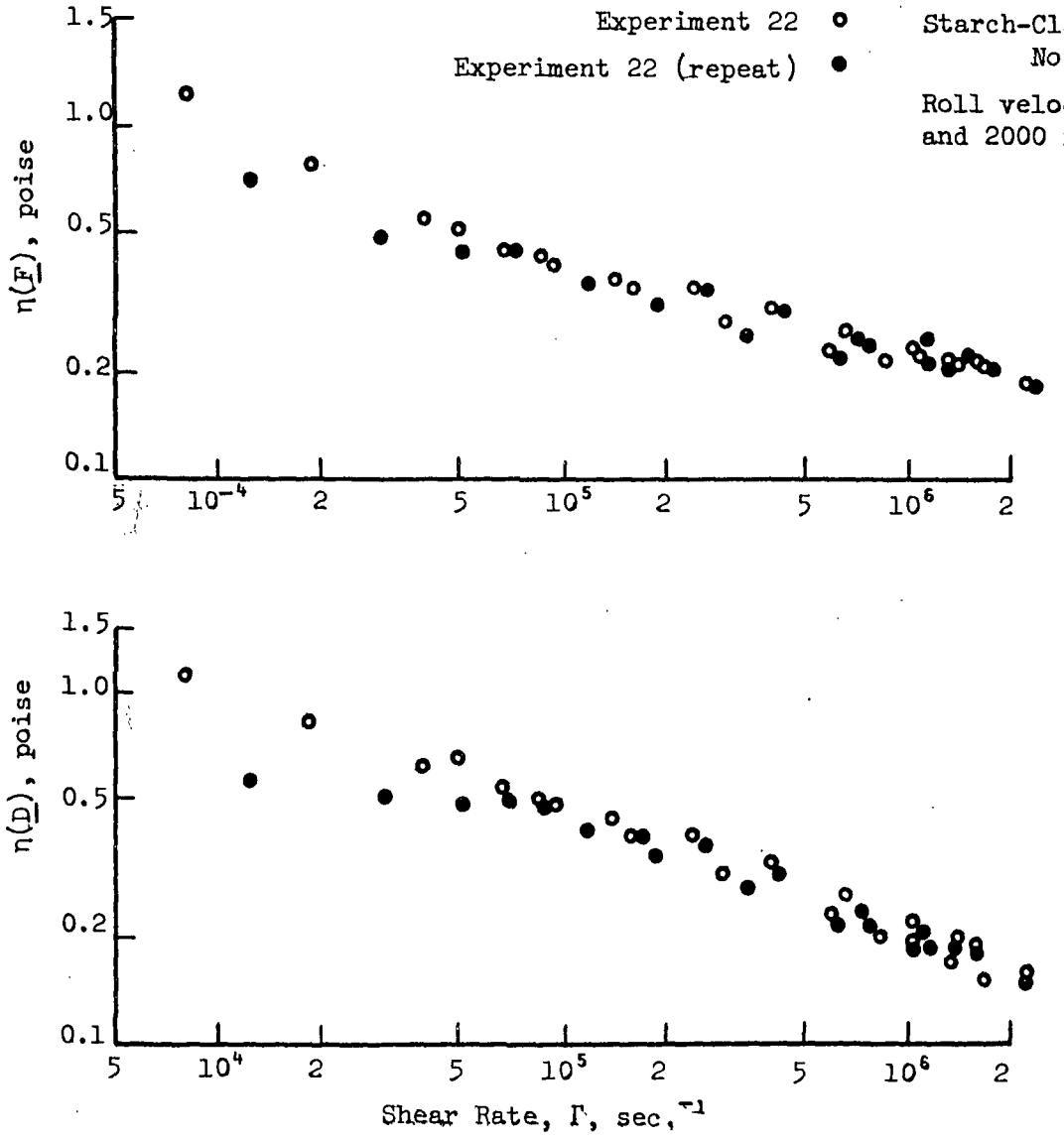

Figure 15. Repeat Experiment to Test Thixotropy

The lines are median values for similar coatings, obtained using the usual experimental procedure, starch-clay coating

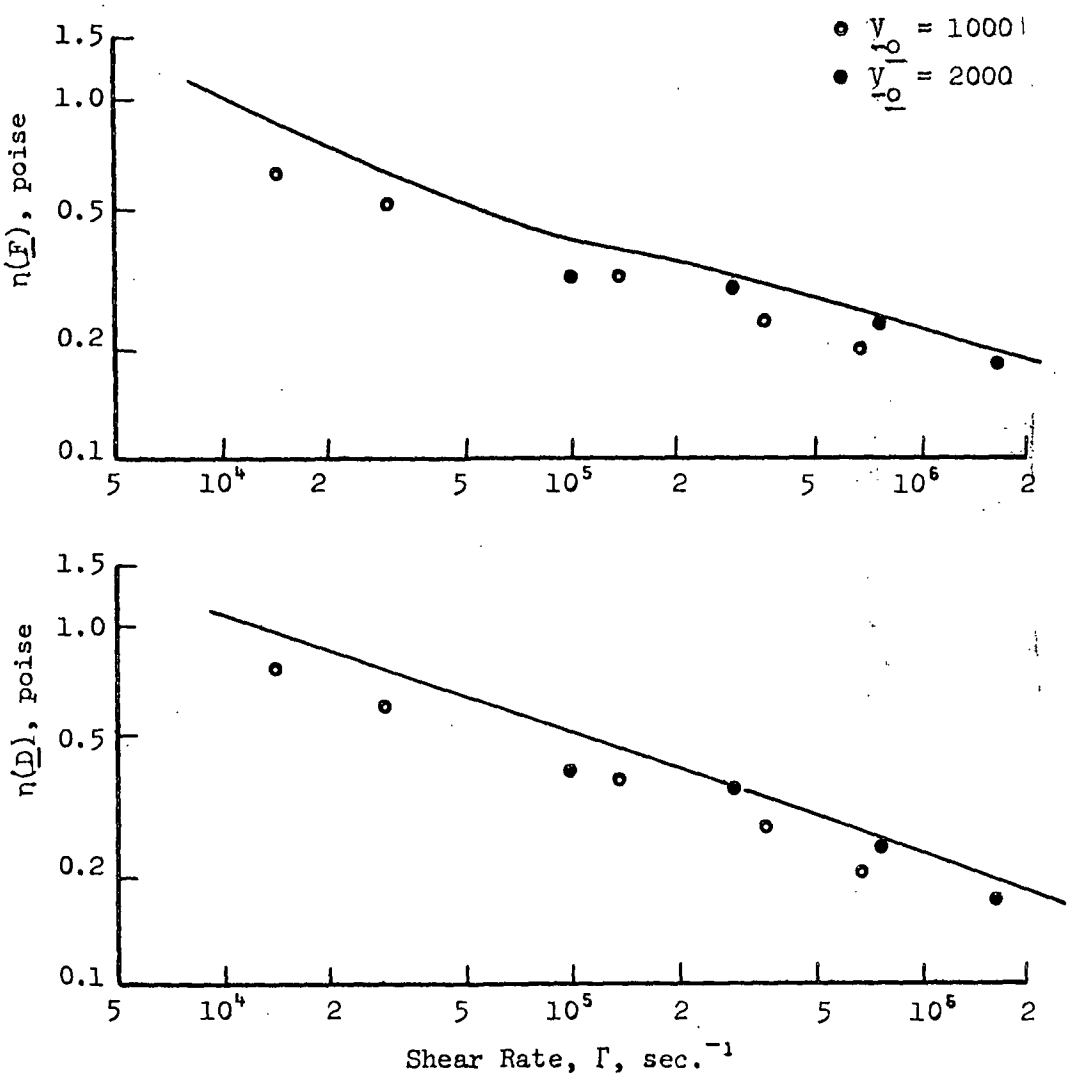

Figure 16. Test of Thixotropy with Results of Experiment 28, Fluid 31

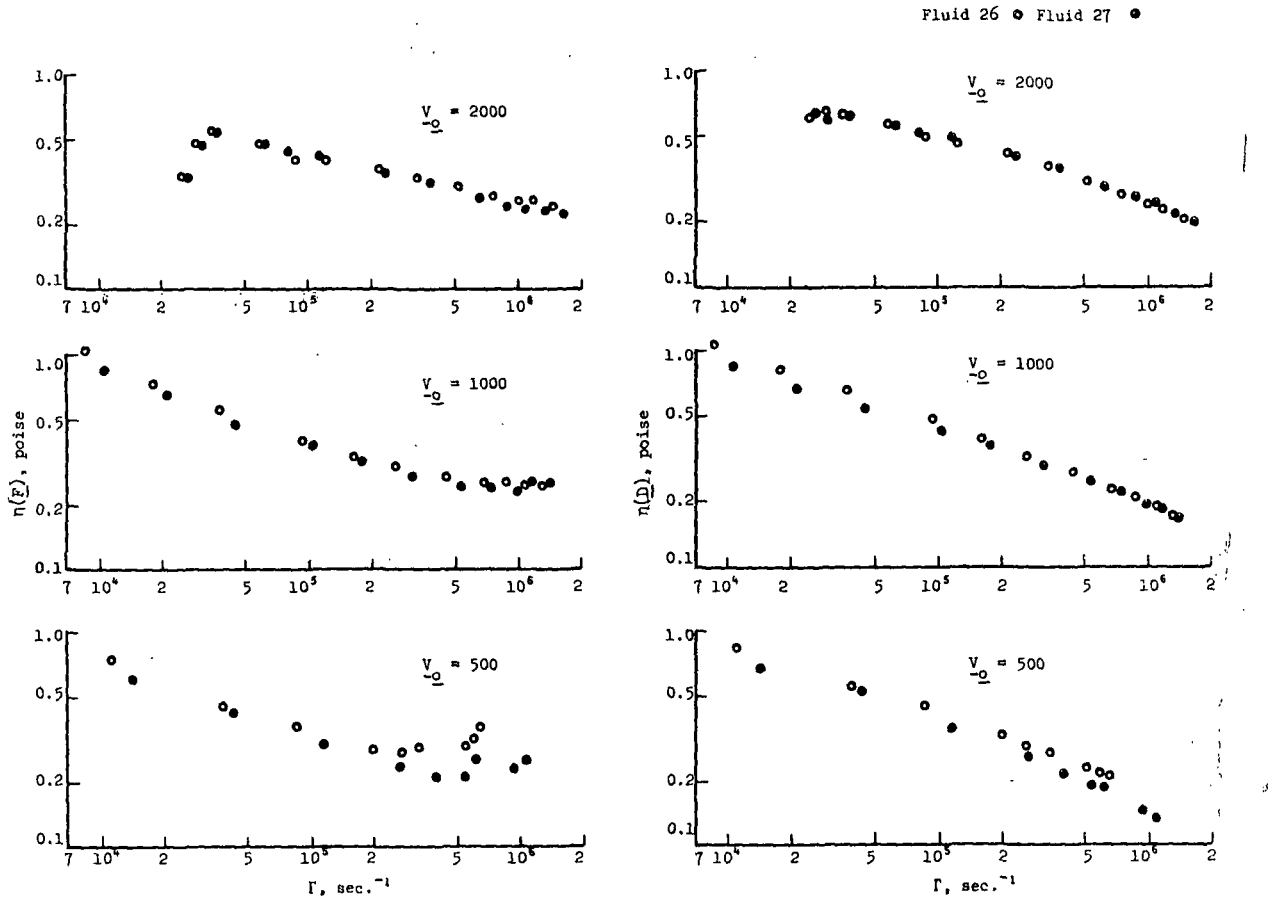

$\underline{V}_o$	Fluid 26 Order Run	Fluid 26 Load	Fluid 27 Order Run	Fluid 27 Load
500	1	Increase	3	Decrease
1000	2	Increase	2	Decrease
2000	3	Increase	1	Decrease

Figure 17. Test of Thixotropy by Variation of Procedure — Fluids 26, 27

The net result of these experiments is that the fluid breakdown at any given point in an experiment is largely constant and due to pumping, and that accumulated breakdown due to shearing in the nips may have some effect but not a major one. It is concluded, therefore, that the fluid being tested in the Rheometer is not virgin, i.e., recovered for an "infinite" time, but is in some state of breakdown characteristic of the circulation system.

Comparison of Rheometer and Hercules Results

It will be seen in succeeding presentation of results that, at comparable shear rates, the Rheometer viscosities are generally higher than the Hercules results. Consider the following arguments that lead to the conclusion that this effect is real and that the Hercules viscosities are artificially low:

(1) The effect of blade force inequality and insufficient feed rate to the nips is to reduce Rheometer viscosities below apparent true results.

(2) In comparing coating and Newtonian results, it is considered more realistic to use Newtonian viscosity values of one poise or greater. At such viscosity values, the Newtonian results are comparable to the true values at low shear rates. The abnormally large experimental viscosities for low viscosity Newtonian fluids are considered to be due to low viscosity in the entrance part of the nip, and coating viscosities are very high at the nip entrance.

STARCH-CLAY COATING RESULTS

General Comments

In most of the experiments conducted in this project, a standard starch-clay coating was tested. The reasons for this were to determine possible

changes in the Rheometer with time, to obtain some idea of the variation in results which might be due to experimental aberrations, and to have a standard coating against which changes in formulation can be compared.

An average power law exponent of 0.71 was used for all coatings and all results were corrected to 30°C. The experimental procedure was the same in all cases except for Coating 26. Normally, runs were made at velocities of 1000 and 2000 ft./min., in that order. For Coating 26 the regular order was preceded by a run at 500 ft./min. It is very unlikely that this affected the results at the higher velocities.

The median results for all of the coatings are given in Fig. 18, and the results for the individual coatings are given in Fig. 19. It is apparent that velocity has a relatively small effect on the results and the median curves include data at both 1000 and 2000 ft./min. The drop in viscosity at 2000 ft./min. and low shear rate is attributed to unequal force on the blades, as discussed earlier, and these values are not included in the median determinations. The single set of results at 500 ft./min. is not considered sufficient to indicate a real change due to velocity.

Comparison with the Newtonian Results

A direct comparison of a shear thinning material like coatings with Newtonian fluids must be approached with considerable caution. Much of the deviation from ideal behavior observed for Newtonian fluids must be due to converging flow under the blade surface. The deviation was generally greater for lower viscosity fluids, especially at low shear rates. Since coatings are shear thinning, the viscosity in the nip entrance is very large, and the net effect might be to make the flow of coatings more ideal than that of Newtonian fluids.

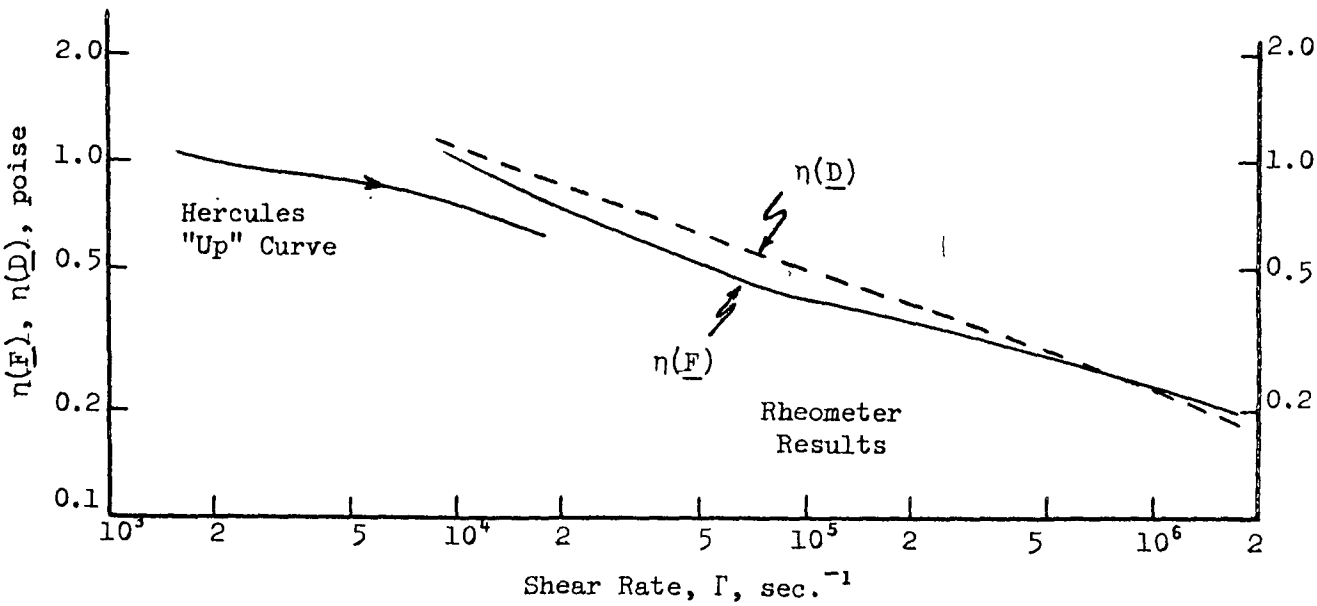

Figure 18. Median Results for Starch-Clay Coatings

It is apparent that the rapid drop in $\eta(D)$ compared with $\eta(F)$ at high shear rate, characteristic of the Newtonian results, is not seen for these coatings. This might suggest that the effect is not, as seems most probable in considering the Newtonian results alone, a result of imperfect blade-roll alignment for extremely thin films but, rather, a question of stabilization of flow due to shear thinning.

Time Change in the Results

A comparison of the six sets of results suggests no consistent change in behavior that could be attributed to machine changes.

Viscoelasticity

The predicted effect of viscoelasticity on results is to leave the $\eta(D)$ curve alone and to cause a rapid increase in the $\eta(F)$ curve at high shear rates. It will be seen later that the true effect is quite different and much more interesting. In only two of the curves is there a marked indication in increase in

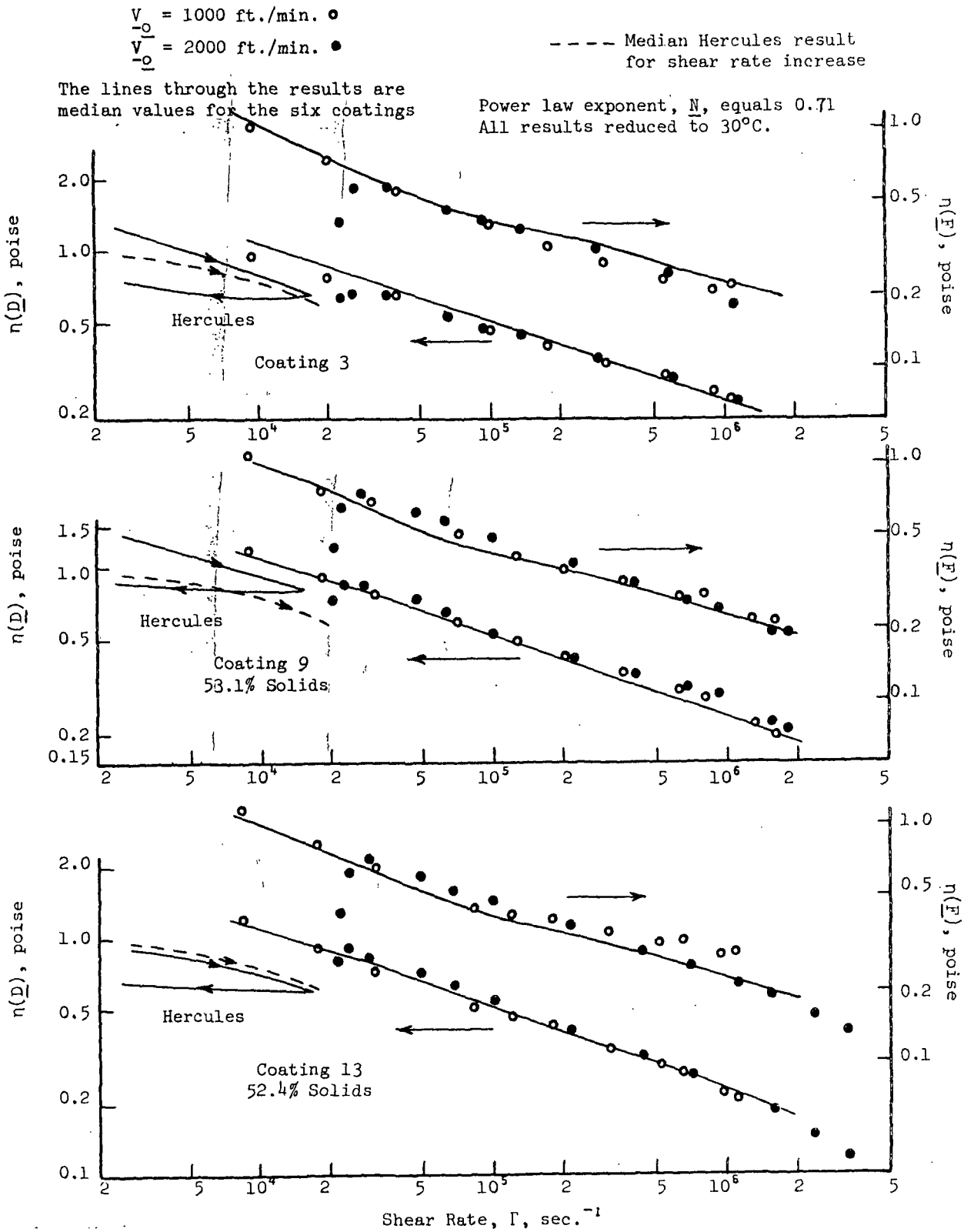

Figure 19. Starch-Clay Coating Results

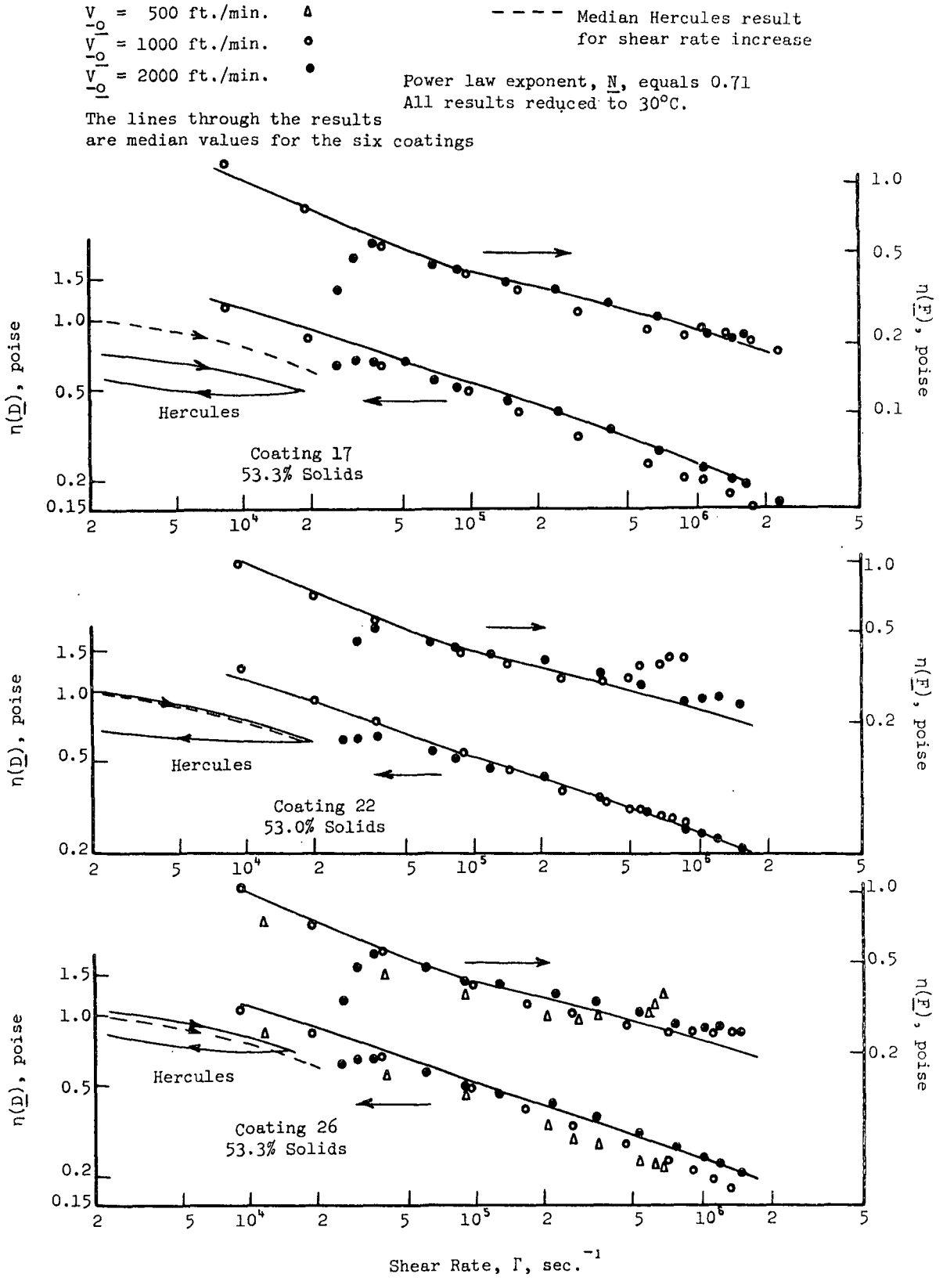

Figure 19 (cont'd). Starch-Clay Coating Results

$\eta(\underline{F})$ at high shear rate (excepting the results at 500 ft./min. for Coating 26). It is concluded that there is no evidence of viscoelastic behavior for these coatings.

Comparison with the Hercules Results

In the previous discussion on thixotropy, it was concluded that the Hercules results at high shear show an artificially low viscosity due to shear thinning. The extent of this effect is apparent in the median curves in Fig. 18.

Individual values of Rheometer and Hercules viscosity are compared in Table XIII. At high shear, $\Gamma = 10^6$, the Rheometer results show somewhat the same changes in relative viscosity values as the Hercules results. At lower shear rate, $\Gamma = 10^5$, the difference is dampened out somewhat. These results suggest a dampening effect due to the effect of viscosity on feed rate to the nips. This effect, in previous discussion of the effect of feed rate on the results, was considered possible but unlikely.

TABLE XIII

COMPARISON OF RHEOMETER AND HERCULES RESULTS

Coating	Rheometer: $\rho = 10^5$		Rheometer: $\Gamma = 10^6$		Hercules "Up": $\Gamma = 10^4$	
	$\eta(\underline{D})$	$\eta(\underline{D})$/av.	$\eta(\underline{D})$	$\eta(\underline{D})$/av.	η	η/av.
3	0.48	0.98	0.250	1.07	0.81	1.07
9	0.52	1.06	0.265	1.14	0.93	1.23
13	0.51	1.04	0.220	0.95	0.70	0.92
17	0.47	0.96	0.215	0.92	0.57	0.75
22	0.49	1.00	0.232	1.00	0.74	0.98
26	0.48	0.98	0.215	0.92	0.81	1.07

COATINGS CONTAINING POLYVINYL ALCOHOL (PVA)

In the first experiment (Experiment 19), coatings composed of clay and various binders were tested. In order to assure one viscoelastic coating, PVA was included as a binder. The Rheometer results obtained with the PVA were so radically different from the other binders that two more experiments were conducted using PVA. In Experiment 20, mixed starch and PVA binders were tested, with the results given in Fig. 20A. In Experiment 23, the pigment content in PVA binder was varied from zero to a regular coating, with the results presented in Fig. 20B. The power law exponents were assigned somewhat arbitrarily since both viscosity curves reflected more than just viscosity. A change in exponent, $\underline{N}$, would change the details of the curves but not the overall form.

According to the theory, the viscosity $\eta(\underline{F})$ should be greater than the true viscosity due to normal stress effects while the viscosity $\eta(\underline{D})$ should be unaffected. Considering all of the results it is apparent that $\eta(\underline{D})$ is affected to an even greater extent than $\eta(\underline{F})$. The probable reason for the effect on $\eta(\underline{D})$ is the emergence of elongational stresses comparable in magnitude to the shear stress, see, e.g., References (14,15). If this is in fact the case, measurements made in the blade nip might be very useful in evaluating a very elusive quantity, the elongational viscosity. It is apparent in any case that, since the Rheometer does not measure reliable viscosity values for these materials, the viscosity function and the first normal stress function, $\underline{p}_{11}-\underline{p}_{22}$, in themselves cannot describe the flow in the nip.

The gradual reduction in viscoelastic behavior in the PVA-starch coatings is apparent as the PVA content is reduced. With only starch in the binder the flow appears to be inelastic.

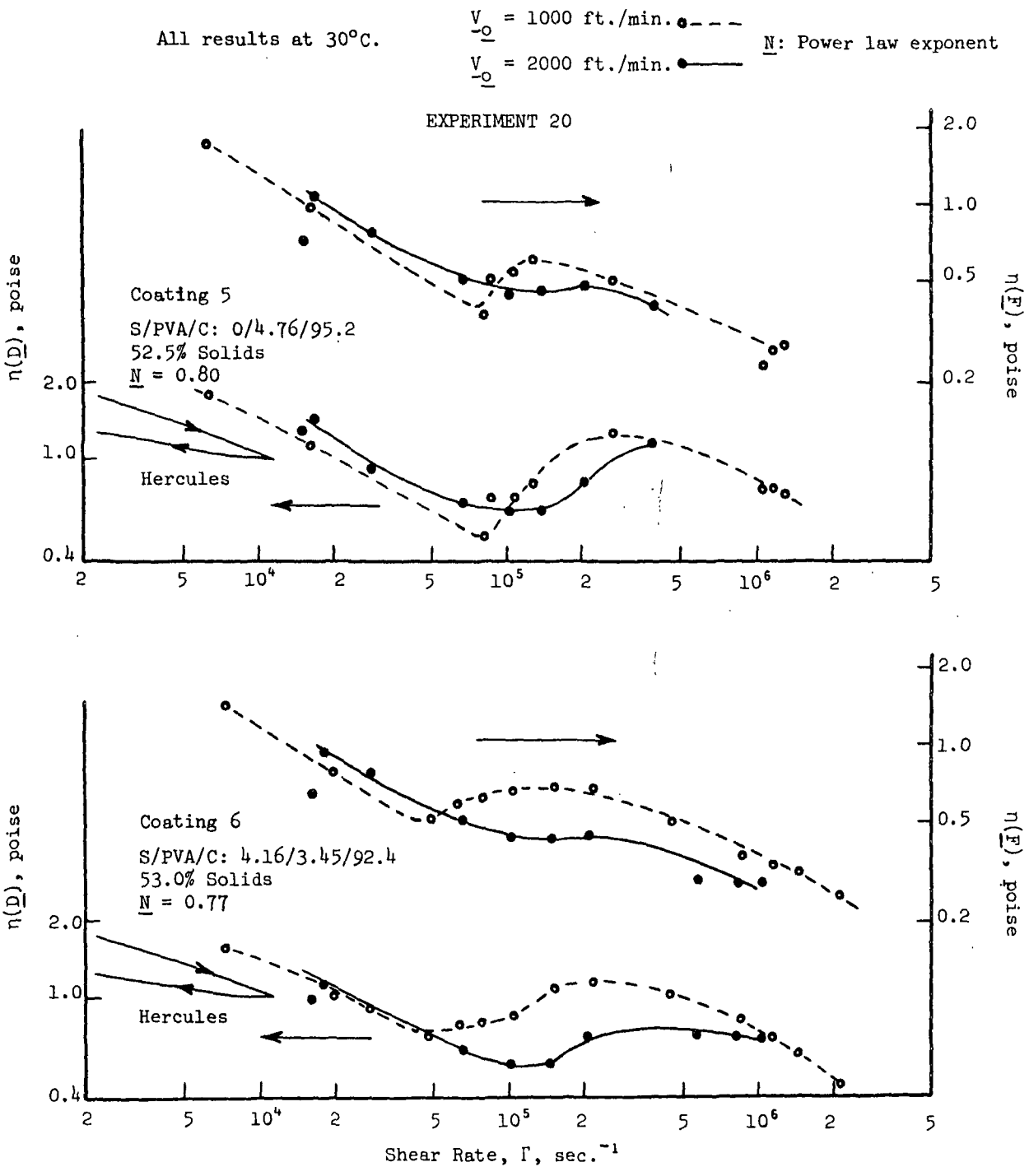

Figure 20A. Starch (S)-Polyvinyl Alcohol (PVA)-Clay (C) Coating Viscosities

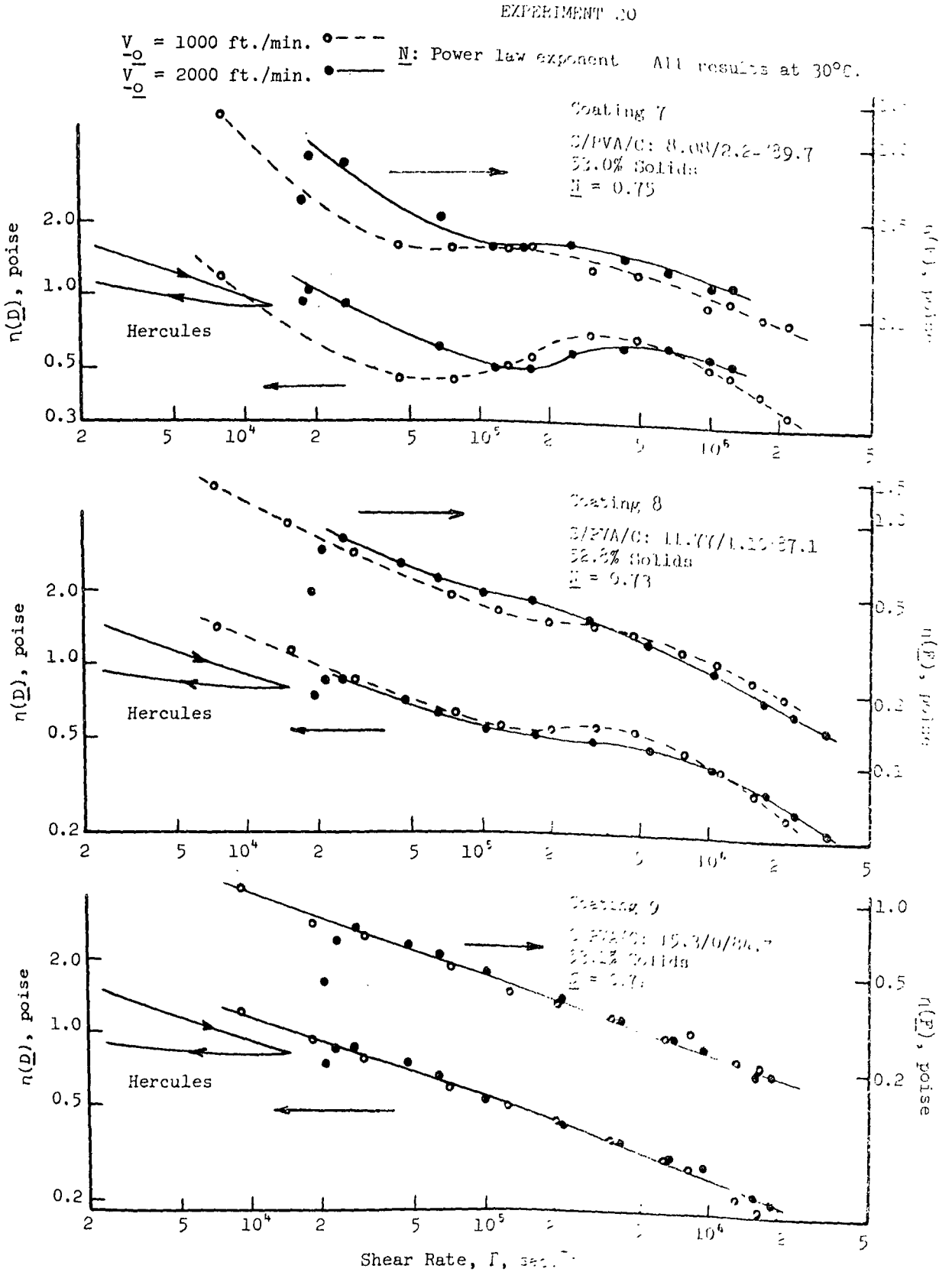

Figure 20A (cont'd). Starch (S)-Polyvinyl [illegible]-Clay [illegible] Coating Viscosities

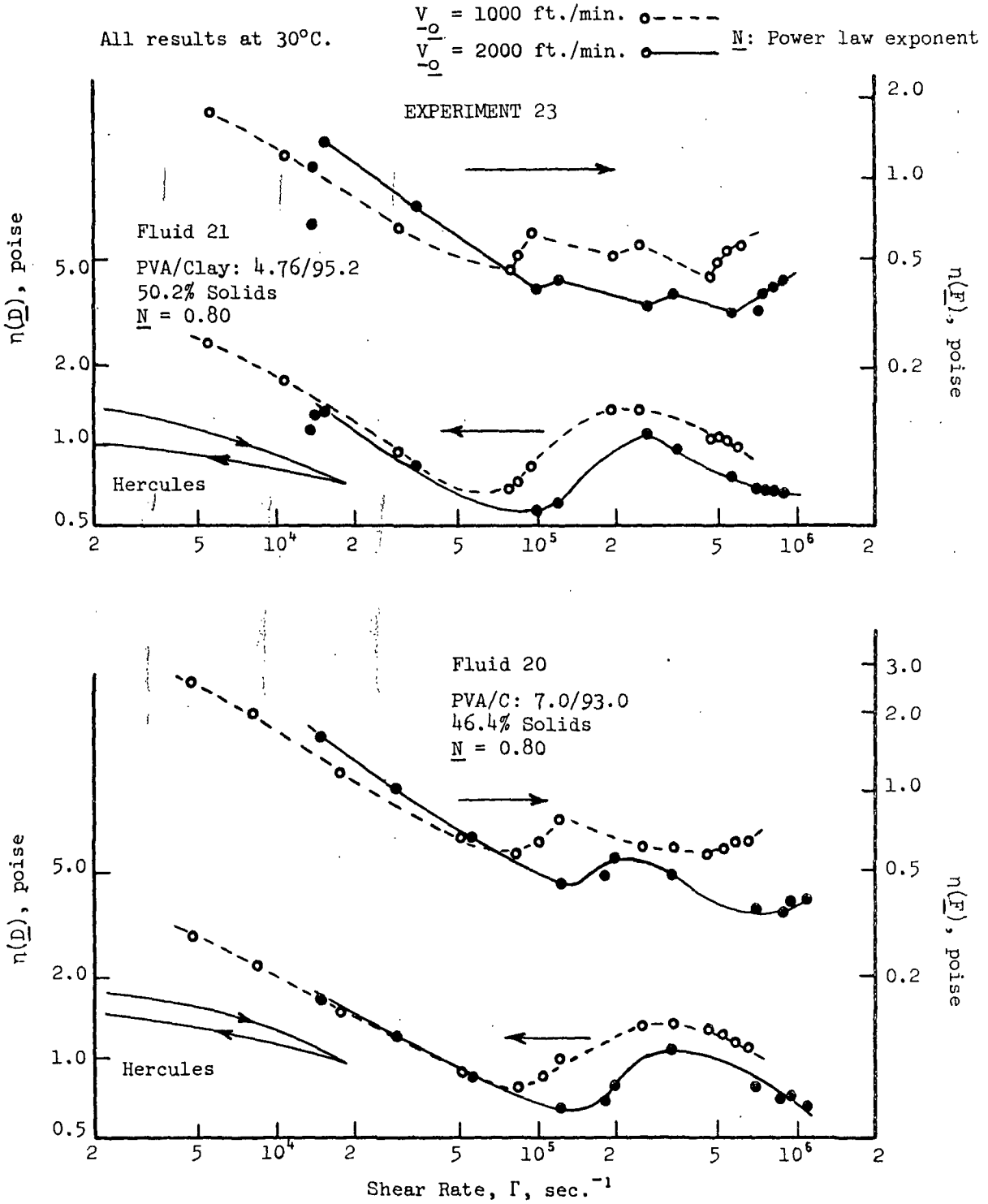

Figure 20B. Variation of Polyvinyl Alcohol (PVA)-Clay (C) Composition

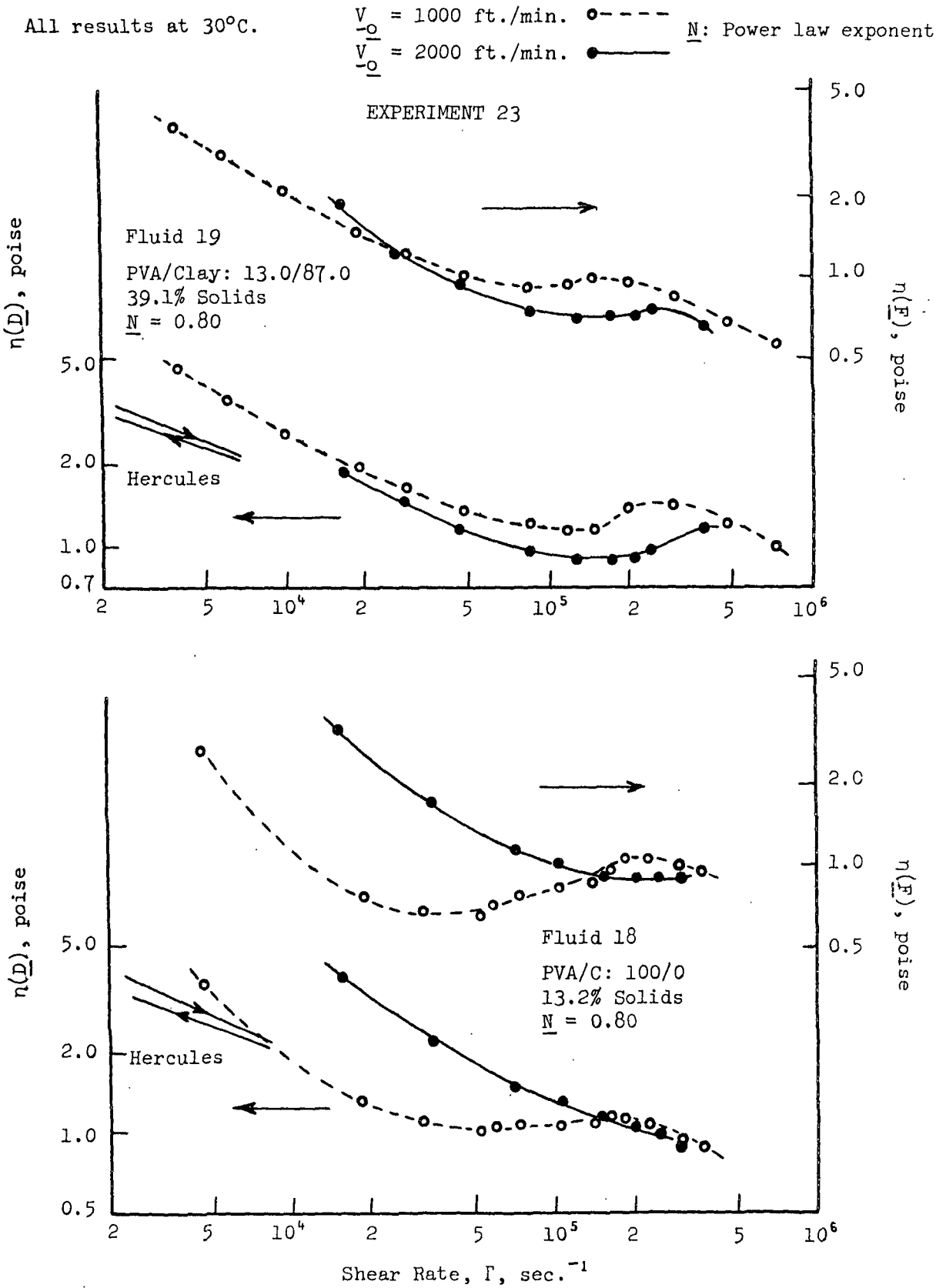

Figure 20B (cont'd). Variation of Polyvinyl Alcohol (PVA)-Clay (C) Composition

Since the function $\eta(\underline{F})$ does rise above what would be expected for the true viscosity, it would be useful to determine how well these curves conform to theory. Results were calculated of relative viscous and viscoelastic blade lift to be expected for fluids with viscous and viscoelastic power law behavior according to the following:

$$\tau \text{ (shear stress)} = K\,\Gamma|\Gamma|^{N-1}$$
$$p_{11}-p_{22} \text{ (first normal stress difference)} = K'\,(\Gamma^2)^{N'} \tag{30}$$

in which Γ is the shear rate, and $\underline{K}$ and $\underline{K}'$ are constant coefficients. The resulting ratios of viscoelastic to viscous blade lift, computed as $\underline{R}'$, is given in Fig. 21 as a function of $\underline{N}$, $\underline{N}'$, and film thickness under the blade tip, $\underline{h}_o$. The significance of $\underline{R}'$ is:

$$\frac{\text{Viscoelastic blade lift}}{\text{Viscous blade lift}} = R'^{*}\,\frac{(p_{11}-p_{22})}{\tau}\,. \tag{31}$$

Since there is a lack of knowledge of true fluid properties for the fluids tested in the Rheometer, some data of Kurath were tested (16). The data are for a PVA-water solution and appear to be of comparable viscosity as most of the fluids in Fig. 20A and 20B. The results of the calculations are given in Table XIV. It is apparent from the results that one would expect a rise in $\eta(\underline{F})$ as observed in the Rheometer results but not the subsequent decline observed at higher shear rates. Even if the normal stress data of Kurath are in error, and the value of $\underline{N}'$ is less than one, the qualitative results would be the same. The continual rise in $\eta(\underline{F})$ with shear rate is due to two factors; it has generally been found that normal stress increases with shear rate considerably more than shear stress for viscoelastic fluids, and the effect of an increase in $\underline{R}'$ with

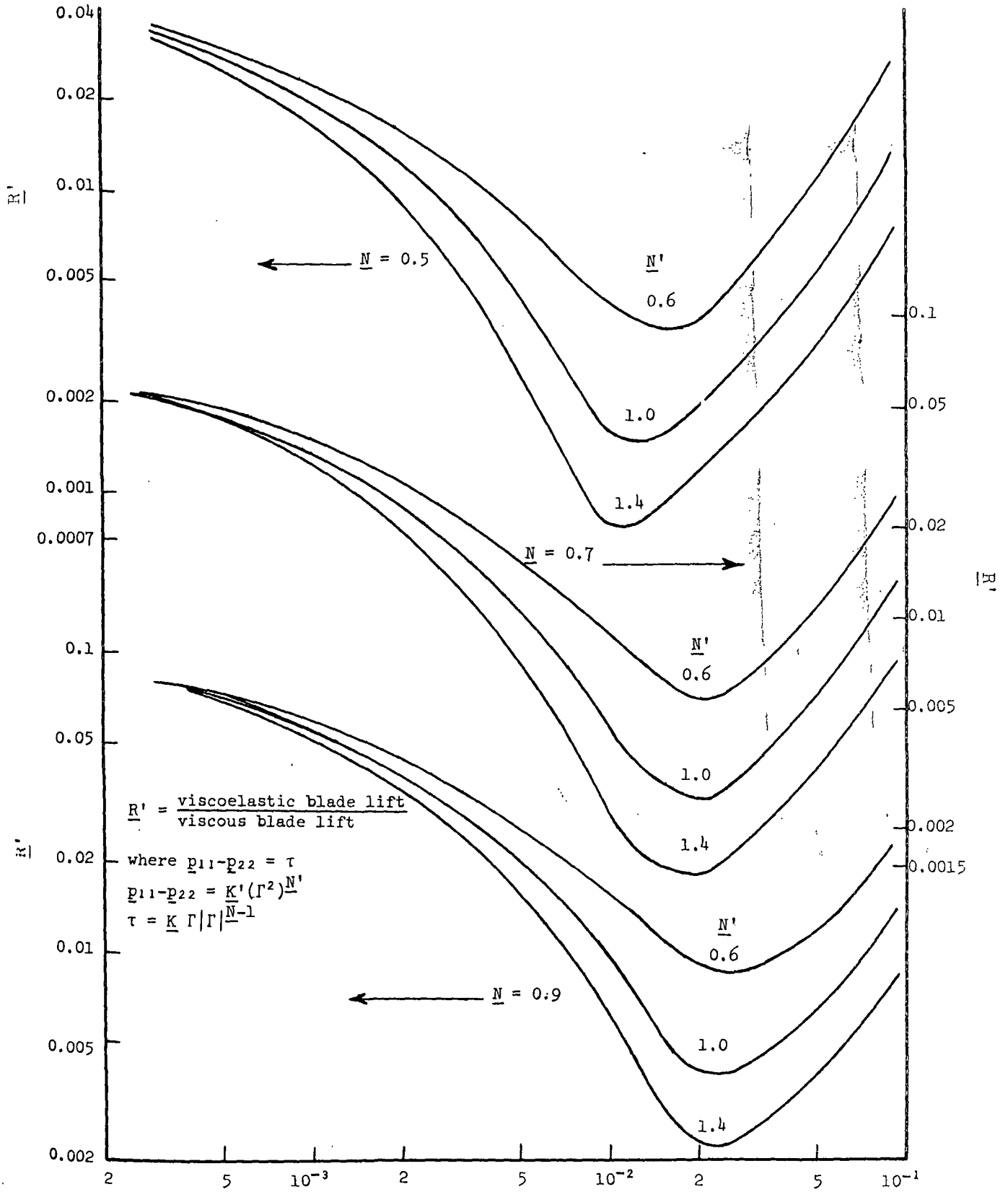

Figure 21. Relative Viscoelastic and Viscous Blade Lift (Theoretical)

TABLE XIV

PROJECTED VISCOELASTIC BLADE LIFT BASED ON DATA OF KURATH (16)

0.0712 G. Polyvinyl Alcohol/Ml. Soln., 25°C.

Shear Rate, Γ, sec.$^{-1}$	Shear Stress, τ, dynes/cm.^{2}	Viscosity, η, poise	Power Law Exponent, N	Normal Stress, $p_{11}-p_{22}$, dynes/cm.^{2}	$\frac{p_{11}-p_{22}}{\tau}$
2.5×10^4	2.2×10^4	0.88	0.82	1.7×10^5	7.7
5	3.7	0.74	0.75	6.7	18.1
1.0×10^5	6.2	0.62	0.65	2.7×10^6[a]	44.0
2	9.1	0.46	0.54	1.08×10^7[a]	118.0
4	1.32×10^5	0.33	0.54	4.3[a]	326.0
8	2.0	0.25	0.54	1.73×10^8[a]	860.0

Γ	h_o, cm.	R' (See Fig. 21)	$\frac{\text{Viscoelastic Blade Lift}}{\text{Viscous Blade Lift}}$	Apparent $\eta(F)$ / True Viscosity[b]
		V_o = 1000 ft./min.		
2.5×10^4	2.03×10^{-2}	0.0032	0.02	1.02
5	1.02	0.0052	0.09	1.09
1×10^5	5.1×10^{-3}	0.0088	0.39	1.39
2	2.54	0.0114	1.34	2.34
4	1.27	0.0197	6.4	7.4
8	6.4×10^{-4}	0.028	24.1	25.1
		V_o = 2000 ft./min.		
2.5×10^4	4.1×10^{-2}	0.0049	0.04	1.04
5	2.03	0.0028	0.05	1.05
1.0×10^5	1.02	0.0035	0.15	1.15
2	5.1×10^{-3}	0.0054	0.64	1.64
4	2.54	0.0114	3.7	4.7
8	1.27	0.0197	17.0	18.0

[a] Extrapolating Kurath's data which are of the form $p_{11}-p_{22} \alpha \Gamma^2$ (i.e., $N' = 1$).

[b] Equal to the total blade lift divided by the viscous blade lift.

decreasing $\underline{h}_o$ (increasing shear rate) is to increase the importance of the normal stress difference as shear rate increases.

The question arises then as to whether there is a normal stress function which behaves contrary to common experience for the fluids tested or whether the flow is changing. The answer is not certain, of course, but it appears probable that when viscoelastic behavior becomes dominant in nip flow there is an adjustment in the flow from viscometric flow. This question is of the greatest theoretical and practical importance and deserves more study in the future.

VARIATION OF STARCH-CLAY RATIOS

In Experiment 21, the effect of varying starch-clay ratios was investigated. The solids levels were adjusted to give results in comparable viscosity ranges. The results are presented in Fig. 22.

As one goes from the standard coating (No. 13) to the starch solution (No. 10), two changes are apparent. The difference between low shear Rheometer and Hercules viscosities decreases as the Hercules viscosity increases. This is characteristic of the apparent dampening effect of insufficient feed to the nips which has been discussed. The other change is that in going from the standard to the starch solutions there is a definite change in shape of the Rheometer curves. This is most obvious in the starch solution (No. 10). The viscosities show a decrease which changes to a leveling out and again a decrease, as shear rate increases. According to theory, viscoelasticity should affect only the $\eta(\underline{F})$ curve, but as seen in earlier discussions of PVA coatings, both curves are affected in the manner indicated. It is concluded that starch binders are marginally viscoelastic and affect the flow behavior in the particular geometry studied only under certain conditions.

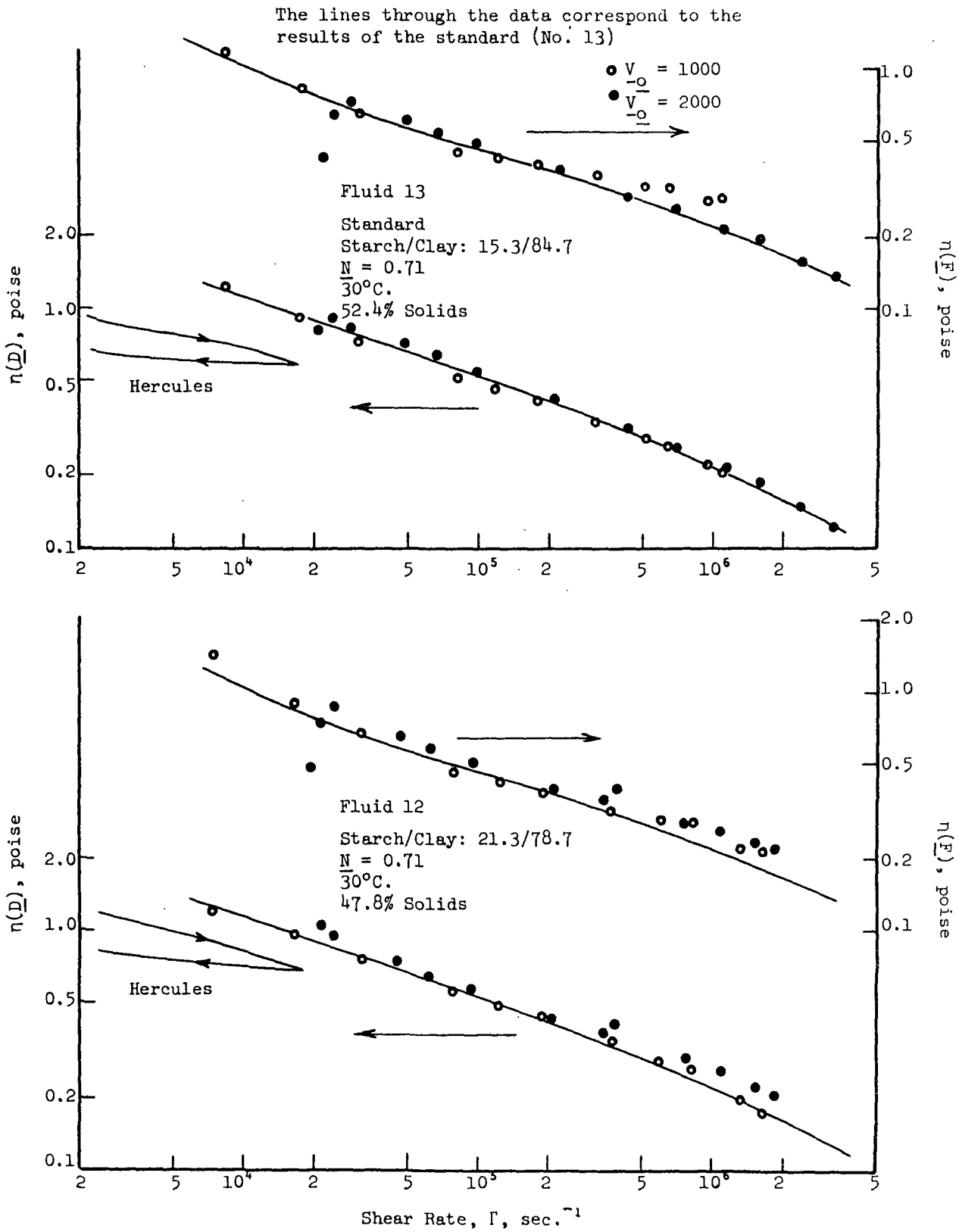

Figure 22. Effect of Starch-Clay Ratio

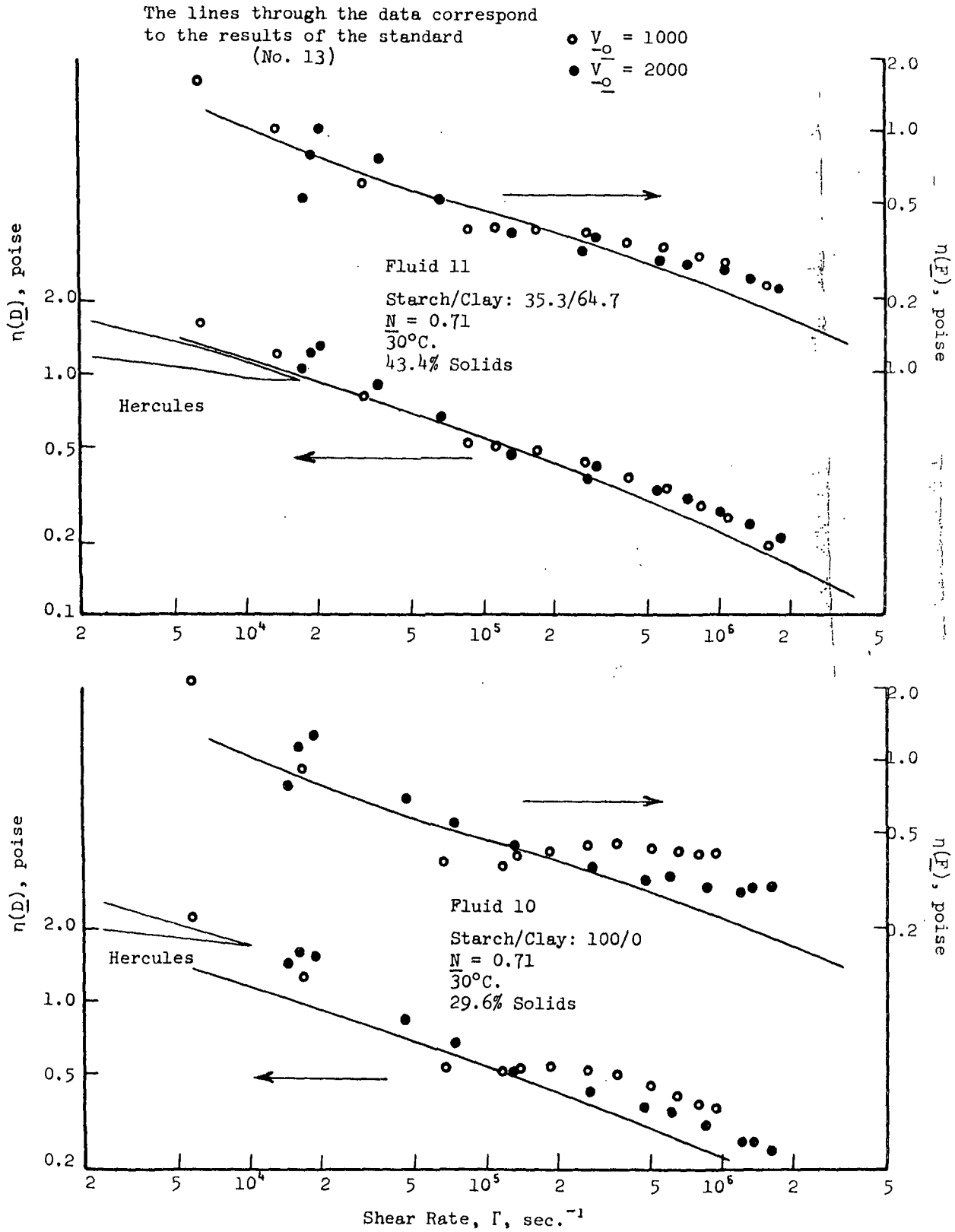

Figure 22 (cont'd). Effect of Starch-Clay Ratio

COMPARISON OF BINDERS IN CLAY COATINGS

Four widely different binders were compared with the same pigment. Coating 2 is polyvinyl alcohol and PVA-containing coatings are discussed elsewhere. The results for the other three binders are presented in Fig. 23.

The latex coating was apparently dilatant with a reverse thixotropy, according to the Hercules rheogram. It appears to be approximately Newtonian in the Rheometer results. An interesting point is the comparison of the Rheometer and Hercules viscosity at common shear rate. For most coatings, the Rheometer viscosity is higher, apparently because of the artificially low Hercules viscosity caused by thixotropic breakdown. The reverse seems to be valid here; the Rheometer viscosity is lower, apparently due to an artificially high Hercules viscosity caused by reverse thixotropic build-up.

At the time these tests were run, the results on protein binder appeared to indicate that protein and starch give the same general type of behavior. In retrospect, considering the consistency with which starch-clay results are reproduced, this may not be the case. If the protein results could be reproduced in another test, particularly the increase in $\eta(\underline{F})$ with shear rate at high shear rate it could indicate a viscoelastic effect.

COMPARISON OF PIGMENTS

Four pigments in the same binder were compared in Experiment 24. The solids level in each was adjusted to yield viscosities in the same general range. The results are presented in Fig. 24. In order to compare each coating with the standard, lines through the starch-clay results are imposed on each set of result

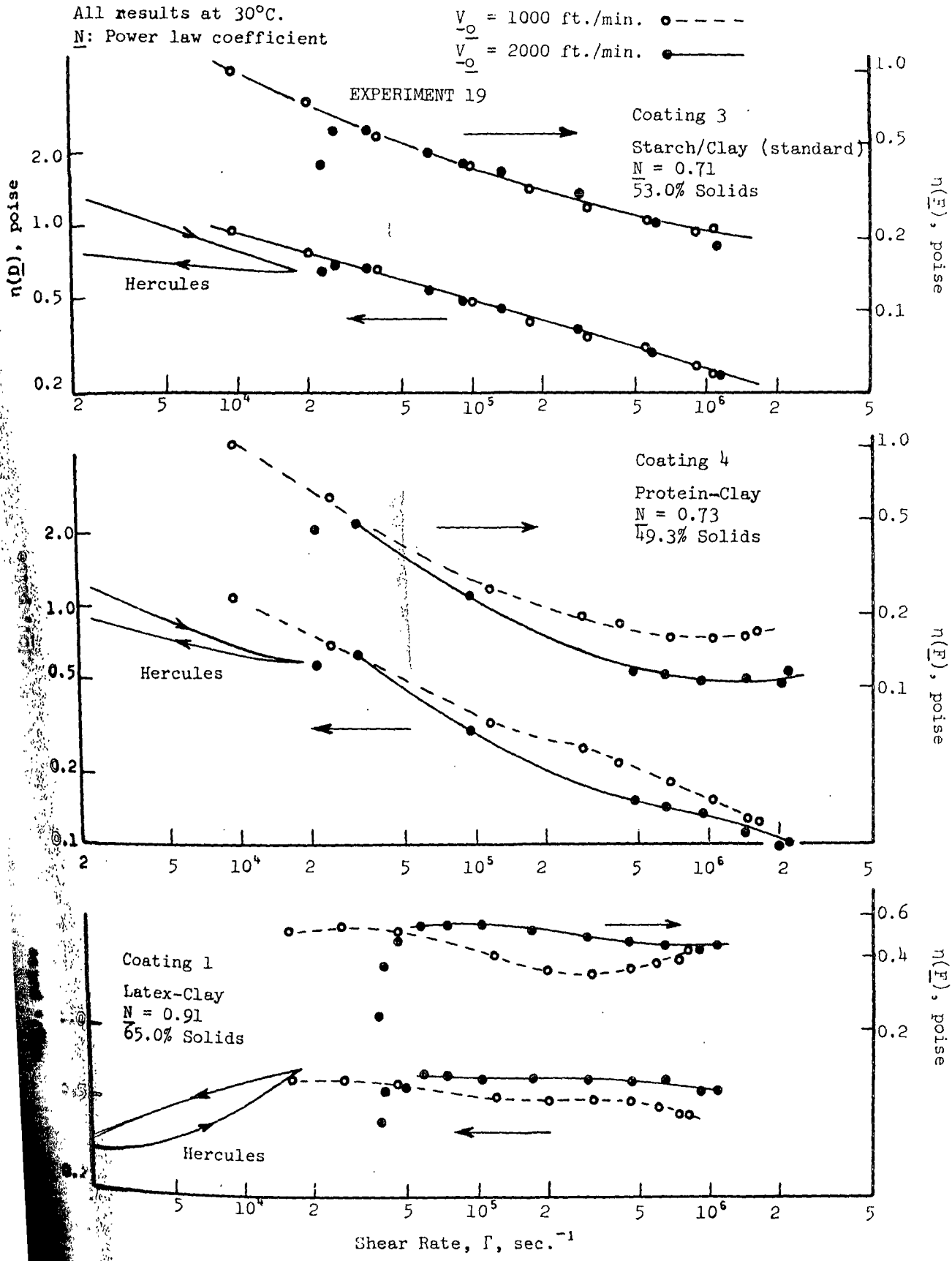

Figure 23. Comparison of Binders

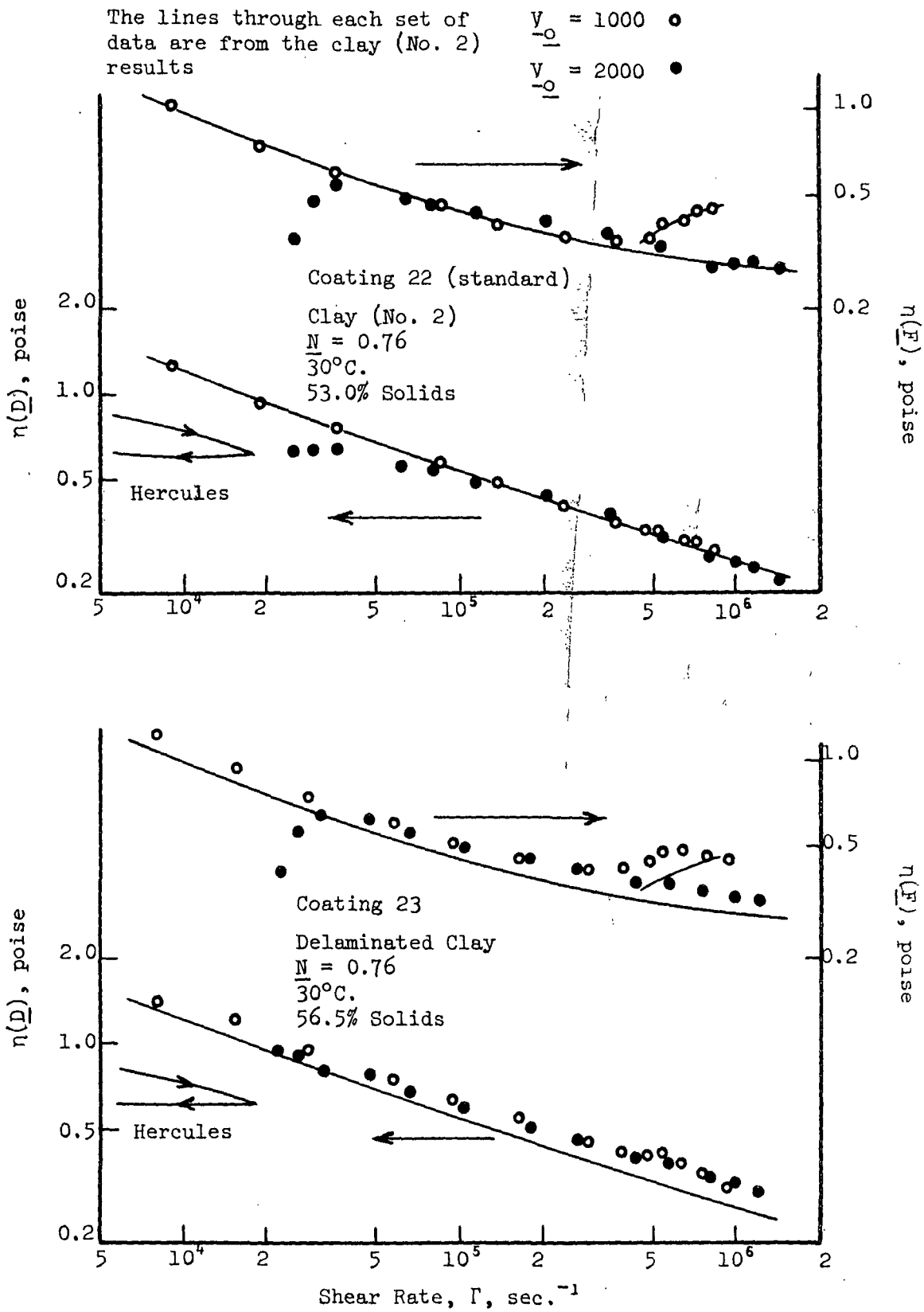

Figure 24. Comparison of Pigments with Starch Binder

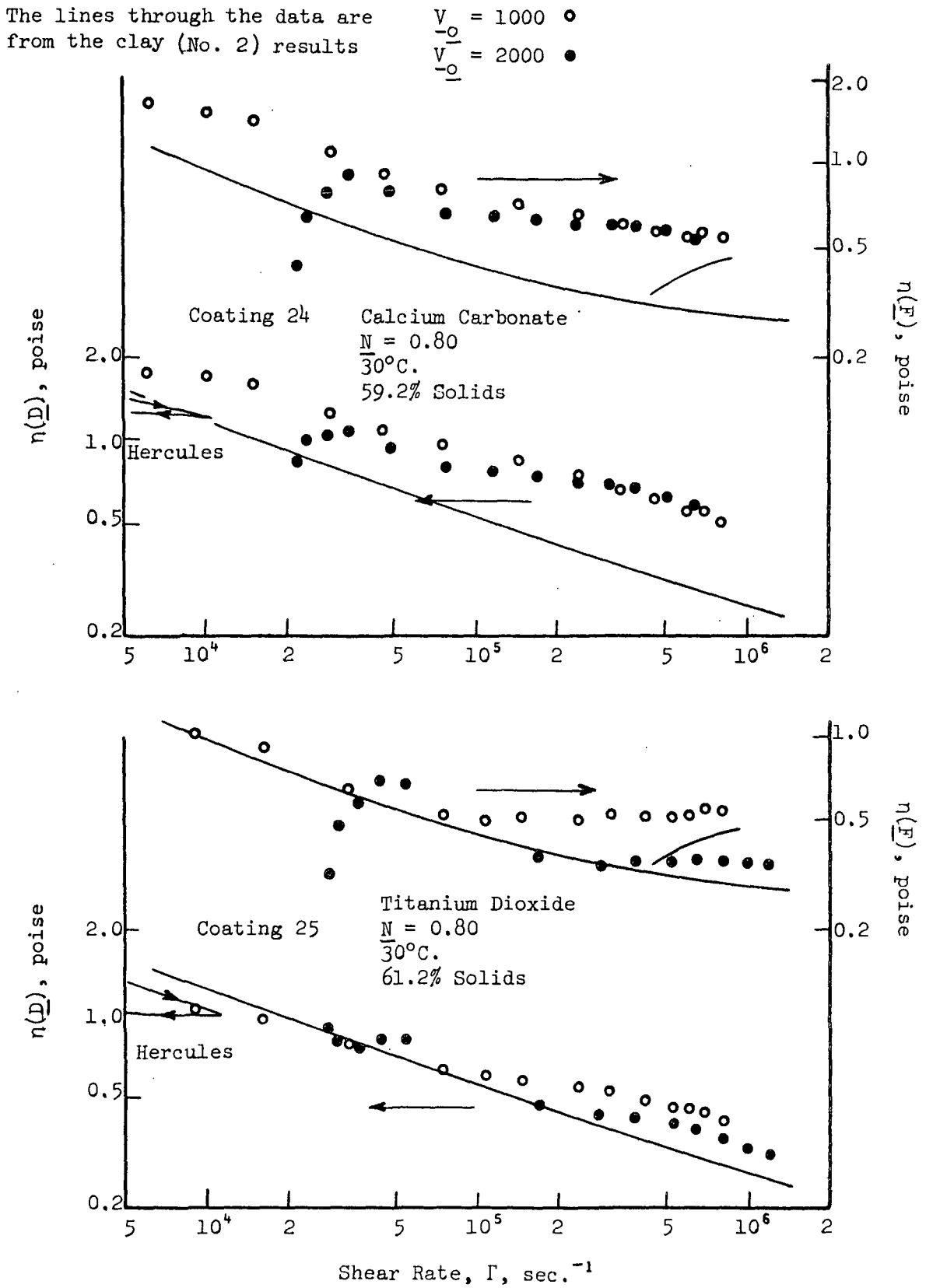

Figure 24 (cont'd). Comparison of Pigments with Starch Binder

The problem of feed rate to the nips has been previously discussed. Because of the importance of this phenomena in comparing different types of materials, the effect is summarized here. According to theory, there is an optimum feed rate to the nips; about 170-200 and 340-400 ml./sec. for $\underline{V}_o$ = 1000 and 2000 ft./min., respectively. Any lower feed rate should result in lower viscosity results. As can be seen from Fig. 14, for starch-clay results, the expected effect is low for high shear rates and high for low shear rates. The effect is greater for $\underline{V}_o$ = 2000 than for 1000 ft./min. The actual feed rate was measured only for the special Experiment 28, resulting in Fig. 14. It can only be presumed that the feed rate for each coating is a function of the viscosity at some unknown low shear rate. In comparing results of different coatings, the effect is probably greater for higher Hercules viscosity at high shear and greater thixotropic or shear thinning increase in viscosity with reduced shear rate.

Consider then the results of Fig. 24. Coating 22 is a standard and has been discussed before. Coating 23 is very similar to the standard. Coating 24 has a high viscosity at $\Gamma = 10^4$ sec.$^{-1}$ and might be expected to show small difference between Rheometer and Hercules results, but the effect of high viscosity is presumably offset by the relatively small shear thinning apparent. For Coating 25, both the viscosity and shear thinning are large and the comparable Hercules and Rheometer results at $\Gamma = 10^4$ is not surprising.

The increase in $\eta(\underline{F})$ for $\underline{V}_o$ = 1000 at high shear rate has been seen to be not characteristic of the standard coatings, and it is probable that this is not an indication of viscoelasticity.

The delaminated clay (No. 23) and the standard (No. 22) are obviously quite similar. The calcium carbonate (No. 24) shows similar behavior with

generally higher viscosity functions. Only the titanium dioxide (No. 25) shows a different type of behavior. However, if the low shear rate data are raised due to the abnormally large feed rate effect, these results would be qualitatively similar to the standard.

These results lend support to a general principle that the viscosity level is affected by the pigment but that the general mode of high shear flow behavior is most dependent on the type of binder.

RHEOMETER TESTING OF PLASTIC PIGMENT

In Experiment 26, coatings were prepared with starch and plastic pigment. The relative amounts of plastic pigment and starch were such that on a volume basis the starch/pigment ratios were the same as in the starch-clay standard coatings.

The experimental procedure for each coating was to test in the order V_o = 500, 1000, 2000, in each case increasing the blade load to the maximum and then reducing again to zero. The results are presented in Fig. 25. The lines through the data are from the standard coating, Fig. 18, for purposes of comparison.

In Table XV, the effects of change in percentage solids on Hercules and Rheometer viscosities are given. A theory describing the effect of insufficient feed to the nips was developed in the section on "The Effect of Feed Rate to the Nips on Starch-Clay Coating Viscosity," and it was seen that a starch-clay coating approximately fit the theory. An effect of feed rate on relative viscosities presumes that higher coating solids give lower pumping viscosity, which in turn leads to lower feed rate and lower experimental viscosity. The net effect is to dampen, or reduce, the change in experimental viscosity with a change in true viscosity.

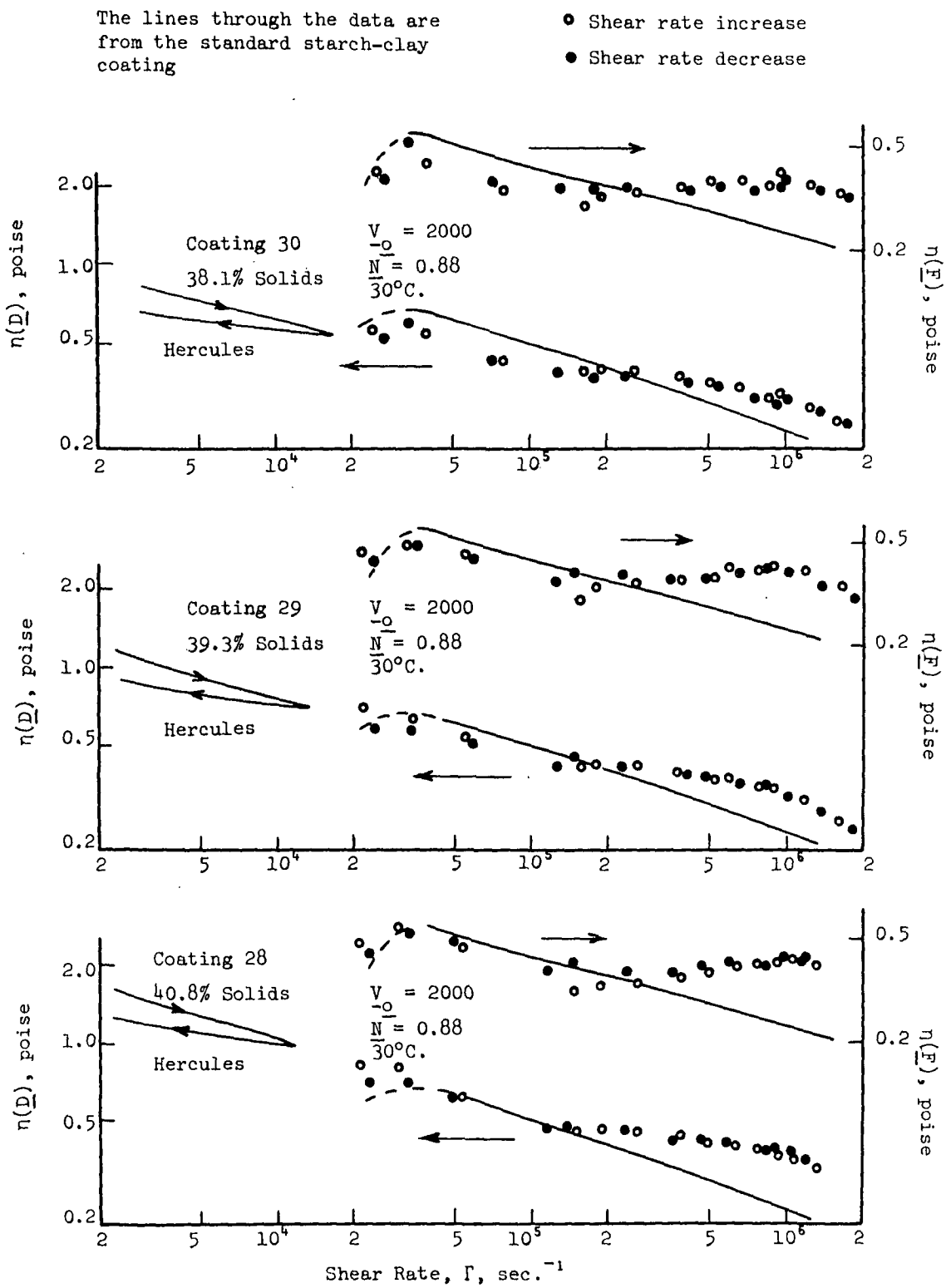

Figure 25. Starch-Plastic Pigment Results

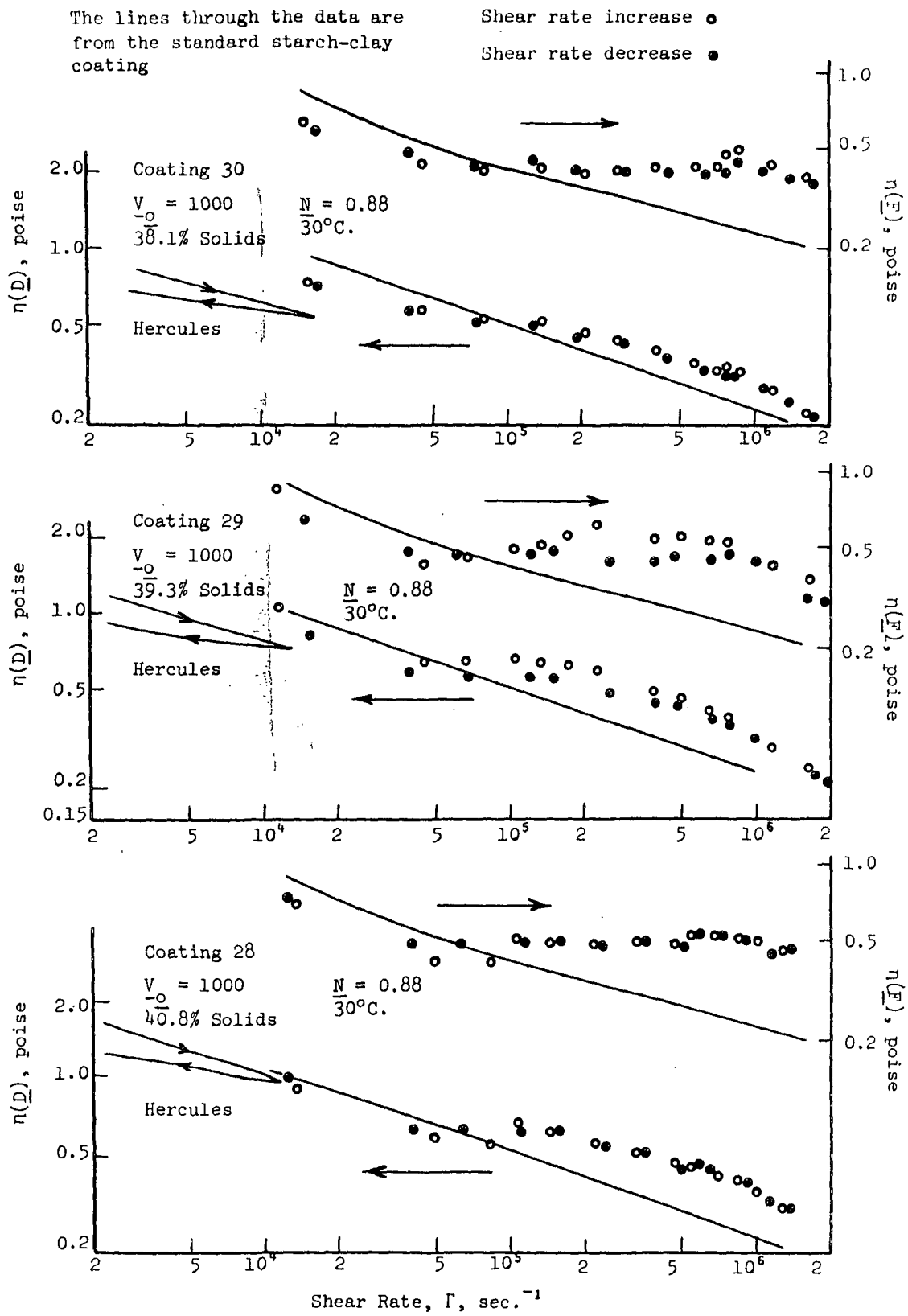

Figure 25 (cont'd). Starch-Plastic Pigment Results

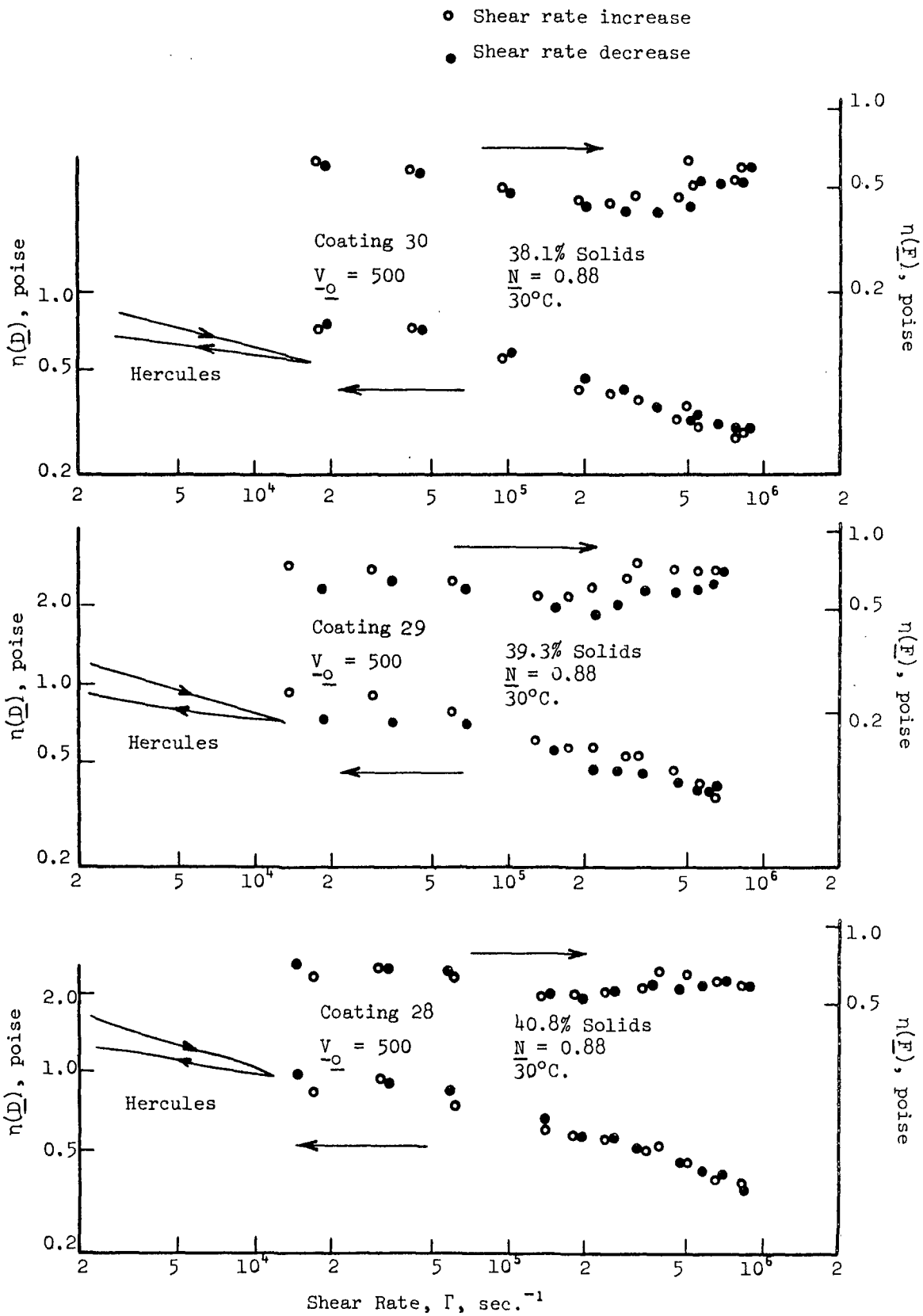

Figure 25 (cont'd). Starch-Plastic Pigment Results

TABLE XV

COMPARISON OF HERCULES AND RHEOMETER VISCOSITIES
FOR STARCH-PLASTIC PIGMENT

Coating		28	29	30	28	29	30
Percent Solids		40.8	39.3	38.1	40.8	39.3	38.1
		Viscosity, poise			Viscosity/Av. Viscosity		
Hercules "Up" Curve $\Gamma = 10^4$, sec.$^{-1}$		1.07	0.78	0.61	1.31	0.95	0.74
Rheometer:							
$\underline{V}_o$, ft./min.	Γ, sec.$^{-1}$	$\eta(\underline{D})$, poise			$\eta(\underline{D})/\eta(\underline{D})_{average}$		
500	2×10^4	0.92	0.86	0.74	1.10	1.02	0.88
	2×10^5	0.71	0.66	0.58	1.09	1.02	0.89
	2×10^6	0.35	0.34	0.27	1.09	1.06	0.84
1000	2×10^4	0.76	0.75	0.68	1.04	1.03	0.93
	2×10^5	0.60	0.60	0.52	1.05	1.05	0.91
	2×10^6	0.36	0.32	0.29	1.12	0.99	0.90
2000	2×10^5	0.48	0.44	0.42	1.08	0.99	0.94
	2×10^6	0.36	0.32	0.31	1.09	0.97	0.94

Application of the theory to the results in Table XV leads to the following very approximate conclusions:

(1) There should be no effect on the relative values at $\underline{V}_o = 500$.

(2) There could be a small reduction in the change of viscosity at $\underline{V}_o = 1000$ and high shear rate.

(3) There could be a small to moderate reduction in the change of viscosity at $\underline{V}_o = 1000$ and low shear rate, and at $\underline{V}_o = 2000$ and high shear rate.

(4) There could be a larger reduction in viscosity change with percent solids change at $\underline{V}_o = 2000$ and low shear rate.

In a very general way these changes are observed in Table XV. However, in no case is the change in viscosity with shear rate nearly as great as that seen with the Hercules results. Two possibilities arise: the theory needs refinement and there is in fact a dampening effect in all cases, or the change in percent solids gives a greater change in Hercules viscosity than Rheometer viscosity. The latter explanation would depend on different relative changes in thixotropic breakdown for the two instruments. Further resolution of this problem must wait for refinement of the Rheometer technique to avoid the feed rate problem altogether.

It is apparent from Fig. 25 that the curves for starch-plastic pigment differ from the standard starch-clay. It is also apparent in comparing these results with those obtained with polyvinyl alcohol (PVA) that these coatings are viscoelastic. The apparent level of elasticity is less than the coatings with high levels of PVA. In both these coatings and those with PVA, both $\eta(\underline{D})$ and $\eta(\underline{F})$ curves are affected by elasticity. In contrast with the PVA fluids, the $\eta(\underline{F})$ curves appear to be more affected than the $\eta(\underline{D})$ curves.

An interesting question concerns the contribution of plastic pigment to viscoelasticity. Does the plastic pigment contribute to elasticity or just alter the starch contribution? That plastic pigment and clay act differently on starch is apparent in the fact that, with the same starch-pigment volume ratio, the solid volume fraction of comparable viscosity coatings is higher with plastic pigment. In Table XVI, various plastic pigment and clay coatings are compared for volume composition and viscoelastic behavior. Apparently, the viscoelastic effect is not simply one of starch volume fraction in the coating or in the starch-water part of the coating. The rheological behavior of plastic pigments compared with mineral pigments deserves more study in future work.

TABLE XVI

RELATIVE VOLUMETRIC BINDER-PIGMENT-WATER VALUES AND VISCOELASTICITY

Coating	Pigment	Volume, %			Volume Ratio, starch/water	Viscoelastic Behavior
		Starch	Pigment	Water		
28	Plastic	8.9	28.5	62.6	0.142	Yes
29	Plastic	8.6	27.4	64.0	0.134	Yes
30	Plastic	8.3	26.5	65.2	0.127	Yes
Standard	Clay	7.8	24.8	67.4	0.116	No
12	Clay	9.2	19.7	71.1	0.129	No
11	Clay	13.2	13.9	72.9	0.181	Slight
10	Clay	21.8	0	78.2	0.279	Yes

THE EFFECT OF ADDITIVES ON STARCH-CLAY COATINGS

The results of these tests are presented in Fig. 26. The only major effect of the additives is the obvious one of changing the viscosity level. The feed rate damping effect already discussed would appear to be responsible for the fact that the low shear Rheometer viscosities are comparable, even though the Hercules results show considerable variation. However, in contrast to the starch results considered earlier, there appears to be no trend in the high-shear Rheometer viscosities to conform to the differences between Hercules results. This may be a real effect of the additives or may be due to random variations in the results.

The only additive that gives an indication of changing the basic nature of the coating rheology is calcium stearate (No. 14). The leveling out and subsequent decrease in viscosities observed on the figure is characteristic of viscoelastic behavior, as was seen earlier. The effect is marginal and may be real or may be due to natural variation in the results.

The lines through the data are for the coating with no additive (No. 17)

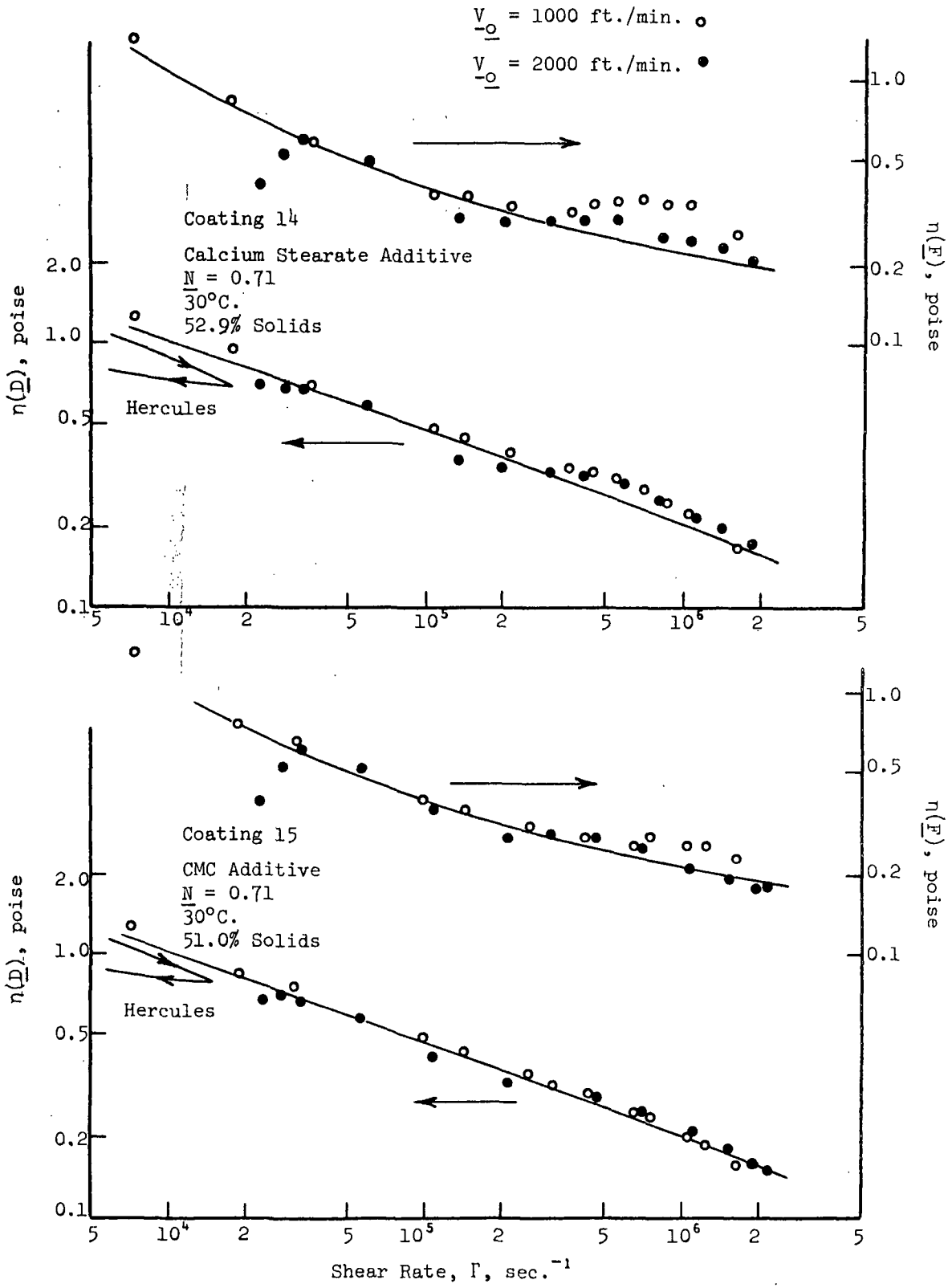

Figure 26. Effect of Additives in Starch-Clay Coatings

The lines through the data are for the coating with no additive (No. 17)

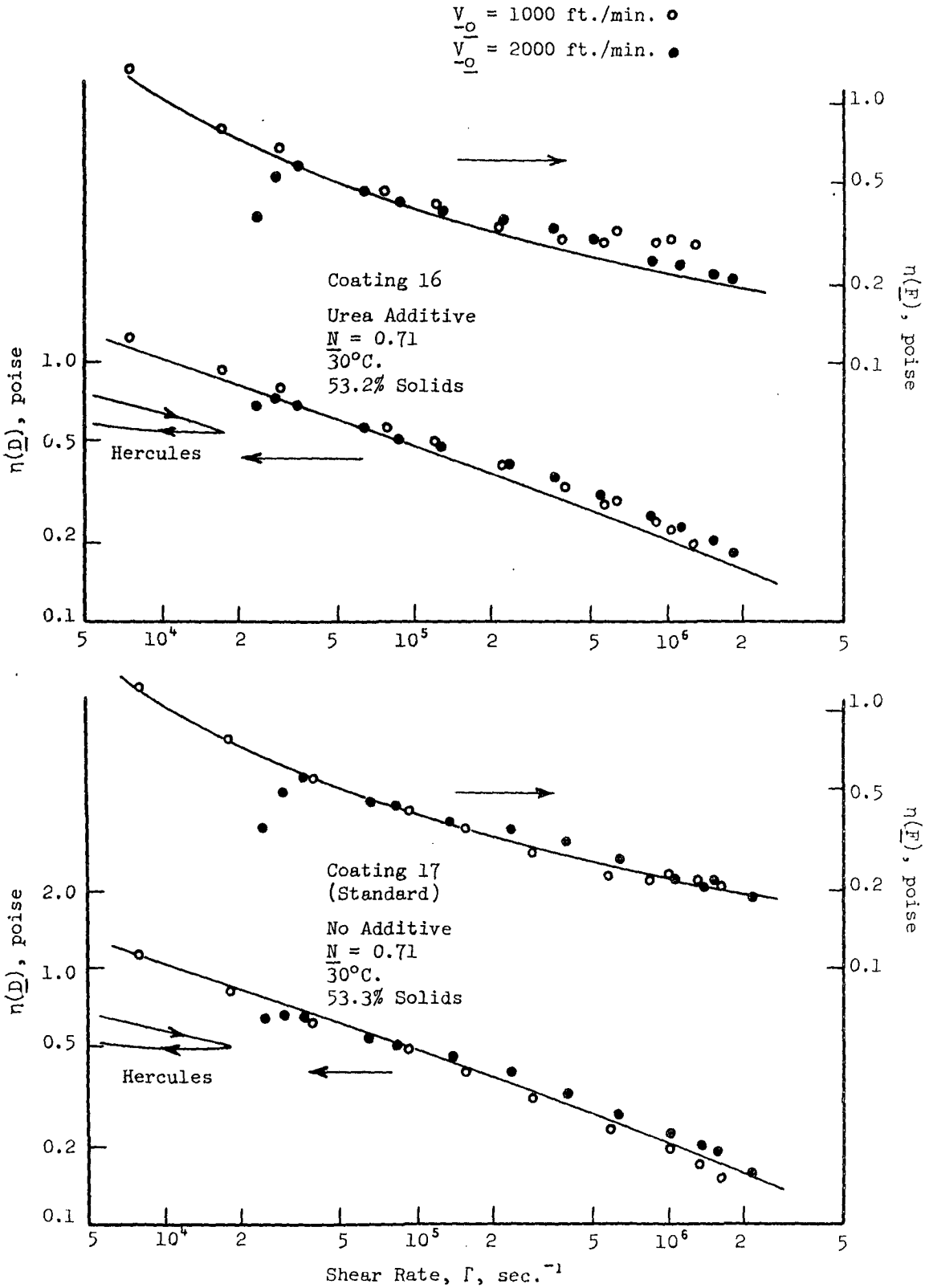

Figure 26 (cont'd). Effect of Additives in Starch-Clay Coatings

LITERATURE CITED

1. Follette, W. J., and Fowells, R. W. Operating variables of a blade coater. Tappi 43:953-7(1960).

2. Clark, N. O., Windle, W., and Restall, C. A. The helicoater — a novel approach to a study of the problems of blade coating machines. Paper Trade J. 150(38):49-54(1966).

3. Modrak, J. P. Effect of coating color rheology on the blade coating process. TAPPI Coating Conference, Miami, Fla., 1973.

4. Hayward, G. Factors affecting the metering characteristics of a blade coater. TAPPI Coating Conference, Miami, Fla., 1973.

5. Windle, W., and Beazley, K. M. The mechanics of blade coating. Tappi 50:1-7 (1967).

6. Windle, W., and Beazley, K. M. The role of viscoelasticity in blade coating. Tappi 51:340-8(1968).

7. Bohmer, E. Shear rates developed in trailing blade coaters. Svensk Papperstid. 67:347-55(1964).

8. Bliesner, W. C. Basic mechanisms in blade coating. Tappi 54:1673-9(1971).

9. Turai, L. L. Analysis of the blade coating process. Tappi 54:1315-18(1971).

10. Turai, L. L. Note to the Editor: Analysis of the blade coating process: response. Tappi 55:262(1972).

11. Ginn, R. F. Note to the Editor: Analysis of the blade coating process: comment. Tappi 55:262(1972).

12. Draper, M. R., and Smith, H. Applied regression in analysis. New York, John Wiley & Sons, Inc., 1966.

13. Smith, J. W., Trelfa, R. T., and Ware, H. O. Casein adhesives in roll coating. Tappi 33:212-18(1950).

14. Metzner, A. B. The significant rheological characteristics of lubricants. Paper No. 68-LRh-2, Presented at the ASME-ASLE, ASTM Symposium on Lubrication and Lubrication Rheology, Ann Arbor, Mich., March 18-20, 1968.

15. Metzner, A. B., and Metzner, A. P. Stress levels in rapid extensional flows of polymeric fluids. Rheol. Acta 9(2):174-81(1970).

16. Kurath, S. F. A jet viscometer for the study of coating colors at high shear rates. Tappi 52:92-9(1969).

17. Flumerfelt, R. W., Pierick, M. W., Cooper, S. L., and Bird, R. B. Generalized plane Couette flow of a non-Newtonian fluid. I&EC Fundamentals 8(2):354-7 (1969).

18. Metzner, A. B., Houghton, W. T., Sailor, R. A., and White, J. L. A method for the measurement of normal stresses in simple shearing flow. Trans. Soc. Rheology 5:133-47(1961).

19. Ginn, R. F. The measurement of normal stresses in viscoelastic fluids. M.Ch.E. Thesis, Univ. of Delaware, Newark, Delaware, 1963.

20. Han, C. D., Charles, M., and Philippoff, W. Rheological implications of the exit pressure and die swell in steady capillary flow of polymer melts. I. The primary normal stress difference and the effect of L/D ratio on elastic properties. Trans. Soc. Rheology 14(3):393-408(1970).

21. Middleman, S. The flow of high polymers. New York, Interscience, 1968.

22. McAdams, W. H. Heat transmission by conduction and convection. In Chemical Engineers' Handbook. J. H. Perry, Editor. 3rd ed. New York, McGraw-Hill, Inc., 1950.

THE INSTITUTE OF PAPER CHEMISTRY

Robert F. Ginn
Research Fellow
Division of Natural
Materials & Systems

Robert M. Leekley
Senior Research Associate
Division of Natural
Materials & Systems

APPENDIX I

GENERAL MATHEMATICAL OPERATIONS

INTRODUCTION

On several occasions in this work it has been necessary to solve differential equations over lines or surfaces. To avoid repetition, the general approach to such solutions is given here.

SURFACE GRIDS FOR THE BLADE NIP

In solving a differential equation over a surface, the surface is laid out in a grid; the equation is then solved as a difference equation at each point of the grid. Normally, it is desirable to make the interval sizes constant in a given coordinate direction, but because of the geometry of the blade nip this is impractical under the blade surface. Figure 27 illustrates the blade nip grid for two sets of coordinates. For calculations along a line, the grid is one dimensional instead of two.

DIFFERENTIALS AND INTEGRALS

Consider a variable f defined at three points on a line in the x direction, as shown in Fig. 28.

Expressing f as a quadratic function of x:

$$f = a + b\,x + c\,x^2. \tag{32}$$

The coefficients of Equation (32) are determined to be the following functions of the given values of f and the grid intervals:

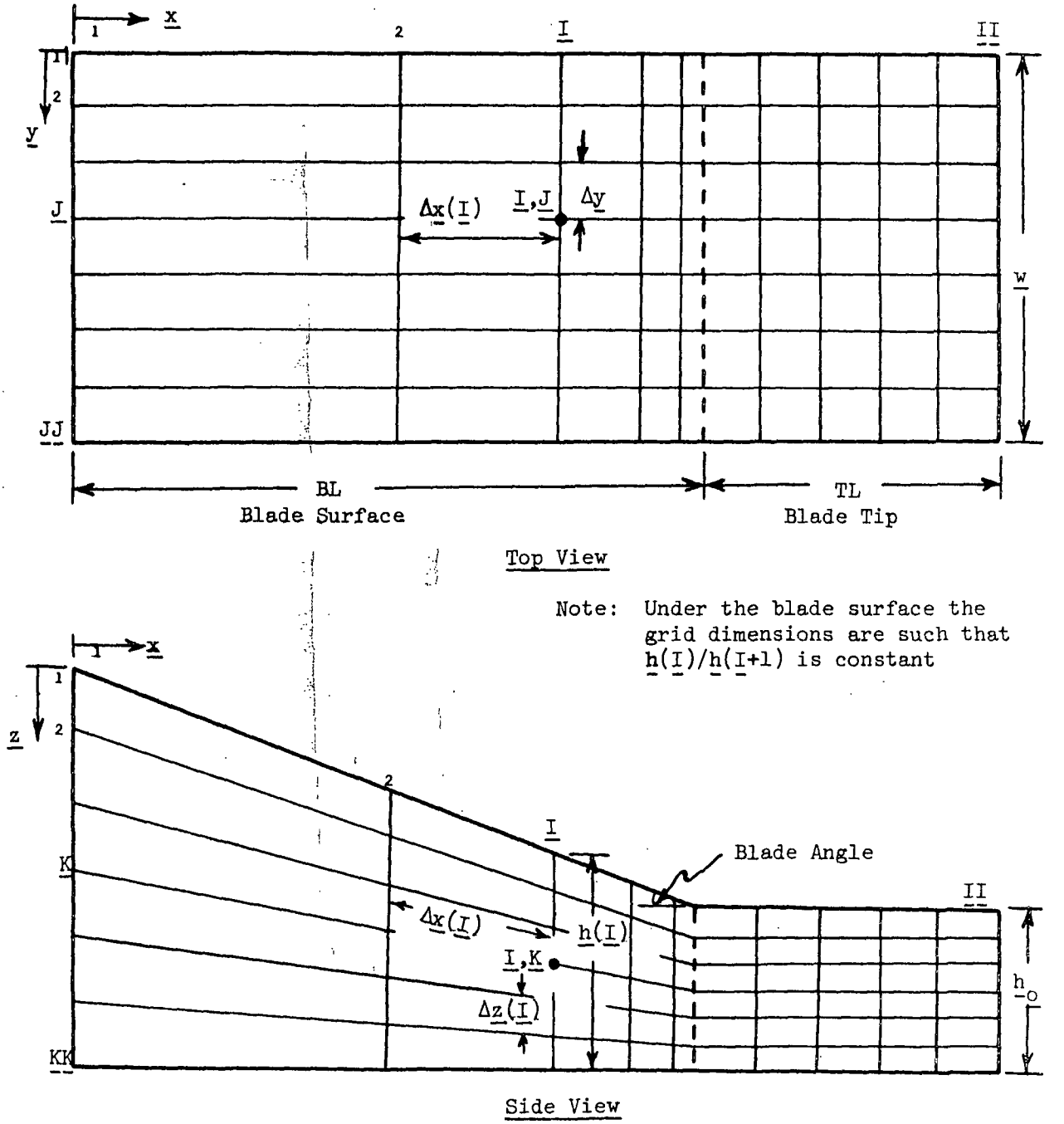

Figure 27. Blade Nip Grid

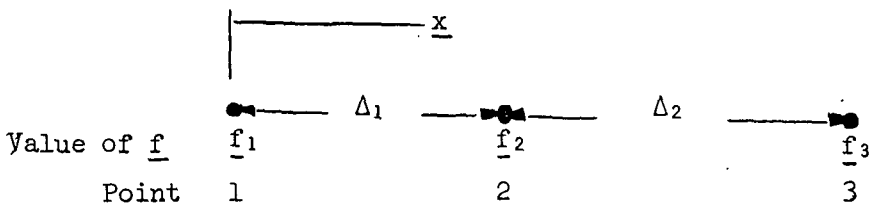

Figure 28. A Variable Defined at Three Grid Points on a Line

$$\left.\begin{aligned} a &= f_1 \\ b &= -\frac{2\Delta_1+\Delta_2}{\Delta_1(\Delta_1+\Delta_2)} f_1 + \frac{\Delta_1+\Delta_2}{\Delta_1\,\Delta_2} f_2 - \frac{\Delta_1}{\Delta_2(\Delta_1+\Delta_2)} f_3 \\ c &= \frac{1}{\Delta_1(\Delta_1+\Delta_2)} f_1 - \frac{1}{\Delta_1\,\Delta_2} f_2 + \frac{1}{\Delta_2(\Delta_1+\Delta_2)} f_3. \end{aligned}\right\} \qquad (33)$$

The differentials of $\underline{f}$ are:

$$\left.\begin{aligned} \partial f/\partial x &= b && \text{at point 1} \\ &= b + 2\,c\,\Delta_1 && \text{at point 2} \\ &= b + 2\,c\,(\Delta_1 + \Delta_2) && \text{at point 3} \end{aligned}\right\} \qquad (34)$$

$$\partial^2 f/\partial x^2 = 2\,c \qquad \text{at all points.} \qquad (35)$$

If $\underline{f}$ is considered the integrand, single integrals are given by:

$$\left.\begin{aligned} \int_0^{\Delta_1} f\,dx &= a\,\Delta_1 + b\,\Delta_1^2/2 + c\,\Delta_1^3/3 \\ \int_0^{\Delta_1+\Delta_2} f\,dx &= a(\Delta_1+\Delta_2) + b(\Delta_1+\Delta_2)^2/2 + c(\Delta_1+\Delta_2)^3/3. \end{aligned}\right\} \qquad (36)$$

Double integrals are determined similarly, with the inner integral being solved and then used as the integrand for the outer integral. For example:

$$\int_{0}^{\Delta_1+\Delta_2} \int_{-\alpha}^{x} f \, dx \, dx = \int_{0}^{\Delta_1+\Delta_2} g(x) \, dx. \tag{37}$$

The values of g corresponding to f_1, f_2, and f_3 of Fig. 28 are:

$$g_1 = \int_{-\alpha}^{0} f \, dx, \; g_2 = \int_{-\alpha}^{\Delta_1} f \, dx, \; g_3 = \int_{-\alpha}^{\Delta_1+\Delta_2} f \, dx. \tag{38}$$

TRIAL AND ERROR SOLUTION OF A TWO-DIMENSIONAL PROBLEM

As an example, consider the solution of Equation (39) in the x-y plane of Fig. 27.

$$\partial f/\partial x + C_1 \, \partial^2 f/\partial x^2 + C_2 \, \partial^2 f/\partial y^2 = C_3. \tag{39}$$

With boundary conditions:

$$\left.\begin{aligned} f(0,y) &= 0 \\ f(BL+TL) &= C_4 \\ f(x,0) &= 0 \\ \partial f/\partial y(x,w) &= C_5 \end{aligned}\right\} \tag{40}$$

in which C_1, C_2, C_3, C_4, and C_5 are constants. The following steps are followed in obtaining a solution for the equation.

Initial Values of f

To assure convergence to a solution in minimum time, "reasonable" initial values of f over $I = 2,II$; $J = 2,JJ+1$ should be set. The manner of setting

reasonable initial values depends on the problem, and may result from simplification of the equation or intuitive physical reasoning.

Determination of f at a Point

Equation (39) is solved at all points on the grid except where boundary values are given. In the general case of J ≠ JJ+1 the solution is as follows:

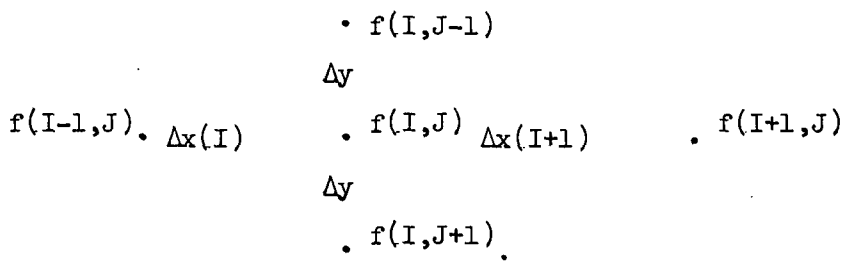

The differentials $\partial f/\partial x$ and $\partial^2 f/\partial x^2$ are determined as described earlier, in which:

$$\left.\begin{aligned} \Delta_1 &= \Delta x(I) \\ \Delta_2 &= \Delta x(I+1) \\ f_1 &= f(I-1,J) \\ f_2 &= f(I,J) \\ f_3 &= f(I+1,J). \end{aligned}\right\} \qquad (41)$$

The differential $\partial^2 f/\partial y^2$ is determined as described earlier, in which:

$$\left.\begin{aligned} \Delta_1 &= \Delta_2 = \Delta y \\ f_1 &= f(I,J-1) \\ f_2 &= f(I,J) \\ f_3 &= f(I,J+1). \end{aligned}\right\} \qquad (42)$$

These results are combined in Equation (39) and the resulting equation is solved for the unknown $f(I,J)$.

On the boundary $J = JJ+1$ the solution is similar to the general case except $f_1 = f_3 = f(I,JJ)$ is used to evaluate $\partial^2 f/\partial y^2$.

The Weighting Factor (W.F.)

To avoid failure of convergence to a solution or promote a more rapid convergence, the calculated value of $f(I,J)$ determined in the preceding section is weighted with the previous value as follows:

$$f(I,J)_{new} = f(I,J)_{previous} + W.F.[f(I,J)_{calculated} - f(I,J)_{previous}]. \quad (43)$$

For all equations considered in this work, W.F. was determined by trial and error.

Test of $f(I,J)$

At each point I,J, f is tested with the previous value and the change is considered error. After all points I,J have been covered, the maximum error is tested with an arbitrary standard. If the error is greater than the standard, the calculations are repeated over all points I,J. If the error is less than the standard, the solution is considered correct.

SEMIPROGRESSIVE SOLUTION OF A TWO DIMENSIONAL PROBLEM

Consider the solution of Equation (39) in which the second boundary condition is changed to:

$$\partial^2 f/\partial x^2 = (0,y) = 0. \quad (44)$$

General Solution on a Line $I \geq 2$

At an arbitrary point I,J on line I, the pertinent values of f and intervals are:

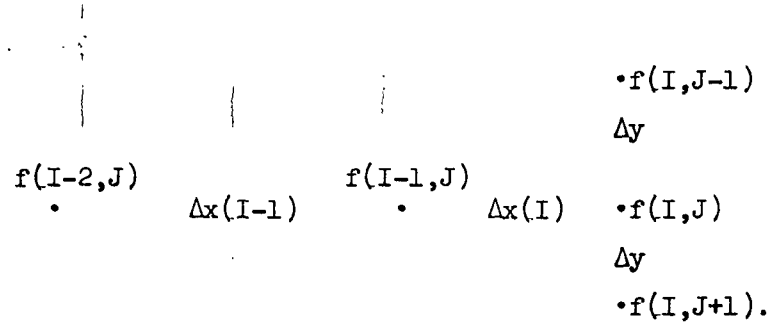

The differentials $\partial f/\partial x$, $\partial^2 f/\partial x^2$, and $\partial^2 f/\partial y^2$ are determined according to the procedures given under Differentials and Integrals (p. 110). Note that the third equation of Equation (34) is used for $\partial f/\partial x$. These results are then substituted into Equation (39) to determine a new value of $f(I,J)$, using the weighting factor described in the Trial and Error Solution (p. 113). This procedure is repeated over all points J on the line I, noting the special case on point $J = JJ+1$ described on page 113. Each new value of $f(I,J)$ is tested for error with the previous value. The procedure is repeated for all points J on line I until the error is acceptably small, and the calculation then proceeds to line $I+1$.

Special Case of Line $I = 2$

The procedure followed here is the same as the general case except the $\partial^2 f/\partial x^2$ differential is zero, due to Equation (44), and it is assumed that the first differential is given by:

$$\partial f/\partial x = [f(2,J) - f(1,J)]/\Delta x(2). \qquad (45)$$

INTERVAL SIZES

Solution of an equation over a surface (or a line) is determined for progressively smaller intervals until the solution is not significantly changed by reducing the intervals.

APPENDIX II

DESCRIPTION OF THE VISCOMETRIC FLOW OF POWER LAW FLUIDS IN NIPS

Nip flow can be simulated by flow between parallel plates in which the fluid driving force is some combination of plate velocities and pressure drop. In a recent paper this was labeled "generalized Couette flow" (17). In this initial step in the development, there are no restrictions placed on the stress/shear rate relationships for the fluid.

The parallel plate geometry is illustrated in Fig. 29. Restrictions and other comments relating to the flow are as follows:

τ = the shear stress

$\Gamma = dv/dy$ = the shear rate

q = volumetric flow rate

w = width of the plates

Ambient pressure is assumed at the right outlet of the plates; the change in the development is trivial for ambient pressure at the left outlet. It is not implied that the pressure within the fluid at $x = L$ is ambient

Entrance, exit, and edge effects are neglected

The fluid is incompressible

Viscous heating is neglected

Gravity and other body forces are absent

There is no fluid slip at the solid surfaces

The stresses τ_w and τ_{yy} are values exerted by the fluid on the plate surfaces

The following are apparent from the system geometry:

$$p = p(x,y) \tag{46}$$

$$\partial P_{xx}/\partial x = \partial P_{yy}/\partial x = \partial\tau/\partial x = \partial\Gamma/\partial x = \partial v/\partial x = 0. \tag{47}$$

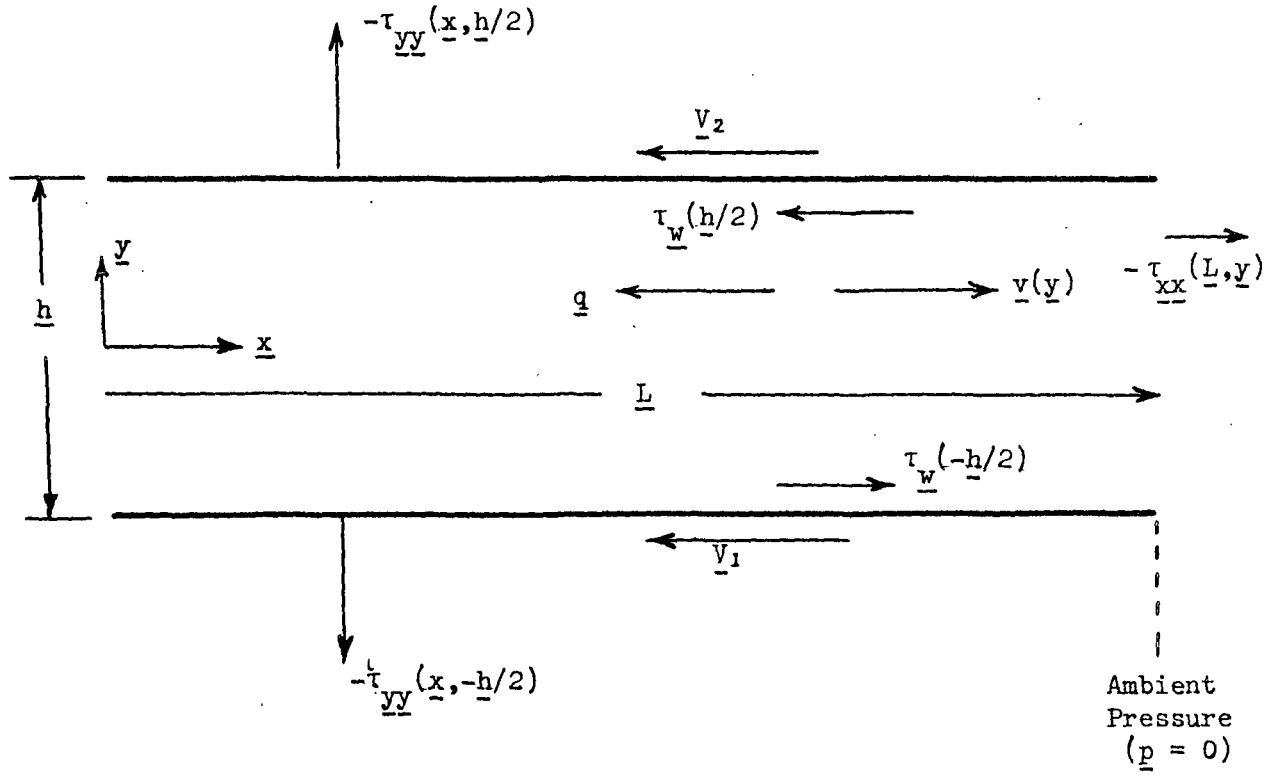

Figure 29. Geometry for Simulated Viscometric Flow in Nips

The equations of motion reduce to the following:

General Fluid	Viscous Fluid	Newtonian Fluid	
$\partial p/\partial x = d\tau/dy$	$dp/dx = d\tau/dy$	$dp/dx = d\tau/dy = \eta d\Gamma/dy = \eta \frac{d^2v}{dy^2}$	(48)
$\partial p/\partial y - dP_{yy}/dy = 0$	$\partial p/\partial y = 0$	$\partial p/\partial y = 0$	(49)

in which η is the fluid viscosity and P_{xx} and P_{yy} are deviatoric normal stresses.

Solving both equations of motion of the general fluid for the pressure:

$$p = (d\tau/dy)x + f(y) + C = P_{yy} + f_1(x) + C_1. \tag{50}$$

$d\tau/dy$ is constant since it is independent of y in Equation (50) and independent of x in Equation (47), and, therefore

$$p = (d\tau/dy)x + P_{yy} + C \tag{51}$$

$$d\tau/dy = \partial p/\partial x = \text{constant} \tag{52}$$

and

$$\tau = (\partial p/\partial x)y + \tau_o \tag{53}$$

with τ_o being constant and equal to the shear stress at $y = 0$.

Since the shear rate, Γ, is a unique function of the shear stress, it is evident that the constant τ_o depends uniquely on the τ-Γ functionality, the constant $\partial p/\partial x$, and the plate velocities V_1 and V_2. It follows that the shear stress, τ, the shear rate, Γ, and velocity profile depend on the viscous fluid properties only and are independent of the elastic properties.

The total stresses exerted by the fluid are determined from Equation (51) to be:

$$-\tau_{yy} = p - P_{yy} = (d\tau/dy)x + C \tag{54}$$

$$-\tau_{xx} = p - P_{xx} = (d\tau/dy)x - (P_{xx} - P_{yy}) + C. \tag{55}$$

Since τ_{yy} is a function of x only, the force normal to the film is the same on the two plates.

In order to determine the stress on the plates, τ_{yy}, it is necessary to evaluate the constant, C, by setting a boundary condition. This is not as simple as it might at first seem; for a viscous fluid one simply sets $p(L) = 0$, but for a viscoelastic fluid there is no boundary condition which will permit all external stresses to be zero at $x = L$. Nothing is lost in the analysis by considering the fluid to terminate prior to the plate exit instead of at the exit; thus, although one is concerned with the boundary condition τ_{yy}, this must be determined indirectly through the boundary condition τ_{xx} at the fluid edge, $x = L$. Considering one

of the two limiting cases, $\partial \underline{p}/\partial \underline{x} = 0$, it is apparent that the appropriate boundary condition is $\tau_{\underline{xx}}(\underline{L}) = 0$. For the other limiting flow, $\underline{V}_1 = \underline{V}_2 = 0$, $\tau_{\underline{xx}}(\underline{L})$ cannot be set equal to zero at all values of $\underline{y}$. Experimental studies for another geometry, flow through capillaries, provide conflicting evidence for the boundary condition [e.g., (18-20)]. Translated to the plate geometry these results would give values of $\tau_{\underline{xx}}(\underline{L}) = 0$ at the center line (18,19), or at the plate surface (20). The applicability of these results, or similar results obtained for flow between plates, is questionable since they may depend on the extruded jet. In the present case the plates are of arbitrary length and the flow is considered to be free of such exit effects. Middleman presents the argument that $\underline{p}(0,\underline{L})$, and thus $\tau_{\underline{xx}}(0,\underline{L})$, should be zero for capillary extrusion since this flow line is free of stresses (21). His argument is weakened for extrusion since the value may be subject to exit effects, but it is appealing in the present case where exit effects are absent. His argument is equally valid for flow between plates and we thus tentatively accept $\tau_{\underline{xx}}(0,\underline{L}) = 0$ for pressure-driven flow. As the flow changes from being pressure driven to velocity driven, the line of zero shear passes from the center toward one plate and eventually disappears. As long as there is a line of zero shear, the Middleman argument is valid for that particular flow line. Extending the boundary condition all the way to velocity-driven flow as a smooth function one arrives at the conclusion that $\tau_{\underline{xx}}$ at the plate outlet is zero at that flow line which is subjected to the minimum absolute value of shear. Solving for $\underline{C}$ and substituting the result in Equations (54) and (55) gives:

$$-\tau_{xx} = -(d\tau/dy)(L-x) - (P_{xx}-P_{yy}) + (P_{xx}-P_{yy})|\Gamma|_{min} \qquad (56)$$

$$-\tau_{yy} = -(d\tau/dy)(L-x) + (P_{xx}-P_{yy})|\Gamma|_{min}. \qquad (57)$$

Consequently, two important conclusions have been arrived at: (1) the velocity profile and shear distribution are a function of viscous fluid properties only, and (2) the force exerted by the fluid normal to the film is the sum of independent viscous and elastic effects. In analyzing flow through nips it is thus possible to consider a general viscoelastic fluid to be purely viscous and to add to the final result the normal force due to elastic stresses. In doing this it is understood that the pressure, $\underline{p}$, and the pressure profile, $d\underline{p}/d\underline{x}$, are not true system parameters but are pseudo values. The assumed boundary condition discussed above affects only the elastic contribution to the normal force and does not affect the conclusion that a general fluid can be considered purely viscous for nip flow.

Since the general fluid can be treated as a purely viscous fluid, with the understanding that $\underline{p}$ is a pseudo value and there is an independent normal force arising from the elasticity, the analysis continues with the viscous momentum equations:

$$\left.\begin{aligned} d\tau/dy = dp/dx = p' \\ \partial p/\partial y = 0. \end{aligned}\right\} \tag{58}$$

It is convenient to define several dimensionless groups:

$$\left.\begin{aligned} \hat{y} &= 2y/h \\ \hat{v} &= v/V_1 \\ \hat{Q} &= 2q/(V_1 hw). \end{aligned}\right\} \tag{59}$$

For the first time in the analysis the fluid behavior is restricted; viscous flow is assumed to conform to the power law model, but the viscoelastic normal stresses remain general. The power law fluid is defined alternatively by:

$$\left.\begin{aligned} \tau &= \eta_o \Gamma |\Gamma|^{n-1} \\ \Gamma &= dv/dy = (2V_1/h)d\hat{v}/d\hat{y} = \tau|\tau|^{(1-n)/n}/\eta_o^{1/n} \end{aligned}\right\} \qquad (60)$$

in which η_o and n are constants for a given fluid.

The boundary conditions are:

$$\left.\begin{aligned} \hat{v}(1) &= -V_2/V_1 \qquad (a) \\ \hat{v}(-1) &= -1 \qquad (b) \\ \hat{Q} &= -\int_{-1}^{1} \hat{v}\, d\hat{y} \qquad (c). \end{aligned}\right\} \qquad (61)$$

The solution of Equation (58) is:

$$\tau = \tau_o(\alpha\, \hat{y} + 1) \qquad (62)$$

in which α and τ_o are constants, τ_o being the center line shear stress, and:

$$\alpha = p'\, h/(2\, \tau_o). \qquad (63)$$

For pressure-driven flow ($V_1 = V_2$), $\tau_o = 0$, and for velocity-driven flow ($p' = 0$), $\tau_o/(V_1-V_2)$ is positive. It is reasonable to assume that $\tau_o/(V_1-V_2)$ is positive in the general case, and it will be seen that this is identically true for the power law fluid. Proceeding on this basis then one obtains from Equations (60) and (62) and boundary condition (61b):

$$\hat{v}\begin{bmatrix} V_1 > V_2 \\ V_1 < V_2 \end{bmatrix} = -1 \pm \left(\frac{h}{2V_1}\right)\left(\frac{+\tau_o}{-\eta_o}\right)^{1/n} \int_{-1}^{y} (\alpha\hat{y}+1)|\alpha\hat{y}+1|^{1-n/n}\, d\hat{y}. \qquad (64)$$

The constant τ_o is obtained from Equation (64) with the application of boundary condition (61a):

$$\tau_o = \left(\frac{2}{hX_1}\right)^n \eta_o\, |V_1-V_2|^{n-1}\, (V_1-V_2) \qquad (65)$$

in which X_1 is the integral:

$$X_1 = \int_{-1}^{1} (\alpha\hat{y}+1)\,|\alpha\hat{y}+1|^{1-n/n}\, d\hat{y}. \tag{66}$$

For all real values of α and positive values of n, $X_1 > 0$, and it is apparent that the assumption $\tau_o/(V_1-V_2) > 0$ is valid.

Applying boundary condition (61c) to Equation (64) and substituting for τ_o from Equation (65), the dimensionless flow rate $\hat{Q}$ is obtained:

$$\hat{Q} = 2 - [(V_1-V_2)/V_1](X_2/X_1) = 2\,q/(V_1\,h\,w) \tag{67}$$

in which the integral X_2 is defined by:

$$X_2 = \int_{-1}^{1} \int_{-1}^{\hat{y}} (\alpha\hat{y}+1)\,|\alpha\hat{y}+1|^{1-n/n}\, d\hat{y}\, d\hat{y}. \tag{68}$$

The integrals X_1 and X_2 have the following solutions:

	General Fluid	Newtonian Fluid ($n = 1$)
$X_1 =$	$\dfrac{\lvert C_1\rvert^{N_2} - \lvert C_2\rvert^{N_2}}{\alpha\, N_2}$	$= 2$
$X_2 =$	$\dfrac{C_2\lvert C_2\rvert^{N_2} + C_1\lvert C_1\rvert^{N_2}}{\alpha^2\, N_2(N_2+1)} - \dfrac{2\lvert C_2\rvert^{N_2}}{\alpha\, N_2}$	$= 2 - 2\,\alpha/3$

(69)

in which

$$\begin{aligned} C_1 &= \alpha + 1 \\ C_2 &= \alpha - 1 \\ N_2 &= (n+1)/n. \end{aligned} \tag{70}$$

The pressure drop is obtained from Equations (63) and (65):

$$p' = [(2\,\alpha)/h]\,\tau_o. \tag{71}$$

The shear stresses at the surfaces are obtained from Equations (62) and (65):

$$\tau_w \Big|_{\text{bottom surface}}^{\text{top surface}} = \tau_o(1 \pm \alpha). \tag{72}$$

Where the plate velocities are equal, a special solution is required. The equations are easily solved and details are not given. In the general case given above, there were separate equations for the pressure drop and volumetric flow rate which were linked through the dummy variable α. In this special case, one equation is sufficient:

$$p' = \left(\frac{2n+1}{n}\right)^n V_1^n \eta_o \left(\frac{2}{\quad}\right)^{n+1} \left|\frac{q}{V_1\, hw} - 1\right|^{n-1} \left(\frac{q}{V_1\, hw} - 1\right). \tag{73}$$

In this special case, the wall shear stresses are given by

$$\tau_w \Big|_{\text{bottom surface}}^{\text{top surface}} = \pm p' h/2. \tag{74}$$

The preceding analysis permits complete characterization of viscometric flow in any nip, restricted to power law behavior for viscosity. A computer program which offers numerical solution to the problem has been written and is available.

APPENDIX III

CROSS-FLOW CORRECTIONS

INTRODUCTION

The pressure in the blade nip is greater than ambient within the nip. Since the pressure at the nip edges is ambient, it follows that there must be flow from the interior out of the edges. The purpose of this appendix is to describe techniques used to predict the effect of cross-flow on blade lift and roll drag, and to predict the rate of fluid flow out of the edges. Calculated values of these results are given.

SOLUTION OF THE MOMENTUM EQUATIONS

It is assumed that the only significant fluid stresses resulting from the flow are due to velocity gradients in the $\underline{z}$ direction, resulting in the following momentum equations:

$$\partial p/\partial x = \partial \tau_{xz}/\partial z = p_x \tag{75}$$

$$\partial p/\partial y = \partial \tau_{yz}/\partial z = p_y \tag{76}$$

in which $\underline{p}$ is the pressure and $\tau_{\underline{xz}}$ and $\tau_{\underline{yz}}$ are shear stresses in the $\underline{x}$-$\underline{z}$ and $\underline{y}$-$\underline{z}$ planes, respectively. The coordinates $\underline{x}$, $\underline{y}$, and $\underline{z}$ are defined in Fig. 27 of Appendix I, except here $\underline{y} = 0$ at the nip center. The boundary conditions are:

$$\partial p/\partial y(x,0,z) = 0 \tag{77}$$

$$p(0,y,z) = 0 \tag{78}$$

$$p(TL+BL,y,z) = 0 \tag{79}$$

$$p(x,w/2,z) = 0 \tag{80}$$

$$v_x(x,y,0) = 0 \tag{81}$$

$$v_x(x,y,h) = V \tag{82}$$

$$V_y(x,y,0) = 0 \tag{83}$$

$$v_y(x,y,h) = 0 \tag{84}$$

in which v_x and v_y are fluid velocities in the x and y directions, respectively, V is the roll surface velocity, and h is the film thickness at x.

Integrating Equation (75):

$$\tau_{xz} = \tau_{xz}^{\circ} + p_x z \tag{85}$$

in which τ_{xz}° is the shear stress on the blade ($z = 0$). By definition:

$$\Gamma_x = \partial v_x/\partial z = \tau_{xz}/\eta = (\tau_{xz}^{\circ} + p_x z)/\eta \tag{86}$$

in which Γ_x is the shear rate in the x-z plane and η is the fluid viscosity. Integrating Equation (86) gives the velocity:

$$v_x = \tau_{xz}^{\circ} \int_0^z dz/\eta + p_x \int_0^z (z/\eta)dz. \tag{87}$$

Applying boundary condition (82):

$$V = \tau_{xz}^{\circ} \int_0^h dz/\eta + p_x \int_0^h (z/\eta)dz. \tag{88}$$

The volumetric flow rate per nip width in the x direction, q_x, is determined by integrating Equation (87):

$$q_x = \tau_{xz}^{\circ} \int_0^h \int_0^z (1/\eta)\, dz\, dz + p_x \int_0^h \int_0^z (z/\eta)\, dz\, dz. \tag{89}$$

It is convenient to define four integrals:

$$z_1 = \int_0^h dz/\eta, \quad z_2 = \int_0^h (z/\eta)\, dz$$

$$z_3 = \int_0^h \int_0^z (1/\eta)\, dz\, dz, \quad z_4 = \int_0^h \int_0^z (z/\eta)\, dz\, dz. \tag{90}$$

Thus, the final results from the x direction momentum equation are:

$$V = \tau_{xz}{}^{o} z_1 + p_x z_2 \tag{91}$$

$$q_x = \tau_{xz}{}^{o} z_3 + p_x z_4. \tag{92}$$

The y direction momentum equation is solved in a similar manner with the results:

$$0 = \tau_{yz}{}^{o} z_1 + p_y z_2 \tag{93}$$

$$q_y = \tau_{yz}{}^{o} z_3 + p_y z_4 \tag{94}$$

in which $\tau_{yz}{}^{o}$ is the y-z plane shear stress on the blade surface and q_y is the volumetric flow rate per nip width in the y direction.

THE z INTEGRALS AS FUNCTIONS OF THE SHEAR STRESSES

The total shear stress, τ, is a combination of the two directional shear stresses:

$$\tau^2 = \tau_{xz}{}^2 + \tau_{yz}{}^2. \tag{95}$$

By the definition of a power law fluid:

$$\tau = \eta_o \Gamma^N = \eta\Gamma \tag{96}$$

in which Γ is the total shear rate and η_o is the viscosity at unit shear rate.

The viscosity is determined as a function of shear stress from Equation (96):

$$1/\eta = (\tau^2)^{\frac{1-N}{2N}} / \eta_o^{1/N}. \tag{97}$$

The z integrals are thus seen to be unique functions of the directional shear stresses. The x direction shear stress is determined from Equations (85) and (91) to be

$$\tau_{xz} = p_x z + V/z_1 - p_x z_2/z_1. \tag{98}$$

Similarly, the y direction shear stress is determined to be

$$\tau_{yz} = p_y z - p_y z_2/z_1. \tag{99}$$

THE MATERIAL BALANCE

The mass balance at a point x,y, averaged over the coordinate z is given by:

$$\partial q_x/\partial x + \partial q_y/\partial y = 0. \tag{100}$$

From Equations (91) and (92), q_x is determined to be:

$$q_x = V z_3/z_1 + p_x(z_4 - z_2 z_3/z_1) = z_5 V + z_6 p_x. \tag{101}$$

From Equations (93) and (94), q_y is determined to be:

$$q_y = p_y z_6. \tag{102}$$

DIMENSIONLESS VARIABLES

Dimensionless geometric variables are defined as follows:

$$\underline{X} = \underline{x}/\underline{h}_o$$

$$\underline{Y} = \underline{y}/\underline{h}_o$$

$$\underline{R} = \underline{h}/\underline{h}_o$$

$$\underline{Z} = \underline{z}/\underline{h} = \underline{z}/(\underline{h}_o \underline{R})$$

$$\underline{L} = (\underline{BL}+\underline{TL})/\underline{h}_o$$

$$\underline{W} = \underline{w}/(2\ \underline{h}_o)$$

$\underline{TBA}$ = tangent (blade angle)

$\underline{SBA}$ = sine (blade angle)

$\underline{CBA}$ = cosine (blade angle)

Other variables are defined using "base" viscosity ($\overline{\eta}$) and stress ($\overline{\tau}$) values defined in Equation (103).

$$\overline{\eta} = \eta_o\ (V/h_o)^{N-1}$$
$$\overline{\tau} = \eta_o\ (V/h_o)^{N}. \qquad (103)$$

The resultant dimensionless variables are defined as follows:

$$\underline{E} = \eta/\overline{\eta}$$

$$\hat{\tau} = \tau/\overline{\tau}$$

$$\underline{P} = \underline{p}/\overline{\tau}$$

$$\underline{P}_{\underline{X}} = \underline{h}_o\ \underline{p}_{\underline{x}}/\overline{\tau}$$

$$\underline{P}_{\underline{Y}} = \underline{h}_o\ \underline{p}_{\underline{y}}/\overline{\tau}$$

$$\underline{Z}_1 = \int_0^1 \underline{dZ}/\underline{E} = [\overline{\eta}/(\underline{h}_o\ \underline{R})]\underline{z}_1$$

$$\underline{Z}_2 = \int_0^1 (\underline{Z}/\underline{E})\underline{dZ} = [\overline{\eta}/(\underline{h}_o\ \underline{R})^2]\underline{z}_2$$

$$\underline{Z}_3 = \int_0^1 \int_0^Z (1/\underline{E})d\underline{Z}\ d\underline{Z} = [\overline{n}/(\underline{h}_o\ \underline{R})^2]\underline{z}_3$$

$$\underline{Z}_4 = \int_0^1 \int_0^Z (\underline{Z}/\underline{E})d\underline{Z}\ d\underline{Z} = [\overline{n}/(\underline{h}_o\ \underline{R})^3]\underline{z}_4$$

$$\underline{Z}_5 = \underline{Z}_3/\underline{Z}_1$$

$$\underline{Z}_6 = \underline{Z}_4 - \underline{Z}_2\ \underline{Z}_5$$

$$\underline{Q}_X = \underline{R}\ \underline{Z}_5 + \underline{P}_X\ \underline{R}^3\ \underline{Z}_6 = \underline{q}_x/(\underline{V}\ \underline{h}_o)$$

$$\underline{Q}_Y = \underline{P}_Y\ \underline{Z}_6\ \underline{R}^3 = \underline{q}_y/(\underline{V}\ \underline{h}_o)$$

THE FINAL RELEVANT EQUATIONS IN DIMENSIONLESS FORM

The $\underline{Z}$ integrals are as follows:

$$\left.\begin{aligned} &Z_1 = \int_0^1 A^B\,dZ, \qquad Z_2 = \int_0^1 Z\,A^B\,dZ, \qquad Z_3 = \int_0^1 \int_0^Z A^B\,dZ\,dZ, \\ &Z_4 = \int_0^1 \int_0^Z Z\,A^B\,dZ\,dZ, \qquad Z_5 = Z_3/Z_1, \qquad Z_6 = Z_4 - Z_2\,Z_5 \end{aligned}\right\} \tag{104}$$

in which

$$\left.\begin{aligned} &A = (P_X\,R\,Z + \frac{1}{Z_1 R} - P_X\,R\,\frac{Z_2}{Z_1})^2 + (P_Y\,R)^2(Z - \frac{Z_2}{Z_1})^2 \\ &B = (1 - N)/(2\,N). \end{aligned}\right\} \tag{105}$$

The dimensionless material balance is

$$\left.\begin{aligned} &\partial Q_X/\partial X + \partial Q_Y/\partial Y = 0 \\ &\frac{\partial Q_X}{\partial X} = R\frac{\partial Z_5}{\partial X} + Z_5\frac{\partial R}{\partial X} + \frac{\partial P}{\partial X}(3R^2 Z_6\frac{\partial R_6}{\partial X} + R^3\frac{\partial Z_6}{\partial X}) + R^3 Z_6\,\frac{\partial^2 P}{\partial X^2} \\ &\frac{\partial Q_Y}{\partial Y} = \frac{\partial P}{\partial Y}\,R^3\,\frac{\partial Z_6}{\partial Y} + R^3\,Z_6\,\frac{\partial^2 P}{\partial Y^2}\,. \end{aligned}\right\} \tag{106}$$

he pressure boundary conditions applied to Equation (106) are:

$$\left.\begin{aligned} P(0,Y) &= 0 \\ P(L,Y) &= 0 \\ \partial P/\partial Y(X,0) &= 0 \\ P(X,W) &= 0 \end{aligned}\right\} \qquad (107)$$

Dimensionless fluid stresses exerted on the blade and roll are functions of the nip geometry and the fluid pressure:

$$T_B = \text{tangential stress (blade)} = 1/(Z_1 R) - (\partial P/\partial X)R\, Z_2/Z_1 \qquad (108)$$

$$T_R = \text{tangential stress (roll)} = T_B + (\partial P/\partial X)R \qquad (109)$$

$$\left.\begin{aligned} P_B = \text{normal stress (blade)} &= P(CBA) - T_B(SBA) && \underline{\text{blade}}\ \underline{\text{surface}} \\ &= P && \underline{\text{blade}}\ \underline{\text{tip}} \end{aligned}\right\} \qquad (110)$$

The effective normal stress on the blade surface has a contribution from drag stress on the blade since $\underline{T_B}$ has a normal component.

The required total forces on the blade and roll are obtained by integrating the stresses as follows:

$$\text{Blade lift (no cross flow)} = W \int_0^L P_B(0)\, dX \qquad (111)$$

$$\text{Blade lift (with cross flow)} = \int_0^W \int_0^L P_B\, dX\, dY \qquad (112)$$

$$\text{Roll drag (no cross flow)} = W \int_0^L T_R(0)\, dX \qquad (113)$$

$$\text{Roll drag (with cross flow)} = \int_0^W \int_0^L T_R\, dX\, dY. \qquad (114)$$

Since the ratios of corrected and uncorrected forces is used it is apparent that the required corrections are functions only of the minimum film thickness, $\underline{h_o}$, and the power law exponent, $\underline{N}$.

The dimensionless flow per nip length out of one side of a nip is given by:

$$Q_Y(W) = P_Y(W)\, Z_6(W)\, R^3. \tag{115}$$

The resulting total flow out of one side of a nip is thus:

$$\left.\begin{aligned} \text{Total flow (dimensionless)} &= \int_0^L Q_Y(W)\, dX \\ \text{Total flow (dimensional)} &= V\, h_o^{\,2} \int_0^L Q_Y(W)\, dX \end{aligned}\right\} \tag{116}$$

SOLUTION OF THE CROSS FLOW EQUATIONS

It is required that the dimensionless pressure P and Z integrals be determined as functions of X and Y such that Equations (104)-(107) are satisfied. Techniques used in the solution are described in Appendix I.

Initial values of the Z integrals were determined by assuming the shear rate at each point to be V/h, independent of the variable Z. The initial pressure profile on the center line, P(X,0), was determined by trial and error without any cross flow contributions. The pressure profile from the nip center to the edges was assumed to be of the form:

$$P(X,Y) = P(X,0)[1-(Y/W)^3]. \tag{117}$$

It was determined that solutions "blew up" when new values of P and the Z integrals were determined at each point. Satisfactory results were obtained by evaluating new values of P at all points and then new values of the Z integrals at all points. Weighting factors used in the calculations were 1.7 for determination of P and 1.0 for determination of the Z integrals.

Correct $\underline{P}$ and $\underline{Z}$ values were then applied to Equations (108)-(116), using the techniques of Appendix I, to obtain the final results.

CALCULATED CROSS-FLOW CORRECTIONS

Calculated results are given in Table XVII. Computer time was quite long for non-Newtonian ($\underline{N} \neq 1$) calculations and convergence to a solution was difficult. Two values in Table XVII show the non-Newtonian effect to be small and Newtonian results were thus used to correct all experimental results.

TABLE XVII

CALCULATED CROSS-FLOW CORRECTIONS

		Number of Intervals			Uncorrected Force/Corrected Force	
$\underline{N}$	$\underline{DR}$[a]	Blade Tip	Blade Surface	Across Nip	Blade Lift	Roll Drag
1	5	6	24	32	1.017	1.005
1	25	6	24	32	1.027	1.013
1	100	6	24	32	1.049	1.026
1	300	6	24	32	1.077	1.039
1	1000	6	24	16	1.119	1.046
1	2000	6	24	16	1.140	1.037
0.9	1000	6	24	16	1.119	1.043
1.0	1000	6	24	16	1.119	1.046
0.9	100	6	24	8	1.073	1.037
1.0	100	6	24	8	1.071	1.035

[a] Minimum film thickness, $\underline{h}_o$, equals $\underline{DR}/16070$, cm.

CALCULATED FLOW RATES OUT OF THE SIDES OF BOTH NIPS

Calculated values are given in Table XVIII.

TABLE XVIII

TOTAL FLOW RATE OUT THE SIDES OF THE BLADES

			V_o, ft./min.	
			1000	2000
N	DR, h_o/16070 cm.	BL, cm.	Flow Rate, $cm.^3/sec.$	
1.0	5	2.0	166	332
		1.0	41	81
		0.5	9	18
1.0	100	2.0	194	388
		1.0	48	96
		0.5	11	22
1.0	1000	2.0	201	402
0.9	100	2.0	194	387
0.9	1000	2.0	196	392

USE OF THE CROSS FLOW CORRECTIONS

Corrections given in Table XVII were empirically correlated with DR to give rapidly available results.

APPENDIX IV

VISCOUS HEAT CORRECTIONS

INTRODUCTION

The energy input to fluids in high-shear viscometers is considerable. Were this heat to remain in the fluids it would generally cause very large temperature rises, and it is apparent that the largest part of the heat passes into the viscometer walls. It cannot be assumed, however, that there is no viscous heat temperature rise, and it is desirable to determine how great this effect is and to correct viscometer measurements for it.

Since the temperature rise in the blade nip is not uniform across the film, the correction is not given simply as an overall temperature rise but the effect on the velocity profile must be considered. It will be seen that the effect is different for the two measurements made in this work, drag on the roll and pressure lift of the blade.

The calculations described in this appendix were difficult and time consuming even for a Newtonian fluid, and consideration of the effect on non-Newtonian fluid behavior was considered impractical. In future work it may be desirable to approximate the effect of non-Newtonian behavior.

THE ENERGY EQUATION

The energy equation is given in Equation (118).

$$\underline{\text{Heat Convection}} \qquad \underline{\text{Heat Conduction}} \qquad \underline{\text{Heat Generation}}$$

$$\rho\, c_p\, v\, \partial t/\partial x = k(\partial^2 t/\partial x^2 + \partial^2 t/\partial z^2) + \eta(\partial v/\partial z)^2 \qquad (118)$$

in which the coordinates x and z are defined in Fig. 27 of Appendix I, and

ρ = fluid density

k = fluid thermal conductivity

c_p = fluid heat capacity

η = fluid viscosity

t = temperature

v = velocity, which is in the x coordinate direction

It is assumed that the viscosity is a function of temperature given by Equation (119).

$$\eta = \eta_o \exp(-\beta t) \tag{119}$$

in which η_o is the viscosity at ambient temperature and β is a material parameter.

In order to express Equation (118) in dimensionless form the following dimensionless terms are defined:

$$\left.\begin{aligned} Z &= z/h_o \\ X &= x/h_o \\ V &= v/V_o \\ T &= k\,t/(\eta_o V_o^2) \\ E &= \eta/\eta_o \\ B &= \eta_o V_o^2 \beta/k \\ A &= h_o \rho c_p V_o/k \\ H &= \exp(-B\,T)(\partial V/\partial Z)^2 \end{aligned}\right\} \tag{120}$$

in which V_o is the roll surface velocity and h_o is the film thickness under the blade tip.

The resulting dimensionless energy equation is:

$$A\ V\ \partial T/\partial X = \partial^2 T/\partial X^2 + \partial^2 T/\partial Z^2 + H. \tag{121}$$

THE MOMENTUM EQUATION

The momentum equations reduce to Equation (122).

$$p_x = dp/dx = \partial \tau/\partial z \tag{122}$$

in which p is the pressure and τ is the shear stress. Integrating Equation (122):

$$\tau = \tau_o + p_x\ z \tag{123}$$

in which τ_o is the shear stress on the blade surface ($z = 0$).

By definition of the shear rate, Γ:

$$\Gamma = dv/dz = \tau/\eta = (\tau_o + p_x\ z)/\eta. \tag{124}$$

Boundary conditions for Equation (124) are:

$$\left.\begin{aligned} v(0) &= 0 \\ v(h) &= V_o. \end{aligned}\right\} \tag{125}$$

Therefore

$$v = \tau_o \int_0^z dz/\eta + p_x \int_0^z (z/\eta)dz. \tag{126}$$

By application of a boundary condition

$$V_o = \tau_o\ z_1 + p_x\ z_2. \tag{127}$$

Also, the total flow rate through the nip per nip width is given by

$$q = \int_0^h v\, dz = \tau_o\, z_3 + p_x\, z_4. \tag{128}$$

The four integrals defined in Equations (127) and (128) are

$$\left.\begin{aligned} z_1 &= \int_0^h dz/\eta, \qquad z_2 = \int_0^h (z/\eta)dz, \\ z_3 &= \int_0^h \int_0^z (1/\eta)\, dz\, dz, \qquad z_4 = \int_0^h \int_0^z (z/\eta)\, dz\, dz. \end{aligned}\right\} \tag{129}$$

In order to express the results from the momentum equation in dimensionless form the following dimensionless terms are defined:

$$\left.\begin{aligned} Z_1 &= \int_0^1 dZ/E, \qquad Z_2 = \int_0^1 (Z/E)dZ, \qquad Z_3 = \int_0^1 \int_0^Z (1/E)dZ\, dZ, \\ Z_4 &= \int_0^1 \int_0^Z (Z/E)dZ\, dZ, \qquad T_o = \frac{2h}{\eta_o V_o}\tau_o, \qquad P_X = \frac{2h^2}{\eta_o V_o} P_x, \\ Q &= \frac{2}{V_o h_o} q, \qquad R = h/h_o. \end{aligned}\right\} \tag{130}$$

The results from the momentum equation in dimensionless form are thus

$$T_o\, Z_1 + P_X\, Z_2 = 2 \tag{131}$$

$$T_o\, Z_3 + P_X\, Z_4 = Q/R \tag{132}$$

$$H = (T_o + P_X\, Z)^2/(4\, E\, R^2) \tag{133}$$

$$V = \tfrac{1}{2}(T_o\, \overline{Z}_1 + P_X\, \overline{Z}_2) \tag{134}$$

in which

$$\left.\begin{aligned} \overline{Z}_1 &= \int_0^Z dZ/E \\ \overline{Z}_2 &= \int_0^Z (Z/E)dZ. \end{aligned}\right\} \tag{135}$$

THE PROBLEM OF REVERSE FLOW

Consider the schematic illustration of flow through the nip given in Fig. 30.

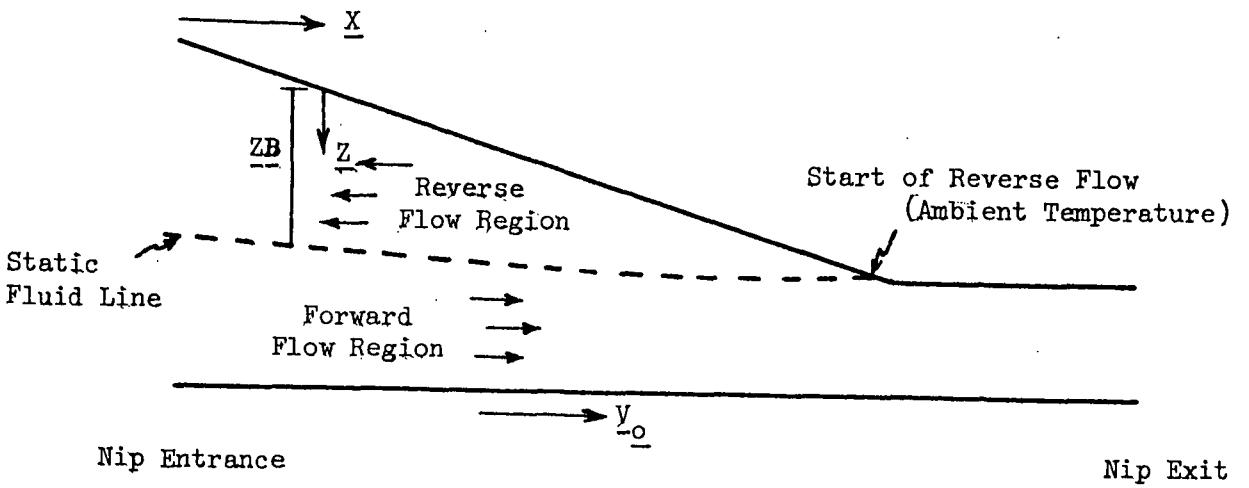

Figure 30. Flow Through the Nip

Reverse flow presents two problems which make an exact solution of the energy equation difficult, if not impossible.

(1) Numerical calculations in the neighborhood of the static fluid line are very difficult to stabilize due to the rapidly changing physical conditions.

(2) Because reverse flow brings heat from the interior to the entrance of the nip, temperature boundary conditions at $\underline{x} = 0$ cannot be fixed.

Because of these difficulties, the effect of viscous heating in the reverse flow region is considered separately using a simple model. The rationale for the model is based on three conditions:

(1) The static fluid line is in a neighborhood of rapid heat generation.

(2) In the interior of the reverse flow region the shear stress changes sign, which suggests a minimum temperature line through the region.

(3) It is assumed that the blade reaches a steady-state temperature and no heat flows between the fluid and blade.

The resulting model has the following characteristics:

(1) The static fluid line is a line of maximum temperature, resulting in zero heat flow across the line.

(2) The start of the reverse flow region is at ambient temperature as indicated in Fig. 30.

(3) The location of the static fluid line is fixed without regard to viscous heating in the nip, which precludes extensive trial and error adjustment of its position.

(4) Viscous heating in the reverse flow region is determined with the fluid at ambient temperature. The heating rate and velocity are determined from Equations (133)-(135). These results are averaged across the reverse flow portion of the film to give average heating rate, HA, and velocity, VA. These values are functions of X but not Z. The energy equation is applied using these average values as:

$$d(TA)/dX = HA/(A*VA) \qquad (136)$$

in which TA is the average temperature at X in the reverse flow region. The boundary condition for Equation (136) is TA = 0 at the start of reverse flow, shown in Fig. 30.

(5) A temperature distribution across the reverse flow portion of the film is required in the solution of Equations (131)-(135). The choice of the form of the distribution is not very critical to the results. The simplified distribution is shown in Fig. 31.

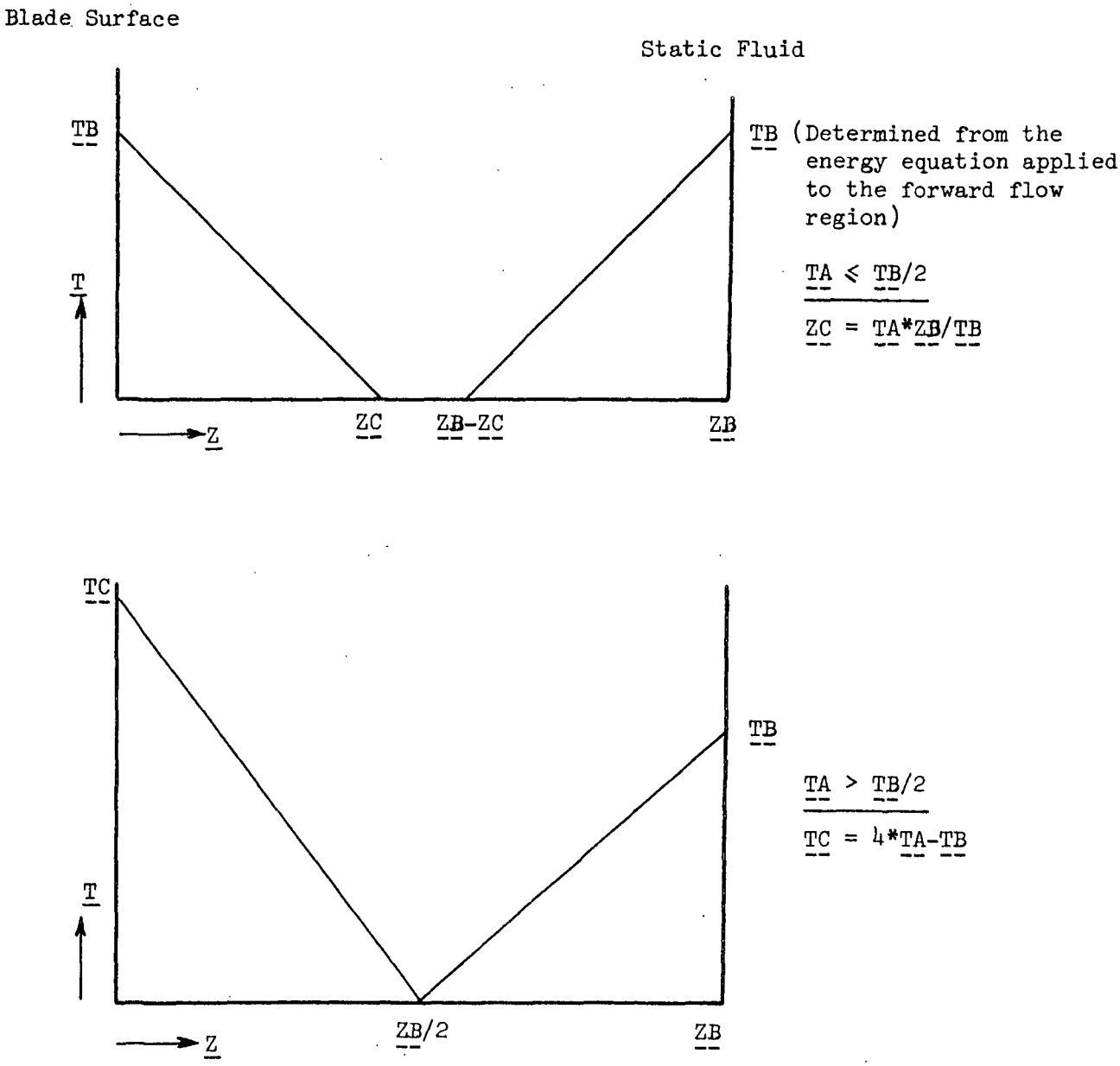

Figure 31. Temperature Distribution Across Reverse Flow Portion of the Film

HEAT CONDUCTED TO THE ROLL

The calculation of heat flow to the roll requires either a continuous calculation of coupled heat balances in the fluid and the roll or the assumption of temperature profile in the roll. The former approach is too complex to be practical in this problem. There is, however, available evidence that a reasonable temperature profile in the roll can be assumed. The solution of the problem of heat flow from a source at an elevated temperature into an infinite body at a lower temperature has been solved (22). The significant result of the solution in the present case is given by Equation (137), valid at all times after the start of heating.

$$\frac{\int_0^\infty T_r \, dZ_r \text{ (true)}}{\int_0^\infty T_r \, dZ_r \text{ (linear temp. profile)}} = \alpha = 1.28 \qquad (137)$$

in which T_r is the temperature in the roll and Z_r is the distance from the surface into the roll.

The significance of Equation (137) is that the temperature profile in the roll can be assumed linear if the heat contained in the roll is multiplied by the factor α.

The resulting energy balance at the roll surface is given by Equations (138) or (139).

$$1/\Delta = - k(\partial t/\partial z)_f/(k' \, t_s) \approx t_s \, \alpha \, \rho' \, c_p'/(2 \, H_R) \qquad (138)$$

or

$$t_s^2 = - 2k(\partial t/\partial z)_f \, H_R/(k' \, \alpha \, \rho' \, c_p') \qquad (139)$$

in which

Δ = apparent distance in the roll to ambient temperature

t_s = surface temperature

$(\partial t/\partial z)_f$ = temperature profile at the surface in the fluid

H_R = heat contained in the roll/nip width/nip length

k' = thermal conductivity of the roll

c_p' = heat capacity of the roll

ρ' = density of the roll

$k' \alpha \rho' c_p' = 0.113$ cal.^{2}/°C.^{2}/cm.^{4}

It is apparent that the boundary condition of roll surface temperature can be determined from Equation (139). As the calculation proceeds from the nip entrance, a constant point on the roll can be considered as the coordinate variable X changes. The value of H_R is thus determined as a continuous function of X by progressively adding heat flow to the roll from $X = 0$ to the value of X being considered.

INPUT PARAMETERS

Viscous heat corrections are functions of the six dimensionless parameters in Equation (140).

$$\left.\begin{aligned} A &= h_o \rho c_p V_o/k \\ B &= \beta \eta_o V_o^2/k \\ C &= BL/h_o \\ AB &= 2k^2/(V_o h_o \alpha k' \rho' c_p') \\ AA &= TL/h_o \\ TBA &= \text{tangent blade angle} . \end{aligned}\right\} \qquad (140)$$

It is convenient to generate the parameters of Equation (140) by a complementary set of dimensionless parameters. By so doing, two geometric parameters are constants for the results presented in this work. In addition, the remaining four are functions of only one operating variable, enclosed in parentheses, which permits useful ranges of variables to be covered without generating superfluous information. These parameters are given in Equation (141).

$$
\begin{aligned}
C_1 &= AA/AB = \frac{TL\ \alpha\ k'\ \rho'\ c_p'}{2\ k^2}\ (V_o) \\
C_2 &= B^*AB^2/AA^2 = \frac{4\ k^3\ \beta}{TL\ \alpha\ k'\ \rho'\ c_p'}\ (\eta_o) \\
C_3 &= AA = TL\ (1/h_o) \\
C_5 &= A^*AB = \frac{2\ c_p\ k}{\alpha\ k'\ \rho'\ c_p'}\ (\rho) \\
C_4 &= C/AA = BL/TL \\
C_6 &= TBA\ .
\end{aligned}
\qquad \text{constant parameters} \qquad (141)
$$

OUTLINE OF THE SOLUTION

Detailed techniques used in the solution are covered in Appendix I. The steps of the solution follow. The solution is trial and error in the Z direction and progressive in the X direction.

Input Variables

Useful ranges of the input variables V_o, η_o, h_o, ρ are selected as independent variables. The dimensionless flow rate through the nip, Q, is a function of the independent variables and is determined by trial and error. Fortunately, it was shown that blade lift, roll drag, and exit pressure are sufficiently linear

functions of $\underline{Q}$ so that only two values of $\underline{Q}$ are required for each set of input variables. In each case the linear relationships are used to determine blade lift and roll drag at zero exit pressure from the nip. The input information is translated to the dimensionless parameters of Equation (140).

Reverse Flow Region

As discussed in the section on The Problem of Reverse Flow (p. 140), the size of the reverse flow region is determined and the average temperature, $\underline{TA}$, determined as a function of $\underline{X}$.

Grid

The nip grid used for the momentum equation results is as shown in Fig. 27 in Appendix I. For application to the energy equation the grid covers only the forward flow region.

Boundary Conditions

The temperature boundary conditions are

$\underline{T}(0,\underline{Z}) = 0$ (forward flow region only)

$\partial^2\underline{T}/\partial\underline{X}^2(0,\underline{Z}) = 0$ (forward flow region)

$\partial\underline{T}/\partial\underline{Z}$ (static fluidline and blade surface) = 0

$\partial\underline{T}/\partial\underline{Z}$ ($\underline{X}$,1) determined as indicated in the section on Heat Conducted to the Roll (p. 143).

Solution of the Energy Equation

Equation (121) is solved along a line across the nip in the forward flow region. The temperature on the static fluid line, $\underline{TB}$, is then used, as shown in Fig. 31, to determine the remainder of the temperature profile across the nip. The temperature on the roll surface is determined by a trial and error solution of Equation (139).

Solution of the Momentum Equation

Equations (130)-(135) are solved on a line across the entire film to determine the Z integrals, T_o, P_X, E(Z), H(Z), and V(Z).

Test of the Solution

Values of T_o and P_X are tested with those determined previously. If succeeding values differ by more than an arbitrary standard, solutions of the energy equation and the momentum equation are repeated; if not, the solution at the particular line at X is considered acceptable and the solution proceeds to the next line.

Evaluation of Blade Lift and Roll Drag

Pressure as a function of X is:

$$P(X) = \int_0^X P_X \, dX. \tag{142}$$

Blade lift and roll drag are given by Equations (143) and (144).

$$\text{Blade lift } \int_0^L \overline{P} \, dX \tag{143}$$

$$\text{Roll drag} = \int_0^L (T_o + P_X R) dX \tag{144}$$

in which $L = (BL+TL)/h_o$ and

$$\left.\begin{aligned} \overline{P} &= P && \text{blade tip} \\ &= P*CBA - T_o*SBA && \text{blade surface} \end{aligned}\right\} \tag{145}$$

in which SBA and CBA are the sine and cosine of the blade angle, respectively.

Values of blade lift and roll drag uncorrected for viscous heating are determined by setting the viscosity-temperature coefficient, β, equal to zero. Since the ratio of corrected to uncorrected blade lift and roll drag are used to correct data, there is no need to transform values to dimensional form.

MAGNITUDE OF THE VISCOUS HEATING CORRECTIONS

The viscosity of coatings is generally not very dependent on temperature and the viscous heat corrections are generally quite small, of the order of 5-10% or less. Corrections for glycerin are greater due to large temperature sensitivity. Some representative results for glycerin are given in Table XIX.

USE OF THE VISCOUS HEAT CORRECTIONS

The generation of viscous heat corrections for every set of experimental data would require too much computer time. Corrections were empirically correlated with the $\underline{C}$ coefficients of Equation (141) resulting in readily available values.

TABLE XIX

VISCOUS HEAT CORRECTIONS FOR GLYCERIN

Terms: η = viscosity, poise

V_o = roll velocity, ft./min.

DR = film thickness under blade tip, cm./16070

$\hat{\eta}(F)$ = ratio of uncorrected to corrected blade lift viscosity

$\hat{\eta}(D)$ = ratio of uncorrected to corrected roll drag viscosity

	DR, 8				DR, 16			
	V_o, 1000		V_o, 2000		V_o, 1000		V_o, 2000	
η	$\hat{\eta}(F)$	$\hat{\eta}(D)$	$\hat{\eta}(F)$	$\hat{\eta}(D)$	$\hat{\eta}(F)$	$\hat{\eta}(D)$	$\hat{\eta}(F)$	$\hat{\eta}(D)$
0.2	1.05	1.03	1.25	1.09	1.04	1.02	1.14	1.05
0.6	1.12	1.09	1.44	1.22	1.12	1.05	1.32	1.28
1.0	1.17	1.13	1.30	1.30	1.20	1.09	1.42	1.40

	DR, 32				DR, 64			
	V_o, 1000		V_o, 2000		V_o, 1000		V_o, 2000	
η	$\hat{\eta}(F)$	$\hat{\eta}(D)$	$\hat{\eta}(F)$	$\hat{\eta}(D)$	$\hat{\eta}(F)$	$\hat{\eta}(D)$	$\hat{\eta}(F)$	$\hat{\eta}(D)$
0.6	1.04	1.02	1.11	1.05				
1.0	1.07	1.04	1.16	1.08	1.02	1.01	1.05	1.03
3.0	1.17	1.09	1.33	1.27	1.06	1.04	1.12	1.08

APPENDIX V

CALIBRATIONS

NORMAL FORCE GAGE

The normal force gage was calibrated using an Instron tensile tester. In order to simulate machine vibration, the gage was lightly tapped during the calibration. The test results are illustrated in Fig. 32.

CORRECTION OF FILM THICKNESS READINGS FOR THE EFFECT OF BLADE LOAD

As the blades are loaded in a direction normal to the roll surface, there is an apparent movement of the roll due to play in the bearings. The extent of this movement was determined in thin film experiments with glycerin. The functionality of Equation (146) is theoretically valid except for viscous heat corrections and deviations from viscometric flow. These effects are not considered important since $\underline{DR}$ is small compared with the correction being measured.

$$F/(\eta V_o) = f(DR) = f(R - R_o) \tag{146}$$

in which $\underline{F}$ is a measure of blade load, η is the fluid viscosity, $\underline{V_o}$ is the roll surface velocity, $\underline{R}$ is the dial indicator reading, $\underline{R_o}$ is the unknown dial indicator reading with zero film thickness, and $\underline{DR}$ is a measure of film thickness under the blade tip. Values of $\underline{R}$ were determined as a function of $\underline{F}$, with $\underline{F}/\underline{V_o}$ constant. Since $\underline{DR}$ is constant, changes in $\underline{R}$ are equal to changes in $\underline{R_o}$.

The results of the calibration are presented in Fig. 33. All experimental readings of $\underline{R}$ are corrected to the standard blade load $\underline{F} = 50$ by Equation (147).

$$R(\text{corrected}) = R(\text{measured}) - 0.0064(50-F)^2. \tag{147}$$

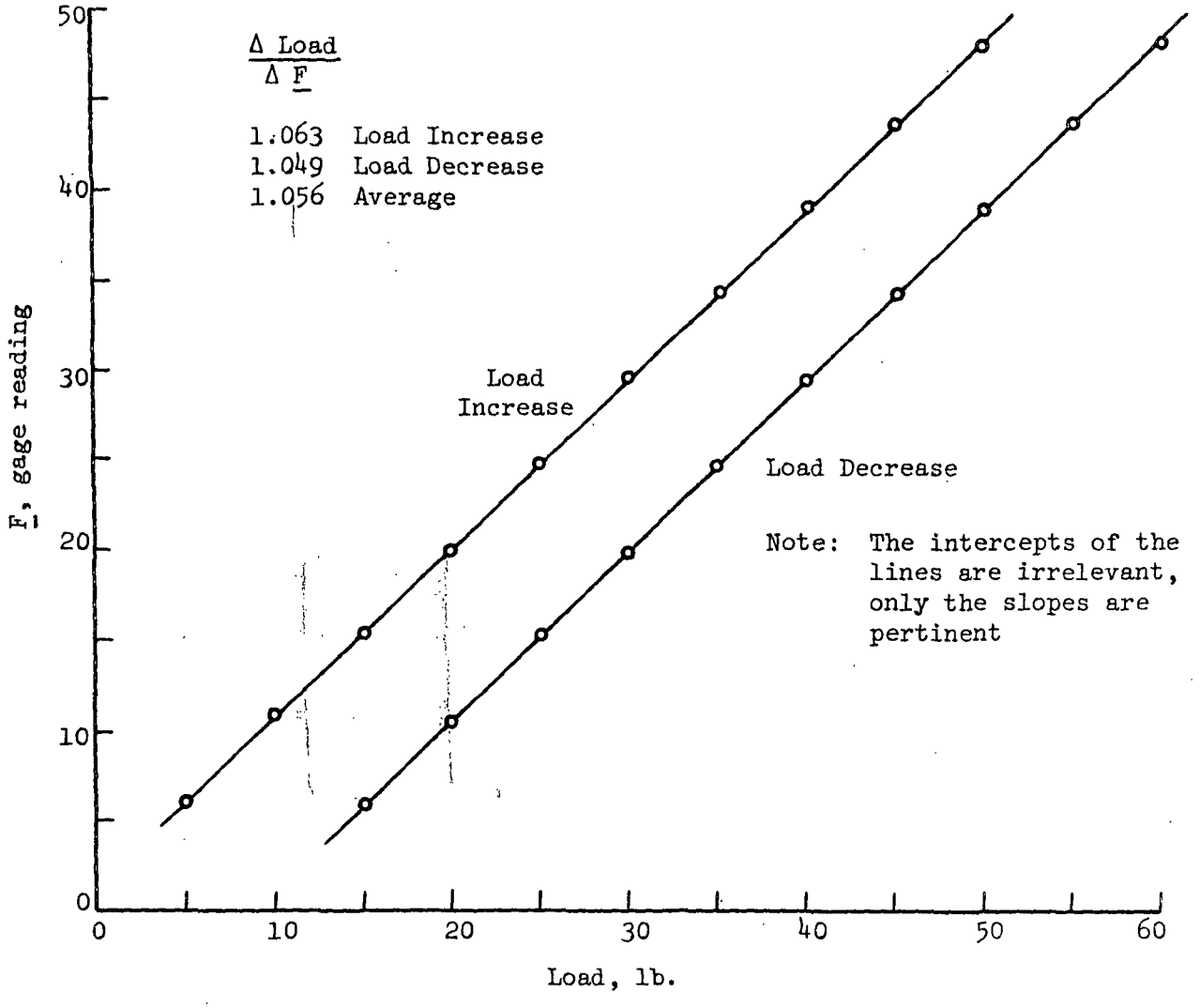

Figure 32. Normal Gage Calibration

ROLL DRAG CALIBRATION

Roll drag is a function of power input to the drive motor. The power input is measured by a voltmeter connected to the SCR drive control. Meter readings are proportional to the actual voltage according to Equation (148).

$$\text{Meter reading } (X)/\text{volts} = 3220. \qquad (148)$$

The calibration was made using the meter and the actual voltage values don't enter into the results.

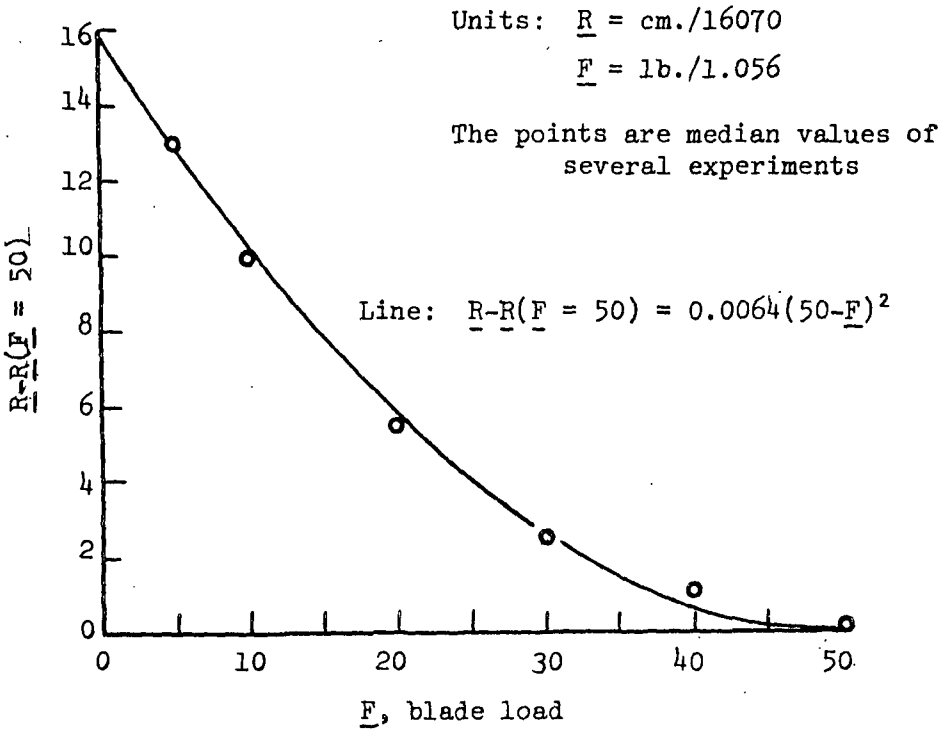

Figure 33. Blade Load Correction of Film Thickness Measurement

The experimental arrangement used in the calibration is shown in Fig. 34. It was determined that this experimental arrangement gave reasonable accuracy in the results despite difficulty in measuring the distance Δ with great precision. The reason for this is the fact that the belt tension W_2-T_1 depends mainly on W_2 which is known precisely.

Equations relating roll drag to Δ and W_2 are as follows:

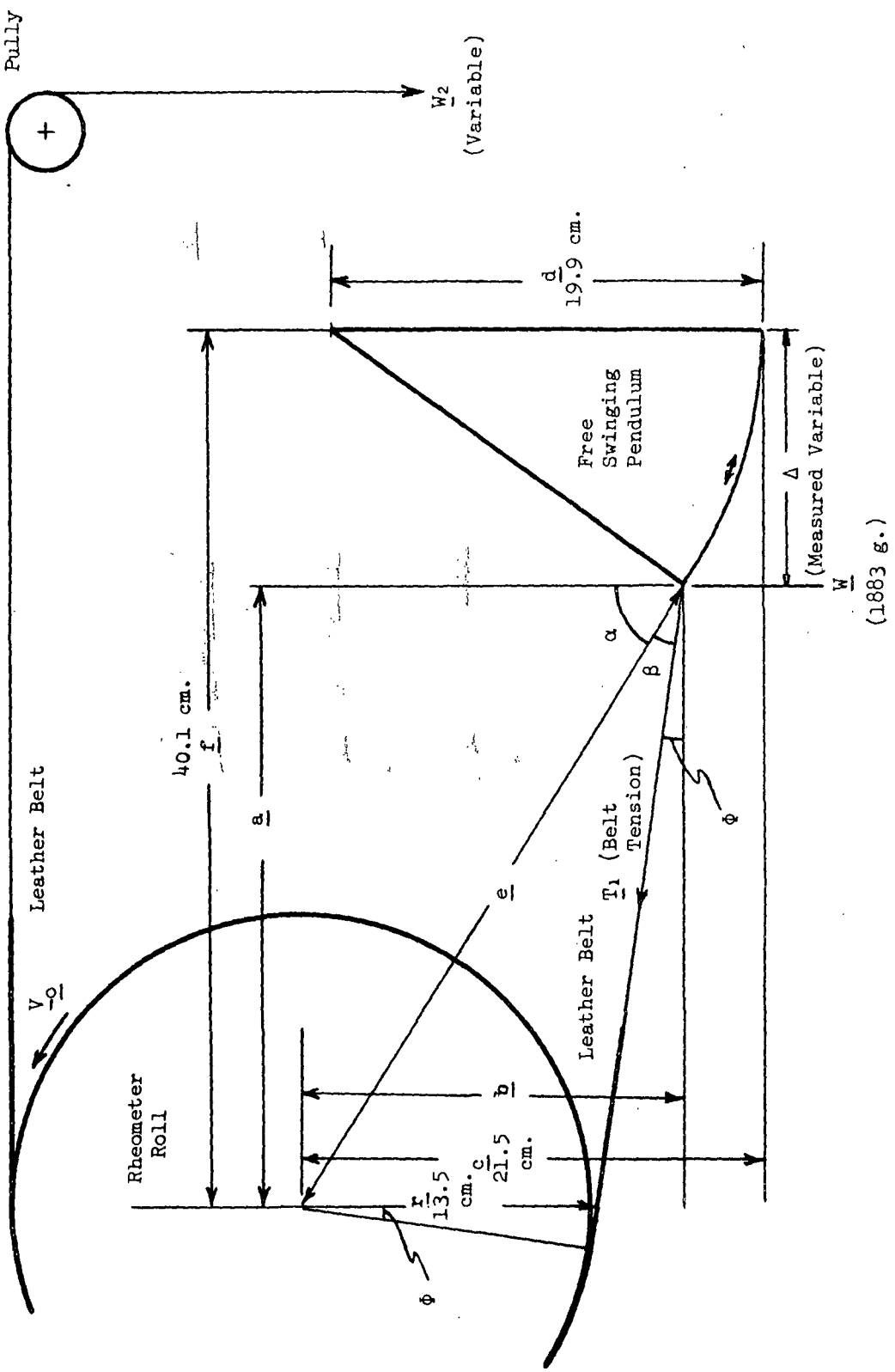

Figure 34. Experimental Arrangement Used to Calibrate Roll Drag

$$\sin \theta = \Delta/d$$

$$a = f - \Delta$$

$$b = c - d(1-\cos \theta)$$

$$\tan \alpha = a/b$$

$$e = b/\cos \alpha \qquad (149)$$

$$\sin \beta = r/e$$

$$\Phi = 90^\circ - \beta - \alpha$$

$$T_1 = \frac{W \sin \theta}{\cos(\theta-\Phi)}$$

Roll drag = belt tension difference = $W_2 - T_1$

The results of the calibration are presented in Fig. 35 and Table XX.

TABLE XX

SUMMARY OF ROLL DRAG CALIBRATIONS

V_o, ft./min.	Blade Load	Δ, roll drag, g./ΔX	Percent Error from Average
300	Increase	14.2	0
	Decrease	14.3	+1
500	Increase	14.4	+1
	Decrease	13.9	-2
900	Increase	14.3	+1
	Decrease	13.9	-2
1300	Increase	15.0	+6
	Decrease	13.9	-2
1600	Increase	14.8	+4
	Decrease	14.1	-1
2000	Increase	14.5	+2
	Decrease	14.0	-1
Average		14.2	

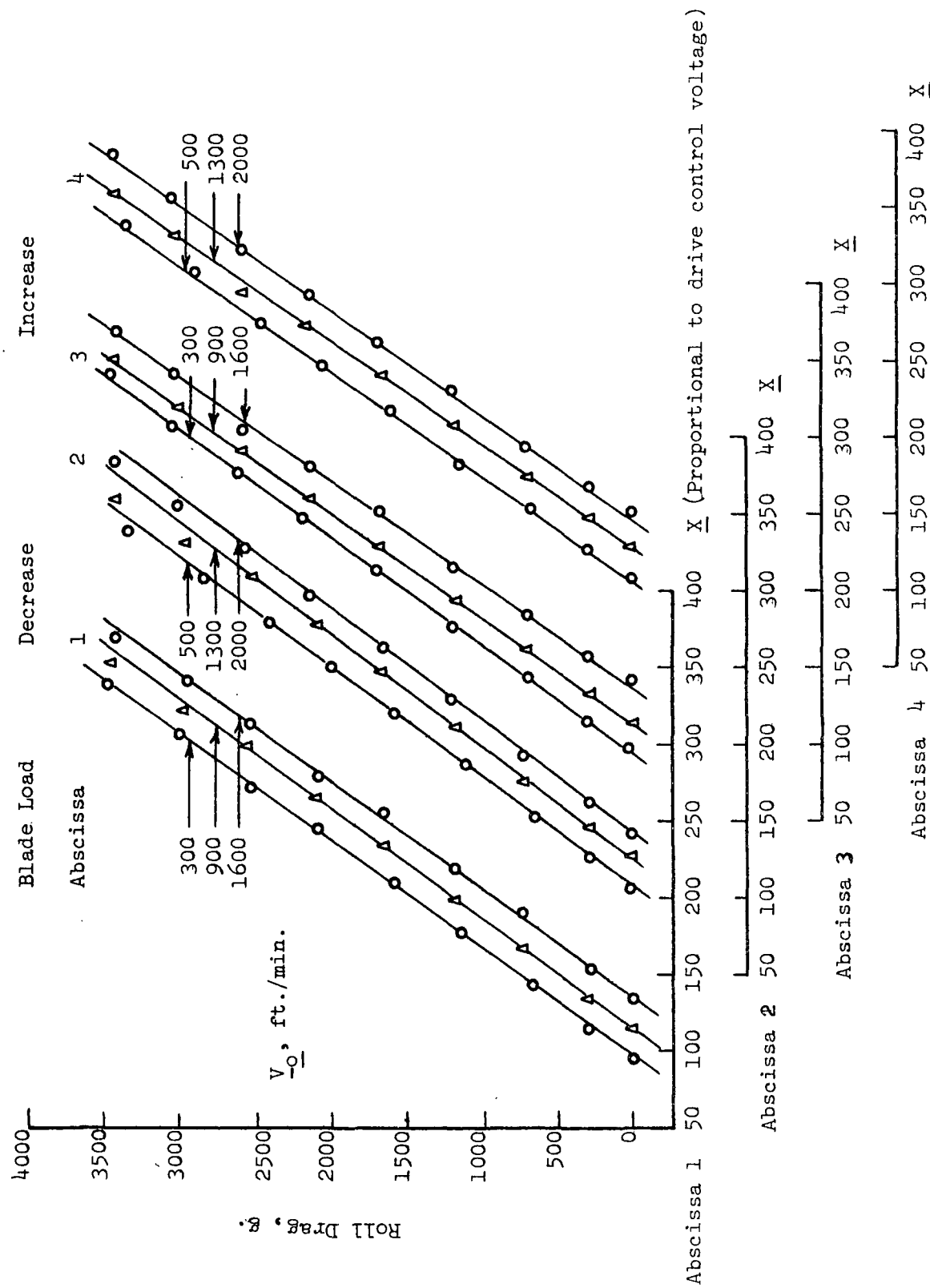

Figure 35. Roll Drag Calibration Results